Qi Wang

DYNAMIC ANALYSIS AND PARAMETER IDENTIFICATION FOR ROBOTIC MANIPULATORS

ACTA UNIVERSITATIS LAPPEENRANTAENSIS 1104

LUT University

Qi Wang

DYNAMIC ANALYSIS AND PARAMETER IDENTIFICATION FOR ROBOTIC MANIPULATORS

Dissertation for the degree of Doctor of Science (Technology) to be presented with due permission for public examination and criticism in the the Auditorium 1316 at Lappeenranta-Lahti University of Technology LUT, Lappeenranta, Finland on the 20th of November, 2023, at noon.

Acta Universitatis
Lappeenrantaensis 1104

Supervisors Docent Huapeng Wu
LUT School of Energy Systems
Lappeenranta-Lahti University of Technology LUT
Finland

Professor Heikki Handroos
LUT School of Energy Systems
Lappeenranta-Lahti University of Technology LUT
Finland

Professor Yuntao Song
Institute of Plasma Physics
Chinese Academy of Sciences
China

Reviewers Professor W.J. (Chris) Zhang
Department of Mechanical Engineering
University of Saskatchewan
Canada

Professor Yan Jin
School of Mechanical and Aerospace Engineering
Queen's University Belfast
United Kingdom

Opponents Professor W.J. (Chris) Zhang
Department of Mechanical Engineering
University of Saskatchewan
Canada

Professor Yan Jin
School of Mechanical and Aerospace Engineering
Queen's University Belfast
United Kingdom

ISBN 978-952-412-002-9
ISBN 978-952-412-003-6 (PDF)
ISSN 1456-4491 (Print)
ISSN 2814-5518 (online)

Lappeenranta-Lahti University of Technology LUT
LUT University Press 2023

Abstract

Qi Wang
Dynamic analysis and parameter identification for robotic manipulators
Lappeenranta 2023
118 pages
Acta Universitatis Lappeenrantaensis 1104
Diss. Lappeenranta-Lahti University of Technology LUT
ISBN 978-952-412-002-9, ISBN 978-952-412-003-6 (PDF), ISSN 1456-4491 (Print), ISSN 2814-5518 (online)

This paper presents a comparative advanced study on parameter identification and dynamic analysis of lightweight and heavy-duty robotic manipulators. The ultimate goal is to enhance the performance and control of these manipulators through precision in parameter estimation.

The initial section investigates the dynamics of harmonic drive systems in lightweight arms. Here, a data acquisition-based algorithm is introduced for offline dynamic parameter analysis. The Markov chain Monte Carlo (MCMC) method is central to this analysis, facilitating accurate parameter estimation for a friction model while considering uncertainty and sensitivity. Furthermore, the prediction of the GMS model, based on the MCMC method, exhibited a commendable improvement in accuracy, further emphasizing the efficacy of the chosen methods.

Subsequent sections explore heavy-duty arms, particularly those with planetary gearboxes. These discussions focus on friction, hysteresis issues, and the complexities of parameter estimation. The Bouc-Wen model is highlighted as a useful tool for identifying and addressing errors caused by hysteresis.

Beyond core analysis, the paper shows the potential combination of digital twin and control robot technologies for remote maintenance, especially in fusion reactor circumstances. Integration of these technologies promises to improve the operational capabilities of robotic systems, resulting in more reliable remote maintenance in challenging conditions.

The results of our various investigations provided a thorough understanding of robot dynamics and advanced parameter estimations. The focus of the first study was on identifying the joint dynamics of the robot. Incorporating the friction model for simulation of harmonic drives, along with the unique perspective of hysteresis characteristics, has enriched this understanding even further. Furthermore, the MCMC and SGHMC algorithms were thoroughly evaluated and validated, with the first exhibiting enhanced prediction accuracy by more than 5% and the second demonstrating

robustness in parameter estimation for heavy-duty manipulators.

Based on our findings, integrating these methods, especially the GMS model, significantly impacts the field. In our subsequent research, the fractional-order Bouc-Wen (FOBW) model has emerged as a key tool for illustrating hysteresis behaviors in different systems. It is based on the popular Bouc-Wen model and has been expanded to include more features. Our research underscores the importance of these advanced tools and models, suggesting an important development in the reliability and accuracy of robotic dynamic control in complex real-world situations.

Keywords: Robotic manipulators, parameter identification, dynamic analysis, heavy-duty arms, light weight arms

Acknowledgements

This work was carried out at the LUT School of Energy Systems, Lappeenranta-Lahti University of Technology (LUT), Finland, between 2010 and 2023.

The author extends her deepest gratitude to Associate Professor Huapeng Wu, Professor Heikki Handroos, and Professor Yuntao Song for their invaluable support and guidance. Their knowledge and distinct insights have been indispensable to the advancement of my research. I also express my sincere appreciation to the Academy of Finland and ASIPP for their financial support. This research was funded through the efforts of Associate Professor Huapeng Wu.

Qi Wang
September 2023
Lappeenranta, Finland

To my parents.

Contents

Nomenclature

Latin alphabet

i	current of the servo motor
$M(t)$	system input control or torque of the motor
T_f	total frictional torque of the robot joint
T_1	driving torque output to the connecting rod by the harmonic reducer
h	height parameter in the gravitational torque equation
g	acceleration due to gravity
m	mass parameter in the gravitational torque equation

Greek alphabet

θ	(angular displacement)
$\dot{u}(t)$	(velocity or derivative of the input position to the joint)
$\Gamma(u(t),t)$	(hysteresis restoring torque in the Bouc-Wen-like hysteresis model)
D	(internal damping coefficient)
$\dot{x}(t)$	(derivative of the state variable in the hysteresis model)
k	(rate-dependent stiffness parameter in the hysteresis model)
$\ddot{\theta}$	(angular acceleration)
τ_1	(joint torque transmitted from the motor side to the input point of the harmonic reducer)
f_c	(Coulomb friction)
f_v	(viscous friction)
f_{τ_t}	(load-dependent friction term)
$G(q)$	(gravitational torque)
$z(t)$	(backlash)
$\Delta\theta(t)$	(joint torsion and position deviation: discrepancies between desired input and actual output in the joint)
τ_m	(torque of the motor)
τ_t	(payload or load)
ω	(angular velocity)
J_1	(moment of inertia on one side of the joint)
q	(angle of rotation of the joint)
$\ddot{q}$	(angular acceleration of the joint)
$C(q,\dot{q})$	(Coriolis term in the dynamic equation)
f	(friction torque)
J_m	(moment of inertia on the motor side)
n	(exponent determining the rate dependence of the hysteresis loop)

Abbreviations

CFETR	China Fusion Engineering Test Reactor
CMOR	CFETR Multipurpose Overload Robot
DOF	Degrees of Freedom
CBW	the classic Bouc-Wen model
FOBW	the fractional-order Bouc-Wen model
MCMC	Markov Chain Monte Carlo
MPD	Multi-Purpose Deployer
PCA	Principal Component Analysis
PLSR	Partial least squares Regression
SGHMC	Stochastic Gradient Hamiltonian Monte Carlo

1 Introduction

1.1 Objective of the research

Robotic arms and their precise parameter identification are important in both industrial applications and scientific research. These versatile mechanical components have applications in fields such as manufacturing, healthcare, space exploration, and more. Their ability to perform complex tasks with speed, precision, and repeatability has revolutionized various industries, leading to increased efficiency and reduced human involvement in hazardous environments. To gain a complete understanding of the importance of this study, we begin with a broader context that underscores the pivotal role of robotic arms and parameter identification in modern technology and industry.

Robotic arms are the basis for contemporary automation. In manufacturing, they assemble complex electronic components with microscopic precision (Metzner et al., 2021), weld large structures (Vasilev et al., 2021), and perform quality inspections with precision (Vojić, 2020). In healthcare, robotic surgical arms aid surgeons in performing delicate procedures, minimizing invasiveness (Kalan et al., 2010) and improving patient outcomes (Marchand et al., 2019). In the domain of space exploration (Ticker, Cepollina, and Reed, 2015), robotic arms in spacecraft have revealed the secrets of distant planets and stars, making discoveries that humans had previously been unable to reach.

The efficacy of these robotic arms is based on a critical factor: precise knowledge of their parameters. These parameters, which range from joint friction and inertia to motor dynamics, govern arm behavior. Accurate parameter identification enables engineers and researchers to develop control algorithms that optimize performance, minimize energy consumption, and ensure safety. Without accurate knowledge of the parameters, robotic arms can malfunction, leading to inefficiency, decreased product quality, and safety risks.

This research aims to comprehensively investigate parameter identification methods for a range of robotic arms, including lightweight models with harmonic drives and heavy-duty versions equipped with planetary gear systems. Accurate parameter identification and dynamic analysis are fundamental to achieving maximum performance, improving safety, and optimizing efficiency in these robotic arms.

Moreover, our research address the distinctive challenges presented by the CMOR robot arm within the CFETR superconducting Tokamak fusion device. Operating within an environment characterized by extreme temperatures, intense radiation, and formidable magnetic fields, this specialized robotic arm poses unique challenges. To address these complexities, we explore the adaptation of advanced Monte Carlo algorithms (MCMC or SGHMC) for precise parameter identification.

In short, the purpose of our research is to provide an understanding of parameter identification methods adapted to the specific requirements of various robotic arms, while also addressing the unique challenges posed by advanced fusion technology.

The effects of friction and hysteresis have been identified as factors that can affect the efficiency of torque transmission in robotic manipulators (Ruderman, Hoffmann, and Bertram, 2009). Estimation of these effects is crucial to improving overall performance. In particular, harmonic drives, commonly used in lightweight robotic arms, are susceptible to these effects due to their nonlinearity and complex structure (Ruderman, Hoffmann, and Bertram, 2009). Various inference methods have been developed to accurately estimate manipulator parameters, including gear stiffness, backlash, and transmission ratios, in lightweight arms equipped with harmonic drives (Hao et al., 2021; Qi, Huapeng, Cheng, et al., 2022).

However, heavy-duty robotic arms often employ planetary gear systems known for their robustness and high torque transmission capabilities. Accurate estimation of parameters, such as gear ratios and stiffness, is vital for the safe operation and longevity of heavy-duty robotic manipulators. The comparative study presented here evaluates different inference methods applicable to heavy-duty robotic manipulators equipped with planetary gear systems, considering factors such as gear wear, system flexibility, and dynamic interactions.

Additionally, this study incorporates the unique challenges posed by the CFETR superconducting Tokamak fusion device's CMOR robot arm. The CMOR arm operates in a demanding environment characterized by high temperatures, intense radiation, and strong magnetic fields. Understanding the parameters of this specialized robotic arm is essential to ensure its reliable and efficient operation in the fusion device. We explore the application of inference methods to accurately identify the parameters specific to the CFETR CMOR arm, facilitating its successful integration into the fusion device (Jiasheng et al., 2020).

To address the challenges of parameter identification in both lightweight and heavy-duty arms, the study incorporates the use of the Markov chain Monte Carlo (MCMC) algorithm and the Stochastic Gradient Hamiltonian Monte Carlo (SGHMC) algorithm. MCMC provides a powerful and flexible framework for parameter estimation by sampling from the parameter space to approximate the posterior distribution. By incorporating prior knowledge and observed data, the MCMC algorithm offers an effective approach to estimate the parameters of robotic manipulators (Brooks et al., 2011).

The SGHMC algorithm is a variant of the popular Hamiltonian Monte Carlo (HMC) method, which uses stochastic gradients to improve sampling efficiency and convergence. By incorporating the SGHMC algorithm, this study aims to enhance the

accuracy and speed of parameter identification in robotic manipulators (Welling and Teh, 2011; Chen, Fox, and Guestrin, 2014).

The following studies have contributed significantly to our understanding of the topic.

(Chunxia et al., 2016) conducted a comprehensive investigation into control strategies to reduce hysteresis effects in robotic systems. The study highlighted the importance of accurately modeling and compensating for hysteresis to achieve precise control. Chunxia's findings provided valuable insights for improving the performance of robotic systems in practical applications.

(Shengzheng et al., 2021) conducted an in-depth analysis of the parameter distributions in robotic arm models. By considering the uncertainties in the model parameters, the authors proposed a robust control strategy that improved the tracking accuracy and robustness of the robotic arm. Their work emphasized the importance of accounting for parameter uncertainties in control design.

(Cai, Dong, and Nagamune, 2023) proposed a novel approach to modeling the dynamic equations of a single-joint mechanism. Their extended model takes into account various factors such as inertia, friction, and external disturbances. The authors demonstrated the effectiveness of their approach through experimental validation. In addition to these influential studies, several other notable works have contributed to our understanding of the subject matter. For example, (Ravenzwaaij, Cassey, and Brown, 2018) proposed an MCMC approach.

These studies, along with numerous other relevant works, have formed the basis for our research. Based on these existing findings, we aim to make novel contributions to the field. In the following sections, we present our research background and scientific contribution.

1.2 Research background

1.2.1 Diverse Robotic Arms for Remote Fusion Maintenance Applications

1. The Articulated Inspection Arm (AIA): Robotic operations pose significant challenges to the maintenance of the ITER and future fusion reactors. In response to this issue, CEA (the French Alternative Energy and Atomic Energy Commission) has successfully developed a versatile carrier capable of performing in-vessel deployments under the Ultra High Vacuum (UHV) and temperature conditioning requirements. Over the span of a six-year research and development program, the CEA-LIST Interactive Robotics Unit and the Institute for Magnetic Fusion Research (IRFM) demonstrated the viability and dependability of an in-vessel inspection robot specifically designed to meet ITER's stringent requirements. The AIA robot carrier, depicted in Figure 1.1a, is a remarkable eight

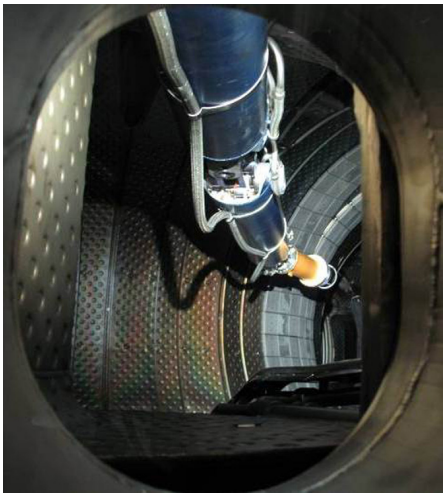

(a) The AIA robot is deployed into the Tore Supra fusion reactor, navigating under the challenging Ultra High Vacuum (UHV)
conditions (Gargiulo et al., 2009).

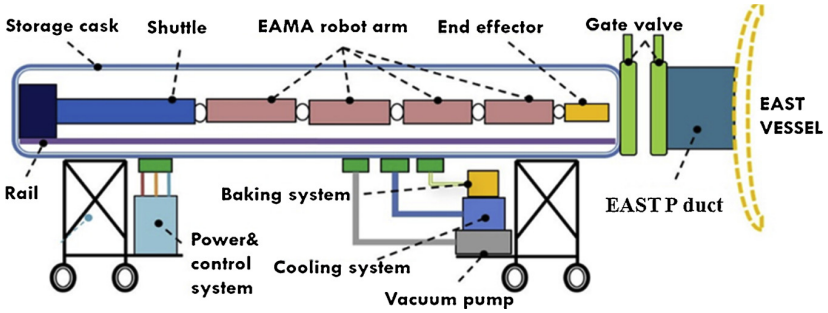

(b) Comprehensive schematic view of the EAMA system (Kun, Qi, Huapeng, et al., 2018; Kun, Qi, Yong, et al., 2019).

Figure 1.1: (a)The AIA robot (b) The EAMA robot.

meter long multilink arm consisting of five modules made of titanium, each with a diameter of 160 mm. These modules incorporate pitch ($\pm 45^\circ$ in the vertical plane) and yaw ($\pm 90^\circ$ in the horizontal plane) joints, offering a unique combination of elevation and rotation motions that provide the robot with a total of eight degrees of freedom. This innovative design allows for comprehensive inspections of Tore Supra plasma vessel components (Team, 2002), all from a single median port. This feature allows the AIA robot to be introduced through a small port of just 250 mm in diameter, showcasing its versatility and adaptability in confined spaces. Operating seamlessly within the challenging environment of the tokamak plasma,

the AIA robot adheres to strict tokamak conditioning conditions, demonstrating its reliability and suitability for in-vessel tasks. This development opens up new possibilities to perform maintenance and inspection tasks remotely and effectively on fusion reactors, significantly enhancing operational efficiency and safety.

2. The East Advanced Superconducting Tokamak (EAST) articulated maintenance arm (EAMA) system: To meet the demanding operational parameters of the EAST, the inner components of the first wall must withstand increasing electromagnetic and heat loads (Shi et al., 2016). Practical experiments have revealed various failures of internal parts, making timely maintenance based on the condition of damaged components essential during the experimental period (Pan et al., 2017). Taking inspiration from the AIA designed for visual inspections inside the Tokamak (Gargiulo et al., 2009), ASIPP and CEA-IRFM collaborated to develop the EAMA system (Shi et al., 2016). The primary objective of this system is to inspect and maintain damaged internal components during plasma discharges without breaking the ultra-high vacuum condition of EAST. The challenging environment of the EAST led to the design of the EAMA as a snake-like robot with a highly redundant articulated series mechanism and several modules, ensuring obstacle avoidance and achieving the required coverage ratio. The EAMA system consists primarily of the highly redundant snakelike robot, the EAMA itself, and a storage cask containing several condition maintenance systems, as shown in Figure 1.1b.

1.2.2 Remote handling system with CMOR

The CFETR Multipurpose Overload Robot (CMOR) motion control system is a specialized system designed to handle heavy loads and perform intricate tasks in challenging environments. The CMOR system in Figure 1.2a comprises a macro arm, which includes the Multi-Purpose Deployer (MPD), and two micro arms.

In general, the CMOR system, with its macro and micro joints, provides a comprehensive solution for the remote control, maintenance, and operation of complex systems. The combination of the macro and micro joints offers versatility and adaptability, making it suitable for a wide range of applications in challenging environments.

The CMOR system in Figure 1.2a is a comprehensive remote handling solution used in various industries to control, maintain, and operate complex systems. It combines advanced robotic manipulators with precise motion control systems to perform tasks in hazardous or challenging environments. CMOR is known as the CFETR (China Fusion Engineering Test Reactor) Multipurpose Overload Robot (CMOR) motion control system (Qin, Cheng, et al., 2022).

The Multipurpose Deployer (MPD), depicted in Figure 1.2b, is an integral component of

the heavy-duty manipulator. The CMOR Multipurpose Overload Robot motion control

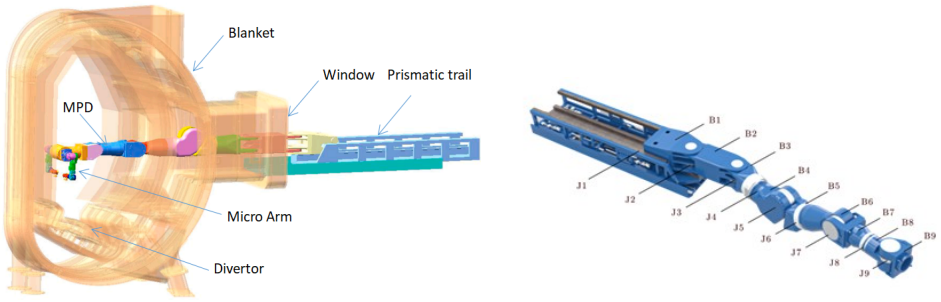

(a) Modeling the operational scenario of the CMOR (CFETR Multipurpose Overload Robot) in the China Fusion Engineering Test Reactor (CFETR).

(b) The configuration of the Multi-Purpose Deployer (MPD).

Figure 1.2: (a) Simulation of CMOR in CFETR and (b) Structure of MPD in Heavy-Duty manipulator

system consists of a macro arm and two micro arms. The MPD is responsible for handling heavy loads and executing complex tasks. It is designed to operate in the challenging environment of the CFETR fusion device, where precision and robustness are crucial. The CMOR consists of nine components labeled B1 to B9 and features eight rotation joints designated J1 through J8. The system possesses a total of eight degrees of freedom, accommodating various joint actuators to meet specific requirements. In particular, horizontal yaw motions are facilitated by J1 and J2, while axial rotational motions are enabled by J3, J5 and J7. Vertical pitch motions, on the other hand, are achieved through J4, J6, and J8 (Qin, Ji, et al., 2021).

The micro arms, on the other hand, are dual 7-DOF robots that provide enhanced agility and precision for delicate operations such as assembly, maintenance, and manipulation of components (Tao et al., 2023).

The integration of these macro and micro joints within the CMOR system enables the remote handling of various components and systems in challenging environments. It offers a versatile and adaptable solution for controlling and maintaining complex machinery and equipment. The CMOR system is specifically designed to meet the requirements of the CFETR project, which aims to develop advanced fusion energy technology in China (Song, Wu, et al., 2014).

To ensure the optimal performance of the CMOR system, advanced parameter identification and dynamic analysis techniques are essential. Accurate modeling of the system dynamics, including the behavior of individual joints and the interaction between the arms and the environment, is crucial to achieving precise control and efficient

operation. Additionally, control algorithms must be designed to handle the uncertainties and complexities inherent in remote handling tasks, ensuring the safety of both the robotic system and human operators.

1.2.3 Lightweight robotic arms and the snake arm manipulator (SAM) in the CFETR system

1. Lightweight robotic arms

Lightweight robotic arms are a key part of the CMOR motion control system for jobs that need to be performed remotely. These arms, which are known for their speed and accuracy, are designed to handle delicate tasks such as assembling, fixing, and moving parts (B'Elanger and Taghirad, 2002). However, challenges arise due to the inherent complexities associated with remote tasks. Friction, harmonic factors, and the robot's interaction with its environment can hinder optimal performance. This study aims to address these challenges by developing improved control algorithms and building accurate models for these systems.

Figure 1.3a presents a 3D model of the CMOR system, which includes the MPD (Multipurpose Deployer) and the lightweight robotic arm. This image provides a visual representation of the CMOR system and the lightweight robotic arm, aiding the reader in better understanding the research background and experimental setup.

Figure 1.3b displays the lightweight robot data acquisition interface, together with the experimental equipment for the fourth joint. The lightweight robotic arm is part of the CMOR system and is used for precise operations. Through this interface, data can be collected and experiments can be controlled to investigate and test the performance and behavior of the fourth joint.

Harmonic drives have been used a lot since 1955 because they have a high torque output, are light, and are more efficient than standard drives (Kennedy and Desai, 2005). They are used in flight, aircraft systems, industrial robots, and heavy-duty and lightweight robotic systems. When studying how robots move, it is important to use correct mathematical models that take into account friction and harmonic drives (Ema et al., 2020).

Accurate prediction of force is important for safety, accuracy and teaching through the introduction (Luca and Mattone, 2005). For example, in robot operations, torque sensing and control are important for the safety of the device, especially when a robot and a person collide (Morel and Dubowsky, 1996). To ensure that people are safe, it is important to know exactly what forces or torques are working on the robot from the outside. Similarly, torque monitoring is of significant importance for flexible production and work scenarios, such as industrial applications like grinding and assembly, where precise control and performance are critical. When it comes to heavy-duty industrial

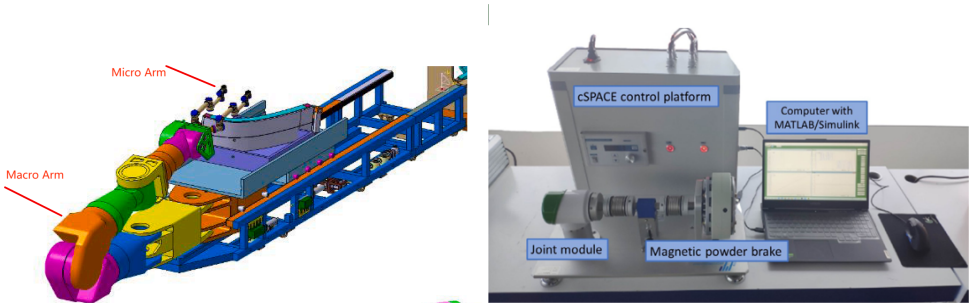

(a) The 3D model of CMOR system that contains MPD and light robotic arm.

(b) Data acquisition interface of the lightweight robot, and experimental equipment of the fourth joint.

Figure 1.3: The CMOR system and lightweight robotic arm: 3D model and experimental setup.

robots, parameter errors become even more important. Because of this, it is important to make control methods that work well with CMOR, CFETR, EAMA, and various other heavy-duty manipulators in industrial settings (Song, Wu, et al., 2014; Shi et al., 2016; Wang et al., 2019).

In addition, dynamic models of manipulators often have many unknown parameters, making it difficult to make accurate models. Static nonlinearity is usually used to describe the friction of harmonic drives. This includes things such as velocity, load, stiffness, hysteresis, and motion error behavior (Kircanski and Goldenberg, 1997; Ruderman, Hoffmann, and Bertram, 2009; Yuhsiu et al., 2019; Kesner and Howe, 2011). Several studies have tried to figure out how harmonic drives work by making dynamic models that take into account transmission wear, kinematic error, and other factors (Tuttle and Seering, 1993; Taghirad and Belanger, 1998). The goal of these models is to make modeling and control algorithms for harmonic drives more accurate. This will make them easier to control and improve their overall performance.

Different friction dynamic models have been suggested, such as Dahl's model, the LuGre model, the Leuven model, and the GMS model (Kennedy and Desai, 2003; Jatta, Legnani, and Visioli, 2006; Marton and Lantos, 2007; Sato, 2012). Some of these models have taken into account temperature effects and the polynomial form of friction models (Simoni et al., 2017; Do et al., 2014; Jan et al., 2000; Dewit et al., 1991; Simoni et al., 2015; Han, Ma, and Li, 2016). Noise, however, makes it difficult to think about how temperature affects output torque and to correctly find parameters using least square methods (Zhiguo et al., 2017; Trumper and Yoon, 2014; Gandhi, Ghorbel, and Dabney, 2002; Astrom and Canudas-De-Wit, 2008), and (Lampaert, J. Swevers, and Al-Bender, 2002).

This study suggests using the Markov chain method to determine the dynamic parameters of flexible manipulators (Tri et al., 2011). This is done to avoid these problems. The method requires figuring out how friction, speed, and load torque depend on each other in a static, nonlinear way. The generalized Maxwell-slip (GMS) model is used to estimate hysteresis features, and the MCMC method is used to find the dynamic parameters of flexible robots with greater precision (Al-Bender, Lampaert, and Swevers, 2005). In parameter fitting, the MCMC method has some benefits over the LS method. Although least-square methods are a classic way to estimate parameters, they may not be strong enough when there is noise and uncertainty. By minimizing the sum of squares difference between the actual data and the model's forecasts, least square methods may give less accurate estimates of the parameters. The MCMC method, which is based on the Markov chain Monte Carlo algorithm, is a more reliable way to estimate parameters, especially when noise and uncertainty are present. It makes it easier to figure things out, such as friction and stiffness, in flexible manipulators. Therefore, the proposed friction model and the MCMC method can improve the control precision based on the model, and can be used to improve the total performance and accuracy of regular industrial robots.

2. Introduce the snake arm manipulator (SAM) into the CFETR system.

Regular monitoring and maintenance of the CFETR through the RH system is necessary for the safe and reliable operation of this test reactor. However, conventional industrial robotics are inadequate for the confined, obstacle-filled, and highly radioactive vacuum chamber of the reactor. This inefficiency in maintenance presents a significant challenge, as it hinders the realization of essential automated equipment for future fusion power plants. The SAM's design and function aim to overcome this challenge.

Hyper-redundant SAMs have attracted attention because of their exceptional adaptability and ability to avoid obstacles. Consequently, the SAM plays a crucial role in monitoring and maintaining complex and expansive apparatuses. It also excels at navigating and managing confined spaces, making it a practical robot.

SAM draws inspiration from natural creatures, such as snakes, an elephant's trunk, and animal tails, due to its multi-jointed hyper-redundancy.

The drive unit (motor, etc.) of an SAM is external to its working space, simplifying its structure, and allowing for a more streamlined posture. This configuration removes all electronics from the robot arm, making it ideal for high-risk, radioactive, and confined environments such as nuclear power plants.

The primary objective of this project was to develop the SAM as a vital subsystem for the CFETR remote handling maintenance system. It performs duties such as visual inspections and dust removal within the complex pipeline areas of the upper window and

bottom diverter of the vacuum chamber. By incorporating SAM onto the quick-change interface at the end of the CFETR multipurpose overload robot (CMOR), maintenance operations in the vacuum chamber's intricate, confined spaces are made possible.

In order to accommodate the tight confines of the CFETR vacuum chamber, we designed a layered drive SAM, as depicted in Figure 1.4. Attached to the CMOR heavy-duty arm, SAM facilitates maintenance, repair, and dust removal of the reactor environment. Its distinguishing characteristics include a capacious operating area and radiation resistance. During reactor operation, it efficiently removes a large quantity of particles generated by the high-temperature plasma, thereby contributing to the efficient operation of the reactor.

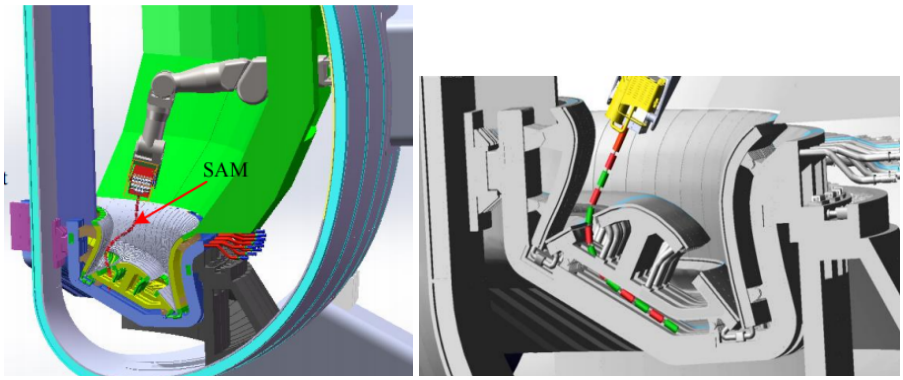

(a) The SAM as a CMOR end-effector for dust cleaning at the bottom of divertors (Qin, Ji, et al., 2021; Qiang, Ling, and Zengfu, 2017).

(b) The SAM robot monitoring and observation in a vacuum chamber environment (Qiang, Ling, and Zengfu, 2017; Qin, 2022).

Figure 1.4: The SAM robot monitoring and observation in a vacuum chamber environment.

In addition to the Micro Arm and Lightweight Robotic Arm, the CMOR system incorporates the 'Snake Arm Manipulator' (SAM), a unique robotic arm resembling a snake. Although specific parameter identification for the SAM snake-like manipulator was not pursued in this study, it plays a crucial function within the CMOR system. Due to its flexible structure resembling a snake, SAM implements precise operations in complex environments. The joint flexibility of SAM, which was inspired by serpentine organisms in nature, enables unrestricted movement in confined or obstructed areas.

Collaboration: SAM and the lightweight robotic arm in action

The incorporation of the Snake Arm Manipulator (SAM) into the CFETR system highlights its function as a flexible and adaptable instrument in complex maintenance scenarios. As SAM excels at traversing intricate and confined spaces, it complements the array of robotic assets in the CMOR system, including the lightweight robotic arm

mentioned previously.

Designed with precision and accuracy, the lightweight robotic arm increases the capabilities of the CMOR system. Its lightweight construction and innovative joint design enable efficient manipulation in restricted environments. Working together with SAM, this arm aids a variety of maintenance tasks, providing a comprehensive approach to overcoming obstacles within the vacuum chamber of the CFETR.

The integration of SAM and the lightweight robotic arm into the CMOR system shows an integrated strategy to address the complex remote maintenance requirements of the CFETR. Next, we detail how to further enhance the capabilities of the robotic arm through digital twin integration to meet the challenges of future fusion energy technologies.

1.3 Enhancing robotic manipulators with digital twin integration

The main goal of this section is to thoroughly explore the application of digital twin (DT) technology in robotic manipulators, and to explore how to use DT technology to enhance the dynamic performance of robotic arms. We will focus on the principles of digital twin technology, its benefits, and how it can be integrated into robotic operations for greater precision, safety, and operational efficiency.

Digital twin technology, as a virtual simulation and simulation method, has attracted widespread attention in many fields. It can be used to build a virtual robot model, simulate the movement and behavior of the robot, and evaluate the robot's performance in tasks. For example, with a digital twin, we can test the dynamics of a robotic arm in a virtual environment and optimize its control algorithms for greater precision and efficiency in real-world operations (Grieves and Vickers, 2017).

The dgital twin concept provides a comprehensive representation of an entity, capturing vital information across its entire lifecycle. Modeling and simulation, which are critical in system design and validation, merge physical and virtual realms, helping various professionals understand and manage mechatronic systems (Boschert and Rosen, 2016). In addition, dgital twin can also be used for remote operation and monitoring of robots, as well as real-time health monitoring and maintenance of robotic systems. In the following sections, we will explore in more depth the specific application of dgital twin technology in the field of robotic manipulators and how it affects the performance and operation of robotic arms.

1.3.1 Fusion of light and heavy load robotic arms and dgital twin

Robotic manipulators come in various designs, from lightweight arms with harmonic drives to heavier arms using planetary gear systems. These designs cater to different needs, including safety, precise control, and operator training. However, they also introduce challenges such as friction, hysteresis, and dynamic response. To address these challenges, a deep understanding of robotic arm behavior is crucial and digital twin technology is instrumental.

Safety is essential in robotic arms, pushing design evolution to ensure human-machine coexistence. Precise control has led to complex mechanical structures with advanced control systems. Additionally, the need for skilled operators of varying levels has driven the development of user-friendly robotic arms.

The heart of these challenges lies in understanding the robotic arm's behavior, from every joint to servo interaction. The digital twin comes into play by faithfully replicating the precise behavior and characteristics of physical robotic arms. It directly addresses challenges such as friction, hysteresis, and dynamic response.

A digital twin is a remarkable digital replica of a physical object, system, or process. It mirrors the real-world entity in real time, using insights from sensors and simulations to mimic its behavior and performance. The primary goal is to gain comprehensive insights into the physical object's behavior, continuously monitor its condition, and enhance its operation, all without direct interaction with the physical counterpart.

The conceptual DT-HRC framework (Chitta et al., 2017) suggested is shown in Figure 1.5. The digital twin is a new idea that has the potential to change many different industries. This approach has enabled the creation of virtual counterparts for physical entities, opening avenues for simulation, analysis, and optimization. Figure 1.5 visually display this framework, with the description of the robot that captures essential attributes such as geometry, structure, kinematics, and dynamics, all the same as in the physical robot.

The system operates through a structured process consisting of six sequential steps, each integral to various key applications. This process follows a two-stage model: the "3C Setup" includes steps one to three, and the "operate" stage covers steps four to six. In the initial stage, the focus is on establishing the system's environment. This involves configuring communication channels, collecting data, merging real and virtual datasets, and superimposing digital content. Through these steps, a comprehensive digital representation of the real world is constructed, enhanced by virtual sensors that mirror physical counterparts. By executing code, the virtual controller simulates the movements of the real robot, thereby demonstrating the capabilities of the framework.

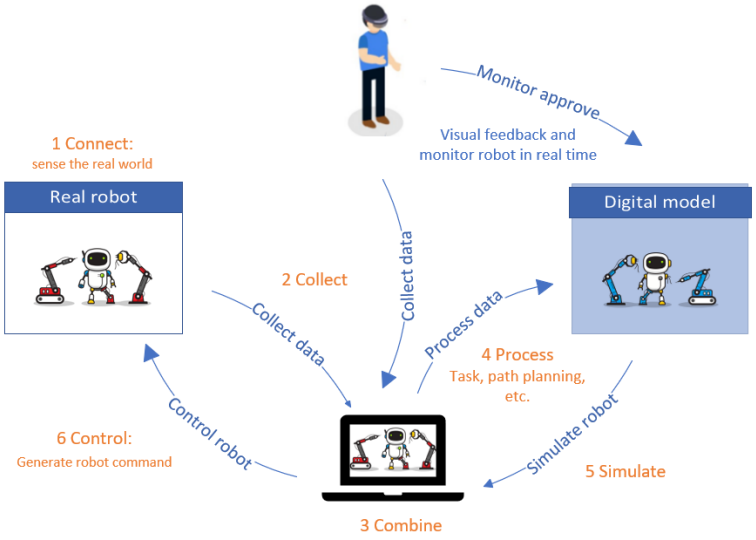

Figure 1.5: The human–robot collaborative (HRC) application of the dgital twin (DT) framework.

The implementation of the digital twin involves several pivotal phases. These include visualizing the corresponding objects and environments, creating sensors and controllers, facilitating communication among these elements, and executing tasks within the virtual domain. A key distinguishing feature of the digital twin, in contrast to standard simulations, lies in its bidirectional communication capacity. This bidirectional capability is achieved by adopting the ROS framework (Chitta et al., 2017), which facilitates data exchange between the physical and virtual domains. Integral to this architecture are the dynamic equations embedded within the robot's Universal Robot Description Format (URDF) file (Yeon, Donghan, and Kwangjin, 2019). This integration underscores the indispensable role of dynamic equations in both the ROS system and the digital twin framework.

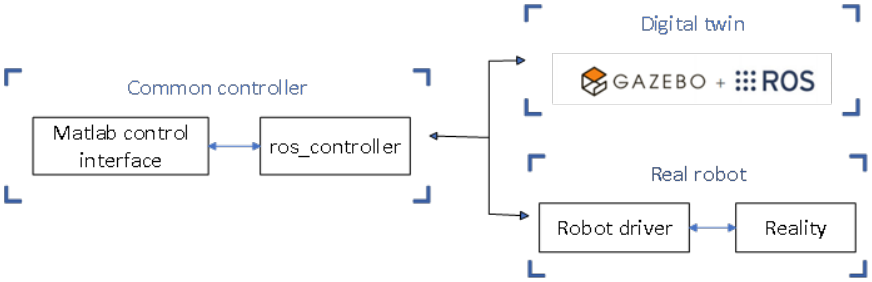

Figure 1.6: The controller of DT and real robot.

1.3.2 Robot operating system: empowering flexible and collaborative robotic control

ROS, short for Robot Operating System, is an open source framework designed to facilitate the control and coordination of robotic components through a computer. It operates under the BSD license and functions as a system that includes multiple individual nodes. These nodes operate independently and communicate with each other using a publishing or subscription messaging pattern. In practical terms, ROS allows for modular and distributed robotics development. Each node can serve a different purpose and interact through message exchange. A prime example is a sensor driver which acts as a node that publishes sensor data in the form of messages. These messages can then be consumed by a variety of other nodes, ranging from loggers to higher-level systems such as pathfinding algorithms.

The attractiveness of ROS lies in its flexibility and adaptability. Nodes within the ROS ecosystem are not restricted to a single system or architecture. This means that nodes could be running on disparate devices, from an Arduino generating messages, to a laptop subscribing to them, and even an Android phone controlling motors. This makes ROS suitable for various applications.

Furthermore, ROS is open source, enjoying contributions from a multitude of developers. This collaborative nature ensures ongoing maintenance and refinement of the framework, keeping it relevant and well maintained. Central to this approach is the ROS server, which enables a cyclic computation process that combines robot, object, sensor, control input, and environment configurations. The final result of this strategy is the construction and use of a parallel world. When the ROS client works with Gazebo, it creates a vivid 3D visualization that shows how the estimated world is set up. Figure 1.6 shows the controller framework for the digital twin, which is controlled by the built-in ROS controller (Chitta et al., 2017).

1.3.3 The role of dynamics in connecting robot control and digital twin technology

The four-layer tower design is a fundamental structure widely utilised in the field of robot control as shown in Figure 1.7. In this design, which is made up of dynamics, parameter identification, motion planning, and motion control, dynamics stands out as the most important part. It is the foundation on which the entire control framework is built.

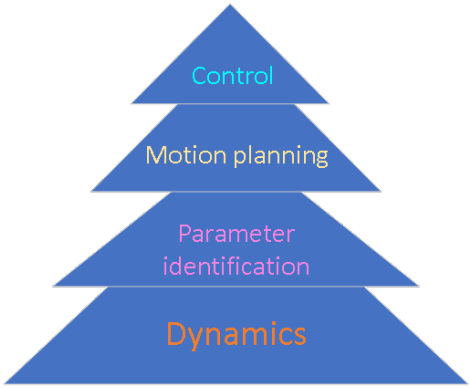

Figure 1.7: A four-level architectural structure for robotic control, with a foundation in dynamics.

Planning and control strategies are based on the layers of dynamics and system identification, which are a crucial basis. Effective control methods are made possible by a deep understanding of a robot's dynamics and an exact identification of its system. Precise trajectory planning is crucial for efficient robot control, optimizing the robot's path, and improving overall performance. Dynamics are fundamental to enhanced control and to ensuring accuracy. These dynamic equations also power digital twin technology, which recreates real-world behavior virtually. When it comes to digital twins, dynamic equations bridge the physical and virtual worlds, allowing accurate simulation. This precision is vital to simulating real-world scenarios, including human interactions, enhancing predictions. Dynamic equations link robot control to digital twins, allowing for more accurate models that help people make better decisions and improve performance.

1.4 Dynamics in modern robotic systems

1.4.1 State of the art in robotic dynamics and digital twins

In recent years, the integration of digital twin technology with the principles of dynamics has enabled significant progress in the field of robotic applications. Through digital twins, engineers have achieved the capability to virtually simulate the dynamic response of robotic systems when subjected to varying input and external forces. Such virtual replications promise enhancements in control algorithms while addressing potential issues before they materialize in real-world scenarios.

A deep understanding of these dynamics is vital for intricate maintenance operations, particularly those pertaining to the internal maintenance of vacuum chambers. Key tasks in this regard include the maintenance and cleaning of deflector tubes, inspection, calibration, and repair of diagnostic components, among others. These tasks are highly

dependent on dual-arm actuators, as depicted in Figure 1.8a. Furthermore, dual arm end effectors, as shown in Figure 1.8b, comprise a multitude of tools, including, but not limited to, external welding tools and non-destructive testing instruments.

In practice, consider a welding robot workstation armed with two robotic appendages. A primary challenge here lies in the synchronization of the robot arm and the workstation to ensure collision-free operations and the preservation of welding quality. The initial tests are conducted in a simulated environment. Upon satisfactory performance in this virtual setup, the programs are transferred to the physical workstation, ensuring seamless coordination between the real and virtual robotic arms.

The synthesis of digital twin technology and dynamics principles not only fosters a deeper understanding of robotic system behaviors but also equips us with the tools to tackle complex challenges. The essence of this integration hinges on the precise modeling of dynamics, as only accurate dynamic equations can enable the intricate controls aforementioned. Such advancements herald a promising future for robotics, especially in the realm of intricate tasks and challenges.

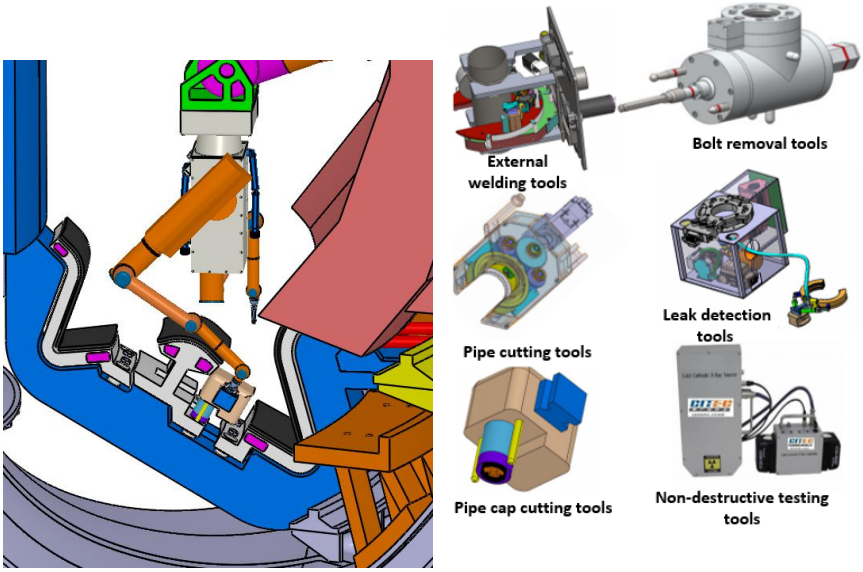

(a) Dual-arm actuator for divertor maintenance.

(b) Actuator for a lightweight robotic arm at the end of a heavy robotic arm.

Figure 1.8: Different actuators for robotic arm systems in maintenance.

1.4.2 Force control methods and applications in robotic manipulation

Precision remains fundamental to robotics. The overall efficacy of the system is determined by the precision of each operation, calculation, and subsequent action. As technology advances, the landscape of problems and applications is in an ongoing process of change. From intricate medical procedures to expansive industrial settings, the need for refined force control is evident. Such precision requires techniques that can handle both mechanical and computational complexities.

Many techniques have emerged to improve force control in robotic manipulators, based on our understanding of robotic behavior and the central role of dynamics modeling. Each technique offers its unique advantages and is adapted to specific applications:

1. Joint torque sensors:
   By fitting single-axis torque sensors on each robot joint, force interactions can be precisely measured. Located close to the motor, these sensors reduce interference from the robot's dynamic body properties. They capture comprehensive torque information, including factors such as gravity and inertia moments. Traversaro (Traversaro et al., 2015) and Suh (Suh, Joonwook, and Dong-Eun, 2020) have explored the potential of this technique. However, the complexity and costs associated with their integration can limit their widespread adoption.

2. End multiaxis torque sensor:
   Employed by many robotic systems, end torque sensors detect forces at the robot's extremity. However, challenges arise due to the separation between the torque sensor and the execution motor. Sun (Sun et al., 2015) worked on designing such sensors for space robots. This separation often limits the robot's force control dynamic performance.

3. Base multiaxis torque sensor:
   Some researchers, including Sim (Sim et al., 2018), have considered installing the torque sensor at the base of the robot to detect interactive force information throughout the arm. But its effectiveness is questioned with non-co-located modes, and calibration becomes intricate.

4. Joint current feedback:
   This method is best for direct-drive robots or those with a small reduction ratio. In such contexts, joint friction remains minimal. Wahrburg (Wahrburg et al., 2018) introduced an approach that employs this method, emphasizing its relevance when joint frictions are negligible.

5. Series elastic drive (SEA):
   The SEA approach uses mechanical deformation to control the force of the robot,

which transforms it into position control. Researchers like Kim (Kim and Oh, 2019) and Ni (Ni et al., 2018) have investigated its dynamics and potential challenges, including the need for complex joint torque sensors.

6. Harmonic reducer:
   Like a torsion spring, the harmonic reducer detects torsional deformation to determine the torque. This method (Song, Huang, et al., 2020) utilizes the inherent elasticity of the harmonic reducer. It is believed that its efficacy is similar to that of joint torque sensors, although comprehensive research remains limited.

Such diverse methods demonstrate the importance of dynamics in robotics. Precise modeling of these dynamics increases robot efficiency across a variety of tasks. Furthermore, understanding the applications of these principles in robotic manipulation reinforces the critical role of dynamics in myriad robotic operations. Whether it is control simulations, position adjustments, or vibration suppression, the granular details of dynamic modeling remain paramount for the success of these endeavors.

In summation, the importance of determining dynamic equations for force control is paramount. A deep understanding of the dynamics underlying robotic systems is essential for force control precision. Our strategies for force control will only be as effective as our ability to identify and model these dynamics with exactitude. Incorporating dynamic principles into robotic applications ensures that they function with heightened efficiency, safety, and precision across a spectrum of tasks.

1.4.3 Dynamics in practical robotic applications

With this foundational understanding of the significance of dynamics in force control, it is crucial to recognize how these principles apply to robotic manipulation. Dynamics not only provides a theoretical foundation but also actively informs and improves a vast array of practical robotic duties. From control simulations to position adjustments and vibration suppression to compliant control, the specifics of dynamic modeling are crucial to the success of these operations.

1. Control simulation: forward kinematics challenges. Dynamics finds a vital application in control simulation, particularly when addressing forward-kinematics challenges. By leveraging dynamic models, simulations can accurately predict the robot's motion and behavior, aiding in optimizing control strategies.

2. Position control: enhancing precision and speed (Wei, 2005)

   (a) High-speed, high-precision position response dynamics are instrumental in achieving precise and rapid position control. By accounting for dynamic effects, controllers can be fine-tuned to deliver swift and accurate responses,

crucial in applications demanding intricate positional adjustments.

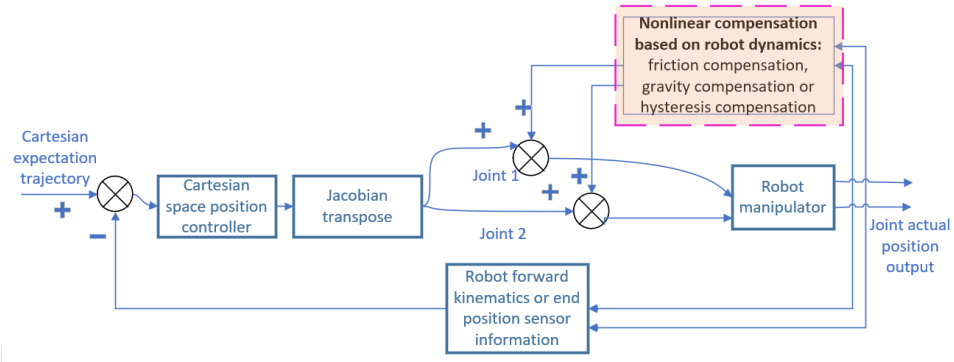

Figure 1.9: Utilizing dynamic equations for precise position control in space.

To show how flexible dynamics can be in robotics applications, we use a specific use case that shows how dynamic equations can be used to control a robot's position precisely in a space environment. This application shows how smoothly dynamic concepts can be used in real-world situations.

The dynamic position control of space robotics follows the following steps:

1. Define the intended Cartesian trajectory for the path of the robot through space. 2. Continuously record the actual position of the robot using joint encoders. 3. Compare the actual position to the desired trajectory to generate a Cartesian position error. 4. Use the position error to alter the control rate, bringing the robot into alignment with the intended path. 5. Use the Jacobian matrix to transform Cartesian errors into joint-specific errors. 6. Apply techniques to compensate for system non-linearities that affect joint movements. 7. Create individualized commands for each joint's actuators based on the refined position errors.

(b) Vibration suppression: resonance frequency identification. Identification and suppression of vibrations are enabled through dynamic analysis. Identifying resonance frequencies allows for the implementation of strategies that mitigate vibrations, enhancing the stability and performance of robotic systems.

(c) Collision detection. Dynamics-based techniques enable effective collision detection. By modeling the robot's dynamics, potential collisions can be predicted and preemptively addressed, preventing damages, and ensuring safe operation.

(d) Flexible joint control: the example of an iiwa robot. Dynamics-based control is crucial in managing flexible joints, as exemplified by robots such as the iiwa. These robots incorporate dynamic models to adaptively control their flexible joints, enabling smoother and more precise movements.

3. Compliant control (Wei, 2005; Qian, Dai, and He, 2007)

   (a) Physical interaction: polishing, guided manipulation. Dynamic principles underpin physical interactions between robots and their environment. Applications such as polishing and guided manipulation rely on dynamic models to facilitate controlled physical interactions, ensuring accurate and controlled movements.

   (b) Compliant control of flexible joints: the case of the iiwa robot. Dynamic approaches also shine in achieving compliant control for robots with flexible joints, similar to the iiwa robot. When dynamics are taken into account, these robots exhibit more natural and adaptable movements, making them suitable for tasks that demand flexibility.

These varied applications underscore the foundational role of dynamics in modern robotic control systems. By integrating dynamic principles into these applications, robots can operate more efficiently, safely, and precisely on a diverse range of tasks.

1.5 Expanded background and selection of inference methods

In this section, we explore the history of parameter identification for heavy-duty manipulators further and expand the discussion to incorporate additional conventional methods for parameter estimation. When estimating model parameters in the domain of dynamic parameter identification, techniques such as least squares or maximum likelihood estimation are frequently employed to acquire point estimates. Although these methods are widely employed, they frequently lack the capacity to completely capture the uncertainty surrounding the model parameters.

1.5.1 Various parameter identification methods in robotics research

Various parameter identification methods are utilized in robotics research to improve the understanding and control of robotic systems. These methods provide an extensive tool for researchers and engineers in the field. They range from classical approaches like least squares methods and extended Kalman filters to cutting-edge techniques involving deep learning. Each method has its strengths and limitations, making them suitable for different scenarios and system complexities. In addition to MCMC and SGHMC, a variety of other parameter identification methods exist within the realm of robotics research. Here, we enumerate some of the prominent parameter identification techniques used in robotics

research and then delve into the motivation behind our choice of MCMC.

1. **Least Squares Methods**:

    - Advantages: Simplicity, broad applicability, and computational efficiency.

    - Disadvantages: Can be ineffective for complex, nonlinear models; sensitive to outliers.

2. **Partial Least-Squares (PLS) Regression** (Llorens-Bonilla and Asada, 2014):

    - Advantages: Manages high-dimensional data, identifies latent variables, adapts to small sample sizes, and exhibits predictive utility.

    - Disadvantages: At risk of overfitting, sensitive to noisy data and outliers.

3. **Gradient-Based Optimization**:

    - Advantages: Systematic iterative optimization, appropriate for convex problems (e.g., Adam (Kingma and Ba, 2014), RMSProp (Ramadhan, Usman, and Pratiwi, 2021)).

    - Disadvantages: Requires good initialization, can get trapped in local minima.

4. **Extended Kalman Filter (EKF)** (Gautier and Poignet, 2001; Nguyen, Zhou, and Kang, 2015):

    - Advantages: Manages nonlinear models through linearization; robust state and parameter estimation.

    - Disadvantages: Sensitive to linearization errors, noise, and computationally intensive for complex models.

5. **Deep Learning Methods** (Shoujun et al., 2020):

    - Advantages: Can handle large datasets, model complex non-linearities, and capture intricate patterns.

    - Disadvantages: Requires significant data and computational resources; interpretability is challenging.

6. **Convolutional Neural Networks (CNNs)** (De León et al., 2022):

- Used for capturing environmental characteristics, anticipating robot state and dynamics through visual input, and improving the accuracy of robot dynamics models.

- Advantages: Reduced parameters, shift-invariant (Krizhevsky, Sutskever, and Hinton, 2012).

- Disadvantages: The computational complexity of the convolutional layers increases with the depth of the network and the size of the filters. It is not suitable for non-image data. The structure of CNN is mainly aimed at image data and needs to be improved for other types of data.

7. **Recurrent Neural Networks (RNNs)** (Mukhopadhyay et al., 2019):

   - Enhancing modeling and control of robot dynamics by distinguish temporal correlations in motion and dynamics, which is especially useful for processing sequential data such as time-series and sensor readings.

Deep learning techniques, despite their prowess in capturing complexities, treat robotic systems as black boxes. While this can produce well-trained networks, it falls short in providing results beyond the training data range. Moreover, pinpointing the specific parameter responsible for unexpected outcomes becomes challenging.

Bayesian methods, such as MCMC, provide a solution by generating posterior distributions of parameters, offering a more comprehensive view that includes optimal estimates and uncertainty indications. Traditional Bayesian methods come with the complexity of intricate integrals that are often infeasible to solve directly. MCMC provides a way of approximating these challenging integrals (Brooks et al., 2011), making Bayesian methods more practical and feasible, which is why we chose MCMC for our research.

1.5.2 Methods and justifications for parameter identification in MCMC and SGHMC

In robotics research, the selection of Markov chain Monte Carlo (MCMC) and Stochastic Gradient Hamiltonian Monte Carlo (SGHMC) for parameter identification in dynamic equations is supported by their special characteristics.

MCMC:

MCMC is an effective method that is ideally adapted to parameter estimation in situations involving complex, high-dimensional models and non-Gaussian probability distributions. Its greatest strength is its capacity to explore parameter spaces by

generating a Markov chain that converges to the posterior distribution. In the context of robotic systems, this convergence provides a robust estimation of parameter distributions and their corresponding uncertainties. Frequently, these systems display nonlinear behaviors and inherent uncertainties.

MCMC comprises two fundamental components: a Markov chain for sampling from arbitrary probability distributions and a Monte Carlo element for addressing complex integral problems. The Metropolis-Hastings (MH) algorithm, one of the foundational MCMC techniques, has gained widespread popularity in various fields due to its simplicity and its ability to sample intricate target distributions (Sarkis and Dhavale, 2015; Thrane and Talbot, 2019; Rens van de Schoot, 2017).

Furthermore, advancements in MCMC methodology have led to the emergence of the Hamiltonian Monte Carlo (HMC) algorithm, which is renowned for its enhanced sampling efficiency. Recent innovations and modifications in the field of computational statistics have given rise to derivative algorithms (Radivojevi and Akhmatskaya, 2019) rooted in the principles of HMC.

Bayesian methods offer several advantages in robotics research when integrated into MCMC:

1. **Uncertainty quantification**: Bayesian methods within MCMC provide posterior probability distributions, encompassing not only point estimates of parameters, but also uncertainty indications. This is crucial in robotics, where uncertainty is prevalent due to sensor noise, environmental variations, and model simplifications.

2. **Robustness**: MCMC, with Bayesian principles, exhibits robustness to outliers and noisy data. It can effectively handle situations where traditional optimization methods might get stuck or provide suboptimal solutions.

3. **Incorporating prior knowledge**: Bayesian approaches allow the incorporation of prior knowledge or beliefs about parameters. This is especially valuable when dealing with limited data, as it provides a way to leverage existing information.

4. **Sampling complex distributions**: MCMC techniques, in particular, excel at sampling complex, high-dimensional parameter spaces. They can explore the posterior distribution effectively, even when it is multimodal or has intricate shapes.

MCMC has clear advantages over other parameter identification approaches, especially for complicated robotics research:

1. Nonlinear dynamics and high-dimensional state spaces are common in robotic

systems. MCMC can solve nonlinear and high-dimensional problems because it explores the entire parameter space, unlike other optimization approaches that tend to find local optimal solutions.

2. Uncertainty and noise: Sensor noise and environmental influences affect robotic systems. MCMC approaches provide a posterior probability distribution for parameters, allowing researchers to estimate their uncertainties and point estimates, improving noise and uncertainty adaptation.

SGHMC:

This is an algorithm that combines the strengths of both MCMC and stochastic gradient descent. It excels in scenarios involving extensive data sets or complex models. SGHMC leverages minibatch gradient information for efficient parameter updates. This makes it particularly valuable in the realm of robotic dynamics, where real-time processing may be imperative, and where high-dimensional and nonconvex parameter spaces are common.

Both MCMC and SGHMC share the feature of providing parameter distribution estimates. This characteristic is important in the context of robotics, where dynamics can be influenced by a wide range of parameters and uncertainties. A probabilistic perspective on parameter estimation, offered by these methods, is indispensable for ensuring robust control and accurate predictions in the dynamic and ever-evolving field of robotics.

Compared with other methods, SGHMC has clear advantages when dealing with some specific challenges of robotics research:

1. Big data and real-time processing: In modern robot applications, it is often necessary to process large amounts of data and perform real-time decision-making and control. SGHMC makes it well-suited for such applications by exploiting mini-batch gradient information for efficient parameter updates.

2. High-dimensional parameter spaces: Robot dynamics often involves high-dimensional spaces. SGHMC is able to efficiently explore such parameter spaces, providing accurate estimates of parameter distributions.

The following is an overview of the advantages of SGHMC compared to the methods listed above.

1. SGHMC offers probabilistic insight into parameter uncertainty, showing improved resilience to overfitting compared to PLS and enhancing adaptability to noisy data. 2. It provides a comprehensive view of parameter distributions, rather than just singular optimal values. 3. Unlike EKF, it is not heavily dependent on linearization, thus reducing

model approximation errors. 4. Compared to deep learning models, SGHMC offers a clearer quantification of uncertainty, bolstering generalization in various scenarios. It also explicitly addresses uncertainties in sequential data, providing profound probabilistic insights into time series. 5. By quickly handling large data sets with stochastic gradients, SGHMC is more efficient than MCMC. Its use of minibatch gradients helps it to converge faster in high-dimensional spaces and reduces the autocorrelation problems that can occur with MCMC. This makes it a good choice for dynamic robotics applications.

1.6 Research methods

This section aimed to comprehensively compare methods for parameter identification and dynamic analysis. Real-world data from robotic arms was collected in various scenarios. A core part of our approach was crafting a dynamic model for robotic motion control. Created using analysis and simulation, the model was validated with real data and compared to existing ones.

Though ROS-MATLAB integration was not pursued, we used tools like sensors to gather data from various robotic joints. Crucial parameters for the manipulators were identified through data collection and sensors. Statistical analysis refined the models by deducing unknown parameters.

In general, these methods improve the understanding of the manipulator and the identification of parameters. The goal is to develop precise dynamic models and improve control. While a full digital twin was not made, the focus on dynamic parameter identification is key for future development.

In accordance with these main goals, the following discussion analyzes the steps that were taken to develop a robust framework for dynamic modeling and parameter identification. This comprehensive strategy not only improves our knowledge of robotic systems, but also provides foundations for future advancements in control methods.

1.6.1 Suggested approach for constructing models.

In this section, we outline a comprehensive strategy for building models and obtaining parameters from real-world data in Figure 1.10. Multiple stages contribute to the successful development of a dynamic model and subsequent parameter identification in this procedure. The overall goal is to accurately capture the complex behavior of nonlinear dynamics.

Step 1: Construct the kinematic structure.

We begin the modeling procedure by constructing a kinematic structure with Denavit–Hartenberg parameters. This foundational stage enables the representation of

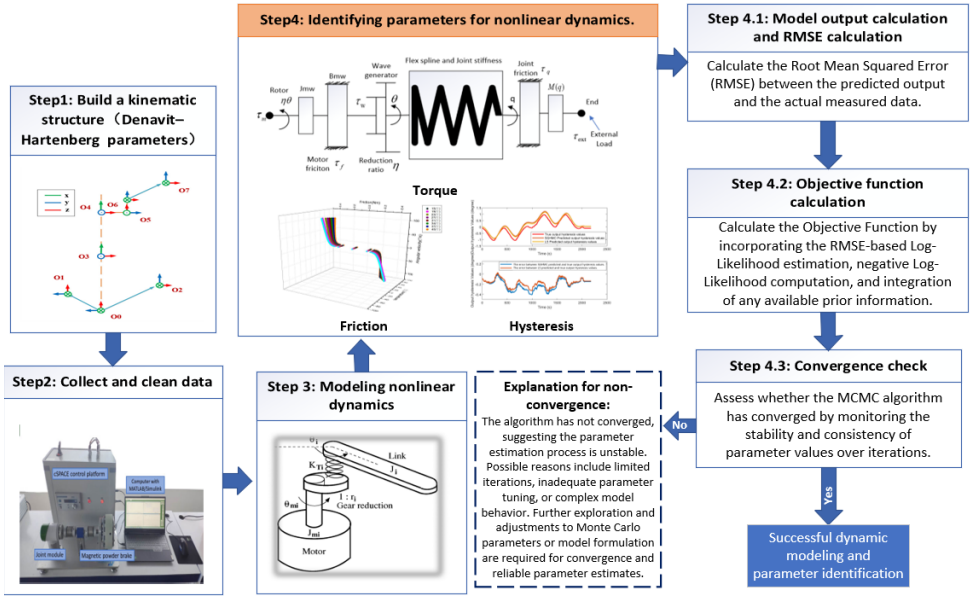

Figure 1.10: Suggested approach for constructing models using collecte real data.

complex system dynamics by establishing the framework for subsequent analysis.

Step 2: Data cleansing and collection.

To guarantee the accuracy of our model, we meticulously collect and preprocess data from the actual world. Thorough data cleaning improves the precision and quality of subsequent analysis.

Step 3: Model non-linear dynamics.

Using the cleansed data, we construct a model capable of faithfully representing the complex behavior of non-linear dynamics. This model is essential for subsequent parameter identification.

Step 4: Identification of nonlinear dynamics parameters

In this important stage, we refine the accuracy and efficacy of our model by identifying the model parameters.

Step 4.1: Model output calculation and RMSE calculation.

We begin by calculating the predicted model output and evaluating its precision by

calculating the root mean square error (RMSE). This metric measures the deviation between the predictions of our model and the actual measured data.

Step 4.2: Calculation of the objective function.

To refine our parameter estimates, the Objective Function is computed. This function includes the estimation of the log likelihood based on RMSE, the negative log-likelihood computation, and the assimilation of any available prior information. The Objective Function is an important criterion for refining our parameter estimations.

Step 4.3: Check for convergence.

To ensure the consistency and dependability of our parameter estimates, we performed a convergence test. By monitoring the consistency and coherence of parameter values across iterations, the convergence of the algorithm is determined. If non-convergence is detected, we investigate potential causes and recommend additional parameter estimation adjustments.

In the case of convergence, our efforts culminate in the accomplishment of dynamic modeling and parameter identification. This success represents the accomplishment of stable parameter values through the iterative process, allowing us to accurately predict and comprehend the underlying nonlinear dynamics.

In conclusion, our proposed method consists of a thorough collection of steps that take us from the establishment of a kinematic structure to the successful identification of complex nonlinear dynamics parameters. This method not only improves our understanding of real-world systems but also provides the basis for accurate model prediction.

1.7 Scientific contribution

This study constitutes a scientific contribution by conducting a comprehensive analysis of inference methods for lightweight and heavy-duty robotic manipulators. Focusing on lightweight arms with harmonic drives, heavy-duty arms with planetary gear systems, and the distinctive challenges posed by the CMOR robot arm of the CFETR superconducting Tokamak fusion device, this study embarks on a comparative analysis. Various inference methods tailored to each gear system are explored and juxtaposed, augmented by the incorporation of the Monte Carlo algorithm. The purpose of the study is to refine and enhance the use of these techniques to precisely determine the parameters of the manipulator. Research aims to enable the development of improved robotic manipulator systems that excel in handling complex tasks with precision, efficiency, and safety in diverse industrial settings.

1.7.1 Comparative study of advanced parameter identification and dynamic analysis

The Figure 1.11 represents three of the most significant technical challenges in the paper and their innovative solutions. In a lightweight manipulator, overcoming friction and hysteresis is the first obstacle. To solve this problem, the GMS model is used to describe the frictional characteristics of the harmonically driven joint, while the FOBW model is utilized to characterize the influence of the hysteresis effect. The second challenge is that the heavy-duty arm has a similar issue.

The third challenge is how to efficiently estimate model parameters and account for uncertainty. The optimal estimate and the uncertainty indication are obtained by adopting the SGHMC method for parameter identification and the Bayesian method for obtaining the posterior distribution. Together, these two creative ideas resolve essential technical issues in heavy-duty manipulators and offer a new method for precise control and optimization in industrial applications.

Designed to address the specific requirements of the CFETR remote handling system and to consider the limitations of current robotic arms, the study is dedicated to overcoming technical challenges in the following domains.

1. Addressing the challenge of accurately identifying and comprehensively characterizing friction within harmonic drive joints of robotic systems. Due to friction, the performance of these joints, which are common in robotics because of their precision and compactness, is impaired. Conventional techniques for friction identification encounter difficulties in comprehensively capturing friction behavior in harmonic drives, particularly when considering factors such as temperature.

The proposed solution involves the application of the MCMC method in conjunction with the generalized Maxwell-Slip (GMS) model. MCMC is a powerful statistical technique that excels in parameter estimation and uncertainty quantification. By combining it with the GMS model, which is adept at capturing the nonlinear and time-dependent characteristics of harmonic drive friction, the authors offer a robust framework for accurate friction identification.

Moreover, the article tackles the challenge of the influence of temperature on friction behavior by incorporating temperature as a variable in the model. This is crucial because temperature fluctuations can significantly alter the friction dynamics within robotic joints. The use of temperature as a factor in the friction identification process improves the accuracy and applicability of the model, allowing a more realistic representation of friction under varying conditions.

By integrating MCMC, the GMS model, and the consideration of temperature, this

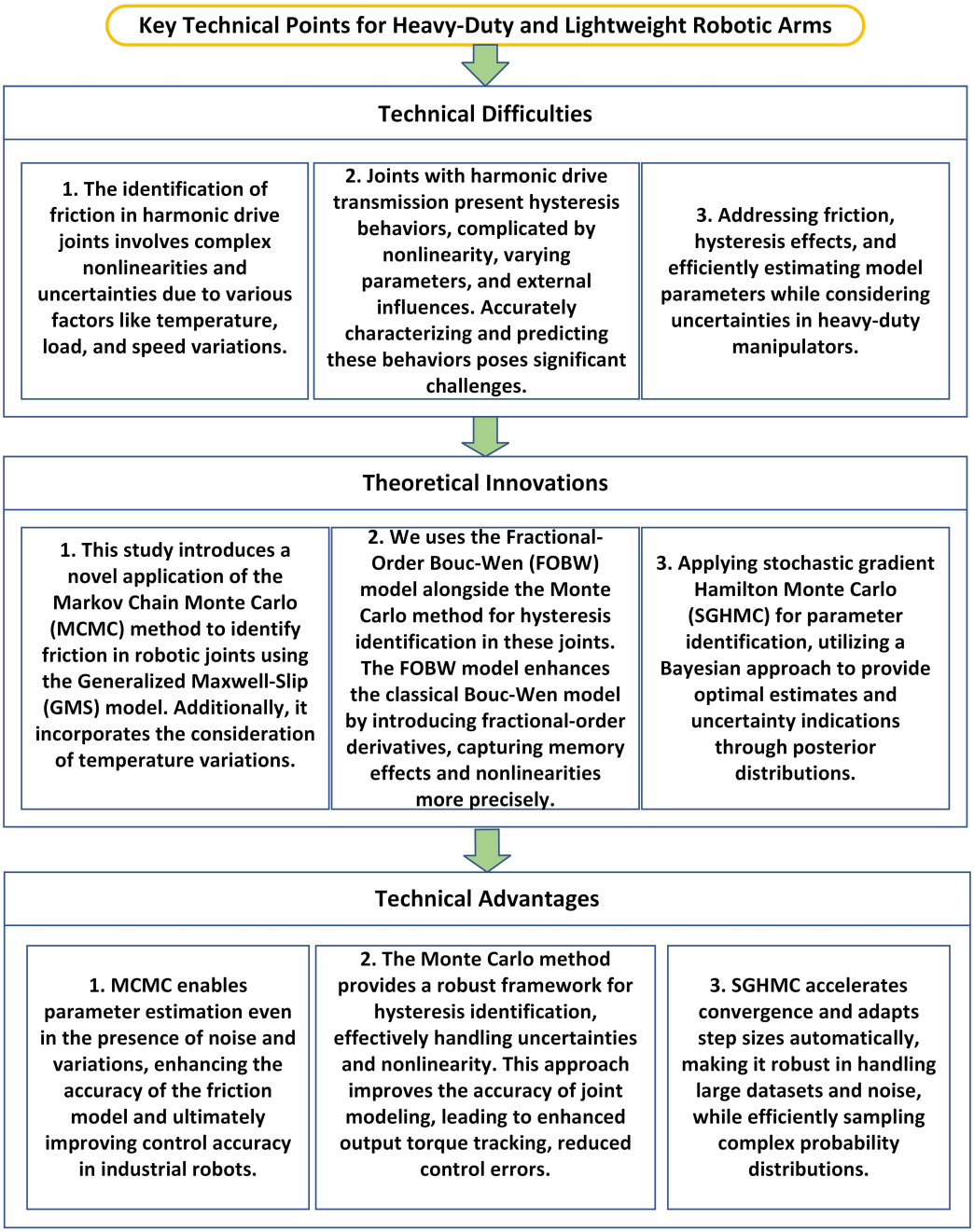

Figure 1.11: Crafting a path forward: technological development roadmap.

article offers a comprehensive solution to the intricate problem of friction identification in harmonic drive joints. This approach not only provides accurate characterization of friction but also contributes to the broader field of robotics by enabling more precise control and better performance of robotic manipulators in various industrial applications.

2. Addressing the challenge involves tackling the accurate identification of hysteresis behavior within robotic joints utilizing harmonic drive transmission. The intricate and complex nature of hysteresis, a non-linear phenomenon characterized by history-dependent effects, poses a primary technical obstacle. In the realm of robotic systems, precise modeling and prediction of hysteresis play a pivotal role in achieving precise control and optimizing overall performance.

The solution to this challenge is introducing the application of the Fractional Order Bouc-Wen (FOBW) model in conjunction with the Monte Carlo method. The FOBW model extends the classical Bouc-Wen model by incorporating fractional-order derivatives, effectively capturing memory effects, and enhancing the model's ability to accurately depict nonlinear behaviors. The Monte Carlo method, a powerful probabilistic technique, is used for parameter identification. It overcomes the limitations of deterministic approaches by taking into account uncertainties and variations inherent in hysteresis behavior.

The synergy of the FOBW model and the Monte Carlo method addresses the technical difficulty through a two-fold approach. First, the capacity of the FOBW model to accurately represent complex hysteresis behavior provides a theoretical foundation. Second, the probabilistic sampling of the Monte Carlo method enables robust parameter estimation even in the presence of uncertainties and variations.

3. Addressing the technical difficulty of accurately identifying parameters for heavy-duty manipulators, particularly focusing on the disruptive influences of friction and hysteresis on torque transmission efficiency. Friction and hysteresis are challenging to quantify due to their non-linear and complex nature, especially in the context of heavy-duty manipulators equipped with differential planetary gears. These effects not only hinder the overall performance of these manipulators, but also complicate their control strategies and dynamic analysis.

The solution introduced in this article involves the innovative utilization of the Stochastic Gradient Hamilton Monte Carlo (SGHMC) method. This Bayesian approach revolutionizes parameter identification by offering posterior distributions of model parameters, allowing a more comprehensive understanding of uncertainties associated with friction and hysteresis effects. The strengths of the SGHMC method, including accelerated convergence, automatic step size adaptation, and scalability, effectively address the challenges posed by the intricate dynamics of heavy-duty manipulators.

Using SGHMC, this study bridges a critical knowledge gap by quantitatively characterizing friction and hysteresis effects, providing accurate parameter estimates, and enhancing the dynamic analysis of heavy-duty manipulators. Consequently, this research contributes to the optimization of control strategies and the overall operational efficiency of these complex robotic systems.

1.7.2 Expectations of control strategy optimization in the digital twin framework

The digital twin framework faces a central challenge: capturing the dynamics of the mechanical system with precision. For precise control of systems such as robotic arms, relying solely on sensors is expensive, while complex control methods require extensive tuning, which poses the risk of decreasing precision. Dynamic equations, which are fundamental to comprehending system behavior, enable informed control strategy design decisions.

Dynamic equations in the digital twin framework expedite the creation of precise control strategies aligned with the system's structure. This improves controller performance, stability, and adaptability. Here is how dynamic equations aid control strategy development:

Model Predictive Control (MPC): MPC uses dynamic equations for simulation predictions, optimizing control inputs to minimize prediction errors (Qahmash et al., 2023). This suits complex control problems considering system dynamics and constraints.

Feedforward Compensation: By identifying key terms in the dynamic equations that affect the response of the system, a feedforward control strategy can anticipate and counteract disturbances, potentially reducing the reliance on feedback tuning (Ema et al., 2021; Chia-Pei et al., 2020).

Control Mode Switching: Dynamic equations guide the strategy to switch between different modes, such as position, velocity, or force control, depending on the dynamics and the state of the system (Zhang, 2013).

In summary, dynamic equations offer detailed insight into the behavior of the system, which guides informed controller design decisions. We select strategies, optimize parameters, and ensure controllers meet performance goals in practical applications.

1.8 Dissertation outline

Chapter 2 of the dissertation provides a comprehensive overview of the parameter identification method in robotic manipulators.

Chapter 3 presents an in-depth analysis of the inference methods used for parameter identification in lightweight arms, including the incorporation of harmonic gear reducers.

Chapter 4 focuses on the CMOR robot arm of the CFETR. It addresses the unique challenges associated with this robotic arm and investigates analytical methods for its parameter identification. Furthermore, it includes an in-depth discussion on experimental methods for the CMOR robot arm, concluding with a comparative analysis.

Chapter 5 concludes the most important results from the comparisons conducted in the earlier sections, with a discussion on the proposed strategies to advance robotic manipulators in industrial applications, providing information on future directions.

2 Bayesian inference for parameter identification

2.1 Introducing the Markov chain Monte Carlo (MCMC) method

Bayesian inference provides a statistical methodology that incorporates prior knowledge and updates it based on observed data. The MCMC methods are instrumental tools for Bayesian inference, allowing sampling from the posterior distribution of parameters. When such methods are employed, it becomes feasible to obtain a probabilistic assessment of parameter values while considering both prior information and observed data.

Nonlinear models with Gaussian noise can be formulated as $Y = f(X,\theta) + \varepsilon$ where X denotes the input and Y represents a measurement of the output. Parameters, denoted by θ, are unknown. Using Bayesian methodology, one incorporates both a likelihood function $\ell(y \mid \theta, \mathscr{M})$ and a prior probability density function $g(\theta \mid M)$ to examine the distributions of unknown parameters. The model, denoted by $\mathscr{M}$, describes the underlying relationships between the data variables.In this context, $\mathscr{M}$ would define how the input X and the parameters θ relate to the output Y in the presence of Gaussian noise ε.

Given a specific parameter value θ, $\ell(y \mid \theta, M)$ offers a probability distribution of the observed value Y, denoted as $P(\theta \mid y)$, which is the posterior distribution. The Bayes formula is outlined as (Llorente et al., 2020):

$$P(\theta \mid y, M) = \frac{\ell(y \mid \theta, M) g(\theta \mid M)}{p(y \mid M)} \tag{2.1}$$

$$Z = p(y \mid M) = \int_{\theta} \ell(y \mid \theta, M) g(\theta \mid M) d\theta \tag{2.2}$$

Here, Z is recognized as evidence (Friel and Wyse, 2012). When assuming that the likelihood follows a Gaussian distribution, the function of this probabilistic relationship can be expressed as detailed in Equation (2.3).

$$\ell(y \mid \theta, M) = \prod_{i=1}^{n} \ell(y_i \mid \theta, M) = \frac{1}{(\sqrt{2\pi}\sigma)^n} \exp\left\{ -\frac{1}{2\sigma^2} SS_{\theta} \right\} \tag{2.3}$$

where

$$SS_{\theta} = \sum_{i=1}^{n} (y_i - f(x_i, \theta))^2 \tag{2.4}$$

The complexity in utilizing the Bayesian approach lies in computing the normalizing constants or the ratios of these constants (Liang, Liu, and Carroll, 2010). However, the MCMC method offers a solution to this computational challenge. This method uses a Markov chain to obtain samples that resemble a distribution of P, followed by a Monte Carlo analysis (Martino, 2018).

The main steps for employing the MCMC method in Bayesian inference are:

1. Define the prior distributions: Based on prior knowledge or hypotheses, specify the prior distributions for the model parameters. These distributions represent the hypotheses regarding parameter values prior to data collection.

2. Define the likelihood function: the likelihood function is formulated to assess the agreement between the observed data and the model predictions, indicating the probability of encountering the observed data with the given model parameters.

3. Calculate the posterior distribution: using the observed data and Bayes' theorem, calculate the posterior distribution of the model parameters. Prior information and the likelihood function are combined to form the posterior distribution.

4. Initialize the Markov chain by assigning an initial value to each model parameter. This initial value may be chosen at random or according to prior knowledge.

5. Sample generation: the MCMC algorithm is employed to generate samples from the parameter space. Starting with the initial parameter values, new samples are generated by proposing updated parameter values based on the current parameter values and a proposal distribution.

6. Acceptance evaluation: the acceptability of each proposed sample is evaluated using the acceptance criteria of the MCMC algorithm. Acceptance criteria determine whether a proposed sample should be accepted or rejected on the basis of the posterior distribution.

7. Parameter update: the parameter values are updated based on whether the proposed samples were accepted or rejected. Accepted samples contribute to the estimation of the posterior distribution, while rejected samples are discarded.

8. Repeat steps: the process of sample generation, acceptance evaluation, and parameter update is repeated iteratively until a sufficient number of samples are collected and the Markov chain has converged.

9. Convergence assessment: the convergence of the Markov chain is evaluated to ensure that the collected samples are representative of the true posterior

distribution. Various convergence diagnostics, such as trace plots, autocorrelation plots, and Gelman-Rubin statistics, can be utilized.

10. Parameter estimation: Based on the collected samples, the model's parameters are estimated. Statistical measures such as the mean, median, or mode of the posterior distribution are used to calculate parameter estimates.

11. Sensitivity analysis: A sensitivity analysis is performed to determine the impact of changes in antecedent distributions or observed data on the parameter estimates, providing insights into the robustness of the estimated results.

12. Validation and interpretation of results: the estimated parameters are validated by comparing the predictions of the model with the observed data. The results are interpreted in the context of the specific problem, drawing conclusions about the significance and impact of the identified parameters on the system.

In the Metropolis-Hastings phase, particularly during the acceptance evaluation, the algorithm ensures that the generated samples align closely with the true posterior distribution of the parameters.

The pseudo-code of the MH algorithm is as follows.

In conclusion, the Bayesian inference method based on MCMC is an effective instrument for the identification of friction and hysteresis in harmonic drive joints. By utilizing a Markov chain process to explore the parameter space, this method permits accurate estimation of the model parameters, resulting in enhanced modeling and control of harmonic drive systems.

2.2 Introducing the Stochastic Gradient Hamiltonian Monte Carlo (SGHMC) method

Building on the foundational concepts of Hamiltonian Monte Carlo (HMC) in (**paper11**), the SGHMC algorithm emerges as a pivotal advancement, mainly marked by the incorporation of stochastic gradients. Such an inclusion is instrumental in optimizing sampling capabilities, particularly in expansive, high-dimensional parameter spaces, typically found in extensive datasets and intricate models (Neal, 2012).

Unlike its predecessor, the traditional HMC, which operates primarily within the bounds of the Metropolis-Hasting mechanism, SGHMC takes a different trajectory.It aims to use Hamiltonian dynamics, which are carried out by specific partial differential equations, to make changes in the initial state. Such an approach results in augmented acceptance probabilities, propelling a faster convergence rate. Equations (2.5) and (2.6) show the

Algorithm 1 The method of sampling used by the Metropolitan Hastings (MH) algorithm

Input: Proposed distribution $q(x \mid x')$, Sampling interval M, sample set $\mathscr{V} = \varnothing$.
Output: Sample set $\mathscr{V}$
Initialization: Random initialization $x_0, t = 0$;
repeat
    Randomly generate a sample $\hat{x}$, according to $q(x \mid x')$;
    Calculate acceptance probability $A(\hat{x}, x_t)$;
    Randomly generate z from the uniform distribution of (0, 1)
    if $z \leq A(\hat{x}, x_t)$ **then**
        $x_{t+1} = \hat{x}$;
    else
        $x_{t+1} = x_t$;
    end if
    $t++$;
    while Steady state not reached **do**
        if $t \mod M = 0$ **then**
            $\mathscr{V} = \mathscr{V} \cup \{x_t\}$
        end if
    end while
until Obtain N samples ($|\mathscr{V}| = N$);
End

Hamiltonian system:

$$H(q,p) = U(q) + K(p) \tag{2.5}$$

$$\frac{\partial q_i}{\partial t} = \frac{\partial H}{\partial p_i} = \frac{\partial K(p)}{\partial p_i}, \frac{\partial p_i}{\partial t} = \frac{\partial H}{\partial q_i} = -\frac{\partial U(q)}{\partial q_i} \tag{2.6}$$

In the HMC model, every state has a representation in two dimensions, where Q and P represent position and momentum, respectively. The fact that SGHMC is good at reducing problems caused by random-walk behavior and the relatively low rejection rates of MH can be acknowledged to a few important items: (a) The conservation law of energy of Hamiltonian holds because Hamiltonian dynamics are always the same. This can be formally expressed as $-\mathrm{H}(\mathrm{Q}*, \mathrm{P}*) + \mathrm{H}(\mathrm{Q}, \mathrm{P}) = 0$. The rejection rate of HMC is, on average, significantly lower than that of many other competing algorithms. (b) The existence of the momentum, P, serves as a regulator of the motion speed in any given state. With each iterative cycle, P undergoes recalibration.

Taking into account the SGHMC methodology, it is imperative to understand the parameters θ and τ^2. In our equation in (Qi, Huapeng, Yuntao, et al., 2023):

$$\begin{aligned} & p\left(\theta, \tau^2 \mid \mathbf{y}\right) \propto p\left(\mathbf{y} \mid \mathbf{X}, \theta, \tau^2\right) p(\theta) p\left(\tau^2\right) \\ & \propto \prod_{i=1}^{N} \mathcal{N}\left(y_i \mid \mathbf{x}_i^T \theta, \tau^2\right) \prod_{j=1}^{5} \mathcal{N}(\theta \mid 0,1) \cdot \text{ Inv-Gamma } \left(\tau^2 \mid 2,2\right) \end{aligned} \tag{2.7}$$

The parameter θ represents a vector of model parameters that interact with predictor variables X to estimate the response $\mathbf{y}$.

$\prod_{i=1}^{N} \mathcal{N}\left(y_i \mid \mathbf{x}_i^T \theta, \tau^2\right)$ represents the likelihood of observing the data $\mathbf{y}$ given the input X, the parameter vector θ, and the variance τ^2.

$\prod_{j=1}^{5} \mathcal{N}(\theta \mid 0,1)$ specifies a prior belief in the parameters θ before any data is observed. It suggests that each parameter in θ is drawn from a standard normal distribution (mean of 0 and variance of 1). The product implies that this prior is applied independently for 5 parameters (hence the range from 1 to 5).

Inv-Gamma $\left(\tau^2 \mid 2,2\right)$ represents the prior distribution of the variance τ^2. The inverse gamma distribution is a common choice for a prior on the variance of a normal distribution in Bayesian analysis. Here, the shape and scale parameters of the inverse gamma distribution are set to 2.

On the other hand, τ^2 means the variance of the errors, which captures the discrepancies between the model predictions and the actual values. Given the equation that describes the posterior distribution of θ and τ^2, we will now outline the procedure of the SGHMC algorithm, specifically tailored for parameter identification, while taking into account the previous distributions for θ and τ^2.

The following is the flow of the algorithm to use SGHMC for parameter identification, considering the prior distributions for θ and τ^2.

1. Initialize parameters: Set initial values for the model parameters θ and τ^2 to start the SGHMC algorithm.

2. Precompute noise: Precompute the stochastic noise for the gradient estimates. This noise term is introduced to make the algorithm robust to noise and sampling errors.

3. Initialize momentum: Set the initial momentum r for each parameter. The momentum is introduced to improve the exploration of the parameter space during the sampling process.

4. Initialize prior distributions: Specify the prior distributions for the model parameters θ and τ^2. Assume a normal distribution for θ and an inverse gamma distribution for τ^2.

5. Iterate over the MCMC Steps: a. Compute stochastic gradients: Compute the stochastic gradients of the log-posterior with respect to the model parameters using mini-batches of data. This step allows the algorithm to handle large datasets efficiently. b. Update momentum: Update the momentum r of each parameter based on the computed stochastic gradients and the precomputed noise term. c. Update parameters: Update the model parameters θ and τ^2 using the calculated momentum and the pre-computed noise term. This step incorporates momentum and noise to explore the parameter space more effectively.

6. Sample from prior distributions: At the beginning of each iteration, sample new values for θ and τ^2 from their respective prior distributions.

7. Accept or reject step: Evaluate the acceptability of the proposed parameter updates using the Metropolis-Hastings acceptance criteria, considering the prior distributions. Decide whether to accept or reject the proposed updates based on the posterior distribution and Hamiltonian dynamics.

8. Repeat steps 5 through 7: Repeatedly perform parameter updates, prior sampling, and accept/reject steps for a fixed number of iterations to collect samples from the posterior distribution.

9. Evaluate the convergence: Assess the convergence of the Markov chain to ensure that the samples obtained are representative of the true posterior distribution.

10. Estimate parameters: Based on the samples collected, estimate the model parameters θ and τ^2 using statistical measures such as the mean or median of the posterior distribution.

The pseudocode of the SGHMC algorithm with prior distributions:

Algorithm 2 SGHMC Algorithm with Prior Distributions

1: **Initialize model parameters** θ, τ^2, momentum r, learning rate η, and pre-computed noise B
2: **Initialize** prior distributions for θ: $\theta \sim \mathcal{N}(\mu_\theta, \sigma_\theta^2)$ and $\tau^2 \sim$ Inv-Gamma$(\alpha_\tau, \beta_\tau)$
3: **while** not converged **do**
4: **Sample mini-batch** of data D_b
5: **Sample new values** for θ from $\mathcal{N}(\mu\theta, \sigma_\theta^2)$ and τ^2 from Inv-Gamma$(\alpha_\tau, \beta_\tau)$
6: **Compute stochastic gradients**: $\nabla_\theta \log p(\theta|D_b)$
7: **Update momentum**: $r \leftarrow r - \frac{\eta}{2}\nabla\theta \log p(\theta|D_b) - \eta Br + \sqrt{2\eta}\varepsilon$
8: **Update parameters**: $\theta \leftarrow \theta + \eta r$
9: **Evaluate acceptance**: Based on the Metropolis-Hastings acceptance criteria and prior distributions
10: **end while**
11: **End Estimate model parameters** θ and τ^2 using collected samples.

2.3 Evaluation criteria for inference methods

In this section, we perform a comparative analysis of the inference methods discussed above for parameter identification in lightweight arms with harmonic gear reducers. We define evaluation criteria to assess the performance of these methods and provide a comprehensive discussion of the results and findings obtained from applying these methods to real-world data.

Selection of evaluation criteria:

Both R^2 (R square) and RMSE (Root Mean Square Error) are widely utilized as evaluation metrics because they intuitively reflect the degree of correlation between model predictions and experimental data.

R^2 offers a statistical measure of the goodness of fit, while RMSE provides a quantification of the prediction error.

Although there are other potential evaluation criteria, such as mean absolute error (MAE) or mean absolute percentage error (MAPE). MAPE expresses the prediction error as a percentage, which can be useful when you want to understand the relative error rather than the absolute magnitude of the error. However, it should be used with caution, especially when the actual values are close to zero, as it can lead to very high or undefined percentage errors. In this context R^2 and RMSE are perhaps considered the most informative. R^2 gives a relative measure of fit, while RMSE provides an absolute measure of fit. Their combination can offer a comprehensive view of model performance.

Evaluation criteria for inference methods for ligthweight robot

We evaluate inference methods based on criteria such as accuracy, computational efficiency, noise resistance, and the ability to handle nonlinearities of harmonic gear reducers. These methods help identify the strengths and weaknesses of each method.

In the comparative analysis of inference methods for parameter identification in lightweight arms with harmonic gear reducers, it is essential to establish evaluation criteria to assess the performance of these methods. Two widely used criteria are fitness (R^2) and root mean squared error (RMSE).

Fitness, also known as the coefficient of determination or R^2, is a statistical measure that indicates how well the model predictions fit the experimental data. It quantifies the proportion of the total variation in the data that is explained by the model. A higher R^2 value indicates a better fit of the model to the data.

The value of R^2 is defined as follows:

$$R^2 = 1 - \frac{\sum_{i=1}^{n} (y_i - \hat{y}_i)^2}{\sum_{i=1}^{n} (y_i - \bar{y})^2} \tag{2.8}$$

where n is the number of data points. y_i is the experimental data observed. $\hat{y}_i$ is the corresponding prediction of the model and $\bar{y}$ is the mean of the observed data. An R^2 value close to 1 indicates that the model's predictions closely match the experimental data, whereas a value closer to 0 suggests poor model performance.

The root mean square error (RMSE) is another commonly used metric to evaluate the accuracy of model predictions. It calculates the average magnitude of the differences between the prediction of the model and the observed data.

The RMSE is defined as follows:

$$RMSE = \sqrt{\frac{1}{n} \sum_{i=1}^{n} (y_i - \hat{y}_i)^2} \tag{2.9}$$

where n is the number of data points, y_i is the experimental data observed, and $\hat{y}_i$ is the corresponding prediction of the model. A lower RMSE value indicates better agreement between the model and the data.

Using R^2 and RMSE as evaluation criteria, we can quantitatively compare the performance of different inference methods to accurately estimate friction and hysteresis

parameters for lightweight arms with harmonic gear reducers. These criteria provide valuable insight into the strengths and limitations of each method and help in selecting the most suitable approach for specific applications.

Evaluation criteria for inference methods for the CMOR robot arm

For parameter identification in the CMOR system, the three main criteria are fitness ((R^2), RMSE, and computational efficiency. A higher R^2 suggests a better fit to the model, a lower RMSE denotes greater precision, and computational efficiency measures the speed and effectiveness of the method. These criteria guide researchers in selecting the best inference method for parameter estimation in lightweight arms with harmonic gear reducers.

In addition to these three evaluation criteria, comparing MCMC and stochastic gradient Hamilton Monte Carlo (SGHMC) for the identification of the heavy duty manipulator parameters in (Qi, Huapeng, Yuntao, et al., 2023) required evaluating both the convergence speed and the computational time.

The autocorrelation time measures how many iterations MCMC or SGHMC needs for the samples to be nearly independent. Shorter autocorrelation times mean faster convergence and efficiency. SGHMC outperformed MCMC in this aspect, suggesting that it converges faster and samples more efficiently.

The Gelman-Rubin convergence statistic (Rhat) is an additional important metric for assessing convergence in the MCMC and SGHMC methods. Rhat compares the variability within and between multiple chains to determine whether convergence has occurred. A value of Rhat near 1 signifies convergence, while values significantly greater than 1 indicate that additional iterations are required. In this study, the Rhat values for the SGHMC algorithm were closer to 1 than for MCMC, indicating that SGHMC estimated the model parameters with greater convergence and stability.

In terms of computational speed and efficacy, the SGHMC algorithm outperformed MCMC. The implementation of the SGHMC method benefited from the use of stochastic gradients, which made it more computationally efficient than the traditional MCMC approach, which requires calculating gradients across the entire dataset at each iteration. The reduced computational burden of SGHMC enables faster parameter estimation and reduces the time required to obtain accurate results.

In the next section, we will explore experimental methods for parameter identification, which supplement analytical approaches by providing real-world data for validation and estimation.

3 Inference methods for the identification of parameters in lightweight arms with harmonic gear reducers

3.1 Parameter identification in lightweight arms with harmonic gear reducers

In this chapter, we focus on the problem of parameter identification in lightweight arms equipped with harmonic gear reducers. Lightweight arms are widely used in various robotic applications due to their high payload-to-weight ratio and flexibility. However, accurate parameter identification is crucial to ensure safe and efficient operation of these arms. Harmonic gear reducers, which are commonly used in lightweight arms, introduce nonlinearities and uncertainties that further complicate the parameter identification process. In this section, we provide an overview of lightweight arms with harmonic gear reducers and discuss the challenges associated with parameter identification in these systems.

3.1.1 Overview of lightweight arms with harmonic gear reducers

Lightweight arms are robotic manipulators designed to be low in weight while maintaining high strength and dexterity. These arms are typically constructed using lightweight materials such as aluminum or carbon fiber composites. Harmonic gear reducers, also known as strain wave gears, are often employed in lightweight arms to achieve high torque density and compactness. Figure 3.1 presents an illustration of a

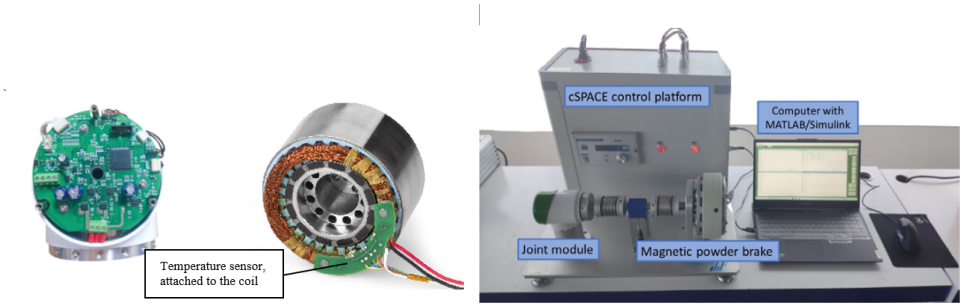

(a) Install the temperature sensor directly onto both the stator coil and the motor driver.

(b) Data acquisition interface, and experimental equipment.

Figure 3.1: (a)The temperature sensor and (b) Lightweight arm with harmonic gear reducers.

lightweight arm with a harmonic gear reducer. The harmonic gear reducer provides torque amplification and speed reduction while maintaining a compact design. The temperature sensor is mounted directly on both the stator coil and the motor driver. Within harmonic gear reducers, three key components are integrated: a wave generator, a

flex spline, and a circular spline. The flex spline is deformed by a wave motion produced by the wave generator, which causes it to mesh with the circular spline. This interaction results in a speed reduction and an amplification of the torque. However, the non-linear and complex nature of the harmonic gear mechanism poses challenges for parameter identification.

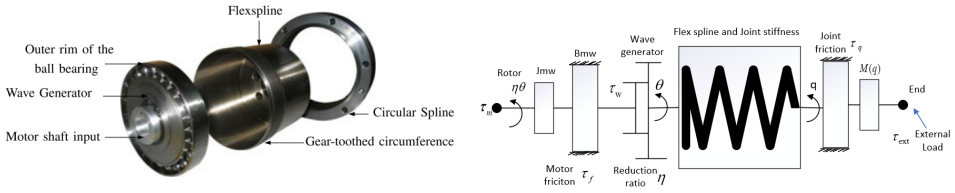

(a) Components of a harmonic gear reducer. (b) Schematic diagram of flexible joint (Dhaouadi, 2003).

Figure 3.2: (a)The temperature sensor and (b) Schematic diagram of flexible joint: lightweight arm with harmonic reducers.

In Figure 3.2a the components of a harmonic gear reducer are shown. The wave generator (top), the flex spline (middle), and the circular spline (bottom) work together to achieve torque amplification and speed reduction.

The parameter identification process for lightweight arms with harmonic gear reducers involves estimating various parameters such as arm mass, link length, joint stiffness, and friction coefficients. These parameters directly affect the arm's dynamics and performance. However, due to the nonlinearities introduced by harmonic gear reducers, traditional parameter identification techniques may not be directly applicable. For the specific parameters in the picture, refer to (Qi, Huapeng, Cheng, et al., 2022).

In the following sections, we will explore analytical and experimental methods for parameter identification in lightweight arms with harmonic gear reducers, and conduct a comparative analysis of different inference methods to evaluate their performance.

3.2 Friction identification

In (Qi, Huapeng, Cheng, et al., 2022), researchers tackled the challenging task of identifying friction in lightweight robotic arms equipped with harmonic gear reducers. Friction is a critical factor that significantly impacts the overall performance of robotic systems, and accurate identification of friction parameters is essential to improve control precision and overall system efficiency.

To address this issue, the authors adopted the GMS model, which is a sophisticated and versatile model that effectively captures various friction effects, including stiction and

hysteresis. The GMS model is used to describe the friction characteristics in harmonic drive joints and is presented in Section 2.2.1 of the paper.

3.2.1 Dynamic model of a joint

A diagram of the flexible joint is presented in Figure 3.2b. In simplified dynamic analysis, the joint module can be regarded as being composed of a permanent magnet synchronous motor and harmonic reducer, as presented in Figure 3.4. In Figure 3.3, τ_m means that the drive torque is applied by the joint motor, where i is the current in the motor.

$$\tau_m = K \times i \tag{3.1}$$

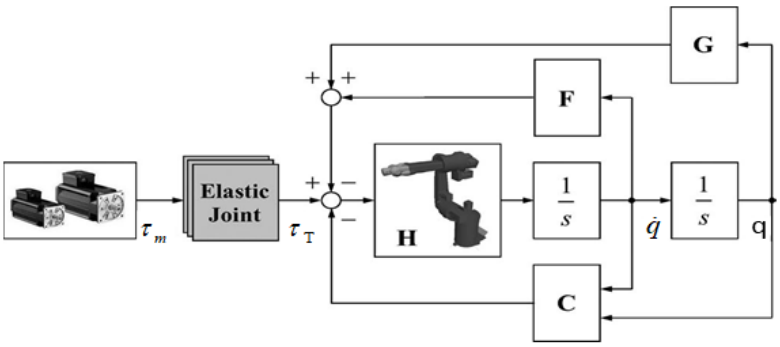

Figure 3.3: Diagram of elastic joints(**paper11**).

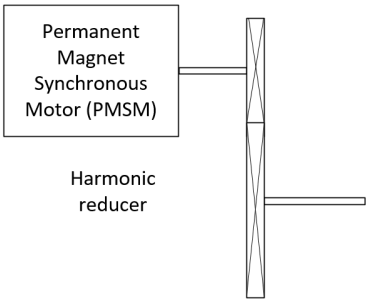

Figure 3.4: The simplified dynamic model of a joint module system (Zhen et al., 2021).

The dynamic model is given in (3.2):

$$\begin{aligned} \tau_m &= J_{mw}\ddot{\theta} + B_{mw}\dot{\theta} + \tau_f + \tau_{ext} \\ \tau_w &= \lambda\eta\tau_{ext} \end{aligned} \tag{3.2}$$

Table 3.1: The parameters of the flexible joint.

Symbol	Quantity
τ_m	motor output torque
K	motor torque coefficient
J_{mw}	Moment of inertia of joint module system
B_{mw}	viscous friction coefficient
τ_f	the friction torque in the harmonic reducer.
τ_w	the harmonic reducer output torque
η	transmission efficiency of the harmonic reducer
λ	the reduction ratio of the harmonic reducer.
q	joint position
θ	motor position
τ_{ext}	Load torque

where τ_f includes Coulomb and viscous friction, as well as static friction. B_{mw} can be included in τ_f. The moment of inertia of the joint module system J_{mw} is 1.65×10^{-3}, and the reduction ratio of the harmonic reducer is 101. The lubrication method of the harmonic reducer is to use harmonic reducer grease. Please, see the paper (Zhen et al., 2021) for other specific data.

3.2.2 Dynamics equations of GMS model and friction

The GMS model is a comprehensive friction model that accounts for multiple friction elements in parallel, including Coulomb, viscous, and static friction components. It also considers the angular velocity $\dot{\theta}$, temperature T, and the torque τ_t applied by the joint motor to accurately model the friction torque τ_f under different operating conditions.

The friction torque τ_f is expressed as follows:

$$\tau_f(\dot{\theta}, T, \tau_t) = \left[f_c + (f_{t0} + f_{vT} \times (T - 15)) \times \left(1 - e^{-\frac{|\dot{\theta}|}{\beta + \alpha \times (T-15)}} \right) \right] \times \operatorname{sgn}(\dot{\theta}) + f_l \tag{3.3}$$

where f_c, f_{t0}, f_{vT}, β, and α are parameters to be identified, and f_l represents the load-dependent friction term.

The first term in (3.3), f_c, represents the Coulomb friction coefficient, which accounts for the friction present when the joint is in a static state. The second term captures the viscous friction component and considers the joint temperature, allowing the model to characterize the variation of viscous friction with temperature. The third term introduces a term related to the joint angular velocity $\dot{\theta}$, modeling the Stribeck effect and capturing the friction dependence on the velocity. The $\text{sgn}(\dot{\theta})$ function ensures the friction torque changes direction when the joint velocity changes direction, accounting for hysteresis.

The final term f_l represents the load-dependent friction component, taking into account the load torque τ_l applied to the joint. This term captures the Stribeck effect under load conditions and further enhances the model's accuracy.

To identify the parameters f_c, f_{l0}, f_{vT}, β, α, and f_l, the researchers employed the Markov chain Monte Carlo (MCMC) method, a powerful statistical approach that effectively deals with complex and nonlinear systems. The MCMC method fits the GMS model to the experimental data at different speeds, temperatures, and load conditions, enabling the precise identification of the friction parameters.

The GMS model describes the friction force, denoted as F, in a robotic joint as the sum of individual friction elements, represented by F_i, and the contribution of viscous friction with coefficient σ multiplied by speed ω. Mathematically, it can be expressed as:

$$F = \sum_{i=1}^{L} F_i + \sigma \times \omega \quad \text{(GMS model)} \tag{3.4}$$

where L is the number of the equivalent friction element of the joint. F_i represents the friction force of a single friction element, and there are L such elements. ω is the angular speed of the joint, and σ is the coefficient of viscous friction. The behavior of each friction element F_i in the GMS model depends on the state it is in.

In the viscous state, the rate of change in friction force with respect to time ($\frac{dF_i}{dt}$) is proportional to speed (ω) with a stiffness coefficient k_i. This can be expressed as:

$$\frac{dF_i}{dt} = k_i \times \omega \quad \text{(Viscous state)} \tag{3.5}$$

where k_i is a coefficient that represents the stiffness of the friction element model.

When the friction element F_i is sliding, the rate of change of friction force with respect to

time is given by:

$$\frac{dF_i}{dt} = \text{sgn}(\omega) \times C \times \left[\xi_i - \frac{F_i}{s(\omega)} \right] \quad \text{(Sliding state)} \tag{3.6}$$

Where $\text{sgn}(\omega)$ is the sign function that returns +1 for positive ω and -1 for negative ω. C is a constant.

ξ_i is a parameter related to the friction element F_i, and is calculated based on the torque at specific points.

By incorporating the parameters ξ_i and k_i determined from the critical points, the authors derive the friction curve $s(\omega)$, which represents the relationship between friction force and speed during sliding. This friction curve $s(\omega)$ is the same as the $\tau_f(\dot{\theta}, T, \tau_t)$ mentioned in the global friction model (GFM). Therefore, in this context, the GMS model and the GFM are closely related, as $\tau_f(\dot{\theta}, T, \tau_t)$ represents the friction curve obtained from the GMS model, incorporating the identified parameters ξ_i and k_i.

In conclusion, the use of the GMS model for friction identification in harmonic drive joints provides a robust and accurate representation of friction behavior. The model successfully captures the complex friction phenomena under various operating conditions. Accurate identification of friction parameters contributes significantly to improving the control precision and efficiency of lightweight robotic arms, resulting in more effective and reliable robotic operations.

3.2.3 Experimental results

Dependence of friction on velocity

Figure 3.5 shows the correlation between joint speed and friction force. In particular, this friction force exhibits symmetry during both forward and reverse rotations. By assessing the friction during these rotations, we can determine the gravitational influence factors and subsequently streamline our equations.

The Stribeck curve shows a decrease as the velocity increases, where the highest point is represented by the static friction Fs and the lowest is represented by the Coulomb friction Fc. However, a distinct non-linear association between friction and velocity can be observed from Figure 3.5. Moreover, despite variations in temperature, the Coulomb friction remains unaltered. Given these findings, it is evident that traditional friction models fail to capture the entire essence of friction dynamics.

Friction's relationship with load torque

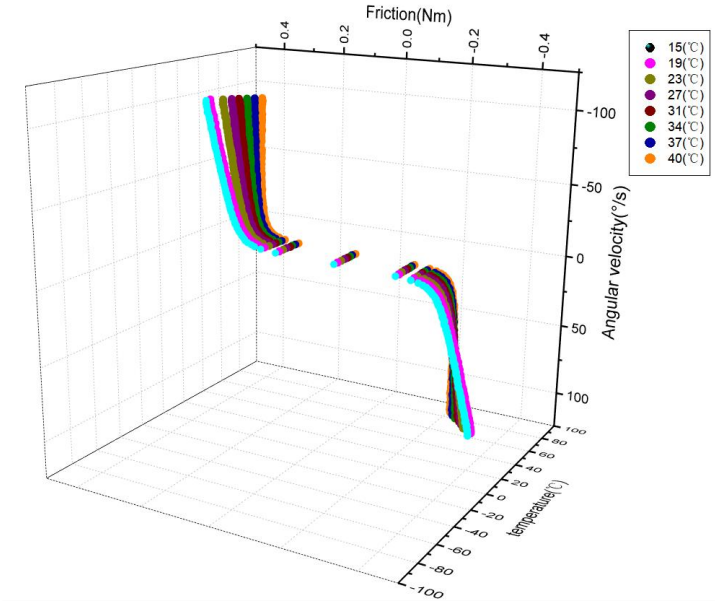

Figure 3.5: The friction changes with velocity and temperature (payload = 0).

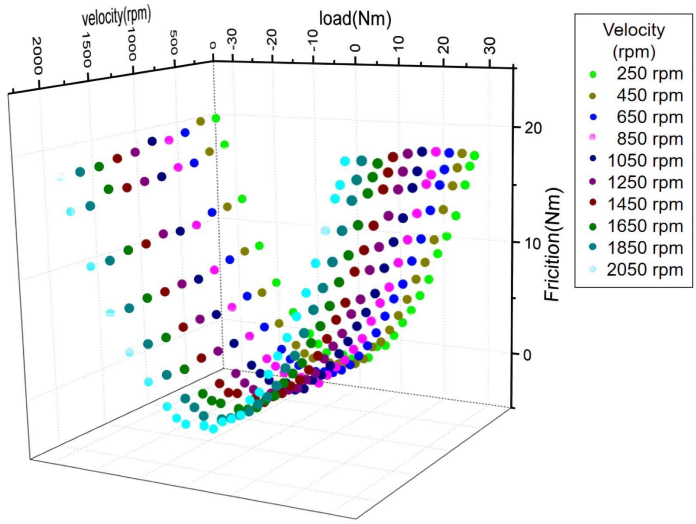

Figure 3.6: The friction changes with joint velocity, and load.

An examination of Figure 3.6 reveals a quadratic relationship between friction and load torque (Ema et al., 2020).

Output torque using the GMS model

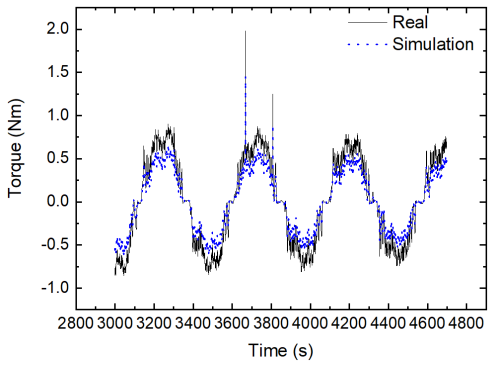

Figure 3.7: Simulation and real friction torque using (3.3). (Without load at room temperature, 15 ° C.)

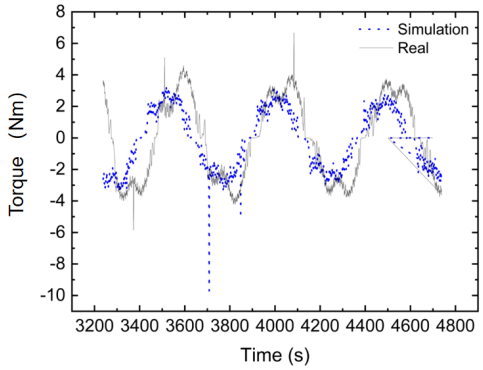

Figure 3.8: Simulation and real friction torque using (3.3). (temperature T = 15 °C, payload is 1 kg).

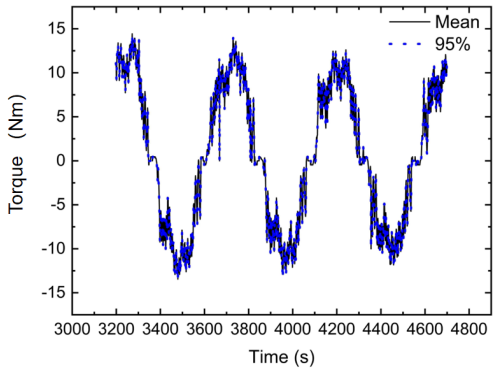

Figure 3.9: The reconstruction of output torque using the GMS model with MCMC and its credible interval (temperature 15°C and load 2 kg).

Regarding Figure 3.7 and Figure 3.8, it becomes evident that precision is reduced when taking into account three parameters, velocity, temperature, and load, in contrast to just considering velocity and temperature. The introduction of more variables tends to increase noise, particularly when the load reaches 15 kg and the temperature increases to 45 °C. Under pronounced noise disturbances, the reconstructive capabilities of the

MCMC method exceed those of the LS method.

The average of the MCMC reconstruction results, along with its 95% confidence range under ambient conditions of 15 °C and a load of 2 kg, is illustrated in Figure 3.9. Beyond providing merely reconstructive results, the MCMC technique also indicates their associated uncertainties. An examination of Figure 3.9 reveals that the 95% confidence bounds for the MCMC samples are quite narrow, which means minimal sample fluctuation. From the 95% predictive bounds of the adjusted models, there is a clear concordance between the predictions of the model and the actual observations.

3.2.4 Discussion

In (Qi, Huapeng, Cheng, et al., 2022), the proposed MCMC method was validated through real-world experiments on a lightweight robotic arm. The experimental setup involved applying different torque inputs to the arm and measuring the displacements of the joints. The collected data was then used in the MCMC algorithm to estimate the friction parameters of the harmonic drive joints. The experimental results demonstrated the effectiveness of the MCMC based approach in accurately identifying friction parameters. The identified friction model significantly improved the joint performance in terms of control accuracy and efficiency, making it suitable for various robotic applications.

The paper presented an innovative approach for the identification of parameters in lightweight arms with harmonic gear reducers using the MCMC method. Through rigorous experimentation, the authors successfully identified friction parameters, crucial for optimizing the arm's performance in various applications. The MCMC-based approach showcased its superiority in accurately estimating parameters in the presence of nonlinearities and uncertainties. This study opens up new possibilities for improving the control and automation of lightweight arms in industrial and robotic applications, contributing to the advancement of precision engineering and automation technologies.

3.3 Hysteresis identification in joints with harmonic drive transmission

This subsection delves deeper into the complexities of hysteresis identification in joints with harmonic drive transmission. The paper introduces the fractional-order Bouc-Wen model (FOBW) as an innovative approach to accurately model hysteresis effects, making it different from traditional models. The Monte Carlo method, which is a key part of this study, is used efficiently to identify parameters. This method shows its strength by making sure that estimates are accurate, which is especially important in situations with a lot of unidentified factors.

In addition to explaining the methods, this part will give a full summary of the most important results and findings of the paper. There is a lot of focus on how well the FOBW model works, showing how much better it is at capturing complicated hysteresis patterns. The Monte Carlo method's ability to capture the complex hysteresis phenomenon in dynamic systems is also emphasized, giving a full picture of its applicability and effectiveness.

3.3.1 Dynamics equations and model description

The paper focuses on the identification of hysteresis characteristics in joints with harmonic drive transmission. It introduces the Fractional Order Bouc-Wen (FOBW) model, an extension of the traditional Bouc-Wen model, to accurately represent the nonlinear hysteresis behavior observed in the system. The harmonic drive-based joint consists of the wave generator (WG), flex spline (FS), and circular spline (CS), connected to the base. The experimental platform system is used to measure the kinematic properties of joints with harmonic reducers and includes a permanent magnet servo motor (PMSM) and the harmonic drive inside the joint module.

The dynamics of the joint with harmonic drive transmission can be described by the following equations.

First, the general dynamics model is:

$$\tau_T = H(\theta)\ddot{\theta} + C(\theta,\dot{\theta}) + G(\theta) + \tau_f \tag{3.7}$$

where τ_T is the joint torque. $H(\theta)$ is the joint inertia matrix. $C(\theta,\dot{\theta})$ is the nonlinear coupling term, including centrifugal and Coriolis forces. $G(\theta)$ is the gravitational torque. $\ddot{\theta}$ is the acceleration of the joint, and τ_f is the friction torque.

For single-axis flexible manipulators, the dynamics model is:

$$\tau_T = Ja \times \ddot{\theta} + Ba \times \dot{\theta} + \tau_f \tag{3.8}$$

$$\tau_f\left(\dot{\theta},\tau_t\right) = \left[f_c + (f_{v0}) \times \left(1 - e^{\frac{|\dot{\theta}|}{\beta}}\right)\right] \times \operatorname{sgn}(\dot{\theta}) + f_l \tag{3.9}$$

where τ_f is the friction torque, $\dot{\theta}$ is the angular velocity, τ_t represents the load, f_c refers to the constant coefficient, f_l represents the load-dependent friction term, f_{v0} is the velocity coefficient, and β is a parameter used to adjust the effect of the exponential term. Please refer to (Qi, Huapeng, Cheng, et al., 2022) for a more detailed explanation.

Second, harmonic drive hysteresis model (classical Bouc-Wen model):

$$\Gamma(u(t),t) = wk|u(t)| + (1-w)k|x(t)| \tag{3.10}$$

$$\dot{x}(t) = \alpha\dot{u}(t) - \beta|\dot{u}(t)||x(t)|^{n-1}x(t) - \gamma\dot{u}(t)|x(t)|^n \tag{3.11}$$

where $\Gamma(u(t),t)$ is the hysteresis component of the transmitted joint torque, w, k, α, β, n, and γ are the model parameters that govern the hysteresis behavior, $u(t)$ is the joint input position, $\dot{u}(t)$ is the velocity of the joint, and $x(t)$ is the hysteresis variable that represents the difference between the input and output positions.

The CBW (Classical Bouc-Wen) model is formulated to characterize the hysteresis effect, and the constants are defined as follows: $ku = wk$,$kh = (1-w)Dkh_0$.

$$T(t) = Ba \times \dot{u}(t) + k_u \times u(t) + k_h \times h(t) + a \times sgn(\dot{u}(t)) \times \tau_l^2 \tag{3.12}$$

$$\dot{h} = D^{-1} \times \left(A \times \dot{u} - \beta \times |\dot{u}| \times |h|^{n-1} \times h - \gamma \times \dot{u} \times |h|^n\right) \tag{3.13}$$

In the hysteresis model, we have the following coefficients and variables:

$\dot{h}$ is the rate of change of the hysteresis variable $h(t)$ over time, D is a coefficient that determines the scaling of the influence of the input velocity on the hysteresis variable, A is a coefficient that scales the contribution of the input velocity $\dot{u}(t)$, β is a coefficient that governs the influence of the velocity-dependent term on the hysteresis variable, n is an exponent that controls the shape of the hysteresis loop and γ is a coefficient that modulates the influence of the velocity-dependent term on the hysteresis variable. These coefficients and variables play an essential role in defining and understanding the behavior of the hysteresis model.

Third, the fractional-order Bouc-Wen model (FOBW): The FOBW model extends the CBW model by introducing fractional derivatives to capture the noninteger order dynamics of the joint. This model is particularly useful for describing systems with memory-dependent behavior, such as joints with harmonic gear reducers. The FOBW model is described by fractional-order differential equations. Its equation is as follows:

$$D^{\lambda_2}h = \rho\left(D^{\lambda_1}u - \sigma\left|D^{\lambda_1}u\right||h|^{n-1}h + (\sigma-1)D^{\lambda_1}u|h|^n\right) \tag{3.14}$$

Equation (3.14) presents an extension of the non-linear hysteresis effect from integer order to fractional order (Shengzheng et al., 2021). It incorporates a fractional derivative

operator and introduces additional parameters to capture the fractional order behavior. Here is an explanation of each parameter:

The fractional derivative operator D^{λ_2} with order λ_2 represents the differentiation of the hysteresis variable $h(t)$ in fractional order.

The hysteresis variable $h(t)$ represents the dynamic response associated with the hysteresis effect.

The coefficient ρ scales the influence of the fractional derivative term on the hysteresis variable. It determines the overall effect of the fractional derivative on the hysteresis response.

The term $D^{\lambda_1}u$ represents the fractional derivative of the input signal $u(t)$ of the order λ_1. It describes the impact of the input signal on the hysteresis variable.

The coefficient σ determines the influence of the velocity-dependent term on the hysteresis variable. It accounts for the non-linearity introduced by the velocity-dependent behavior.

The exponent n controls the shape of the hysteresis loop. It affects the nonlinearity and sensitivity of the hysteresis response.

The term $(\sigma - 1)$ captures the difference between the velocity-dependent term and the elastic term in the hysteresis model.

In summary, Equation (3.14) provides a fractional-order extension of the hysteresis effect, allowing for a more comprehensive representation of complex hysteresis phenomena in dynamic systems. By incorporating fractional derivatives, this model offers increased flexibility and accuracy in capturing the intricate dynamics of hysteresis.

The fractional-order Bouc-Wen (FOBW) model for asymmetric hysteresis is as follows:

$$\frac{\mathscr{D}^{\lambda_2}\hbar}{\mathscr{D}^{\lambda_1}u} = \rho\left(1-\hbar^n\right), \quad \hbar \geq 0, \mathscr{D}^{\lambda_1}u \geq 0 \tag{3.15}$$

$$\frac{\mathscr{D}^{\lambda_2}\hbar}{\mathscr{D}^{\lambda_1}u} = \rho\left(1+(2\sigma-1)\hbar^n\right), \quad \hbar \geq 0, \mathscr{D}^{\lambda_1}u \leq 0 \tag{3.16}$$

$$\frac{\mathscr{D}^{\lambda_2}\hbar}{\mathscr{D}^{\lambda_1}u} = \rho\left(1-(-1)^n\hbar^n\right), \quad \hbar \leq 0, \mathscr{D}^{\lambda_1}u \leq 0 \tag{3.17}$$

$$\frac{\mathscr{D}^{\lambda_2}\hbar}{\mathscr{D}^{\lambda_1}u} = \rho\left(1+(-1)^n(2\sigma-1)\hbar^n\right), \quad \hbar \leq 0, \mathscr{D}^{\lambda_1}u \geq 0 \tag{3.18}$$

where $\mathscr{D}^{\lambda_2}\hbar/\mathscr{D}^{\lambda_1}u$ is the fractional derivative of the hysteresis variable $\hbar(t)$ with respect to the input position $u(t)$. $\hbar(t)$ represents the hysteresis variable (scaled version of $x(t)$) with fractional order dynamics. λ_1 and λ_2 are fractional orders, and ρ, σ, and n are model parameters that control the fractional-order hysteresis behavior. The FOBW model extends the traditional Bouc-Wen model to capture asymmetric and rate-dependent hysteresis behavior, providing a more accurate representation of the system dynamics. The paper also compares the FOBW model with the traditional dynamic equation to demonstrate its improved accuracy in modeling hysteresis.

3.3.2 Experimental results of identification using Least Squares and MCMC

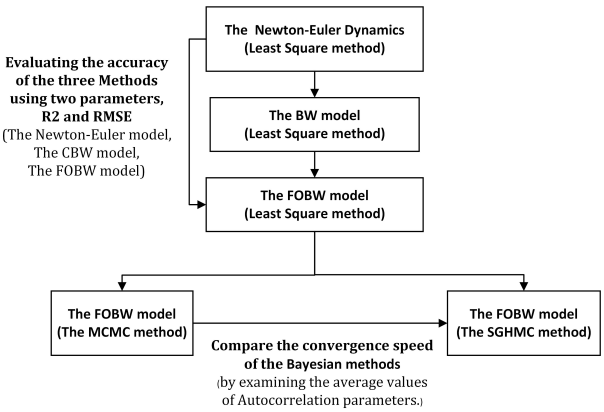

Figure 3.10: Comparison of parameter identification methods: the Least Squares, the MCMC, and the SGHMC for the Newton-Euler Dynamics model Equation (3.8), the CBW model Equations (3.12) and (3.13), and the FOBW model Equations (3.12) and (3.14).

The relationship graph compares the accuracy and convergence speed of LS, MCMC, and SGHMC for parameter identification in three models: the Newton-Euler model, the CBW model, and the FOBW model.

R2 and RMSE are used to assess the accuracy of the method. These metrics quantify the fit of the model using identified parameters. We may compare the accuracy and performance by computing R2 and RMSE for each approach in the three models.

Furthermore, the convergence speed of the Bayesian methods (MCMC and SGHMC) is examined by analyzing the average values of autocorrelation parameters. Autocorrelation measures the correlation between subsequent samples and is a diagnostic parameter that indicates convergence of the Markov chains used in Bayesian inference. By comparing the average autocorrelation values for MCMC and SGHMC, we can assess the convergence speed of these methods and determine which one converges faster.

We can completely evaluate the three techniques in parameter identification for the Newton-Euler model, CBW model, and FOBW model considering accuracy (R2 and RMSE) and convergence speed (Autocorrelation).

The parameter results from applying the LS approach to determine the FOBW, BW and Equation (3.8) formulas are shown in Table 3.2, Table 3.3, and Table 3.4, respectively. In Figure 3.11 to Figure 3.15 you can find the specific graphics.

The identification results of the CBW models in Equation (3.13) are shown in Figure 3.11. The red line represents the actual model hysteresis value in the upper image, the blue line represents the simulated hysteresis loop, and the error value is shown in the lower picture. There is a 7.5 $N \cdot m$ payload. The maximum load was chosen because the effect of hysteresis is more significant the higher the load.

The identification results of the CBW models of Equation (3.12) are shown in Figure 3.12. The red in the upper image represents the actual torque output value of the model, while the blue value in the lower image represents the model torque output error. The loads are 0 $N \cdot m$, 2.5 $N \cdot m$, 3.75 $N \cdot m$, 5 $N \cdot m$, 6.25 $N \cdot m$ and 7.5 $N \cdot m$, respectively.

The identification results of the suggested FOBW models are shown in Figure 3.13 of Equation (3.14). The red one is the actual model hysteresis value in the upper image. Bleu one shows the simulated hysteresis loops, and the lower image shows the error value. There is a payload of 7.5 $N \cdot m$.

The identification results of the suggested FOBW models are shown in Figure 3.14 of Equation (3.12). Red in the top image represents the actual torque output value of the model, while blue in the lower image represents the model torque output error. The loads are 0 $N \cdot m$, 2.5 $N \cdot m$, 3.75 $N \cdot m$, 5 $N \cdot m$, 6.25 $N \cdot m$ and 7.5 $N \cdot m$, respectively.

Table 3.2: Paremater identification results of the single joint system using FOBW model in Equations (3.12) and (3.14) using the LS method.

Notation	Definition	Value	Unit
Ba	the output torque coefficient of PMSM motor	1.4e-4	$N \cdot m/\circ/sec$
ku	the post-yield stiffness	-0.0169	$N/\circ$
kh	the initial stiffness of the hysteretic part	25.989	$N/\circ$
ρ	the shape constant of the hysteresis curve	3.286e-05	$1/\circ$
n	the shape constant of the hysteresis curve	0.855	-
σ	the shape constant of the hysteresis curve	1411.64	-
λ_1	the fractional order	1.479	-
λ_2	the fractional order	0.98	-
a	the friction constant at the load end	0.384	-

Table 3.3: Parameter identification results of the single joint system using the BW model in Equations (3.12) and (3.13) using the LS method.

Notation	Definition	Value	Unit
Ba	the output torque coefficient of PMSM motor	1.4e-4	$N \cdot m/\circ/sec$
ku	the post-yield stiffness	0.0038	$N/\circ$
kh	the initial stiffness of the hysteretic part	22.34	$N/\circ$
D	the shape constant of the hysteresis curve	80.00	$1/\circ$
n	the shape constant of the hysteresis curve	0.9988	-
A	the shape constant of the hysteresis curve	0.1341	-
β	the shape constant of the hysteresis curve	50.00	-
γ	the shape constant of the hysteresis curve	3.00	-
a	the friction constant at the load end	0.3466	-

Table 3.4: Parameter identification results of the single joint system in Equation (3.8) using the LS method.

Notation	Definition	Value	Unit
Ja	the moment of inertia of joint module system	0.00165	$kg.m2$
Ba	the output torque coefficient of PMSM motor	1.4e-4	$N \cdot m/\circ/sec$
f_c	the constant Coulomb friction	-0.2384	N
f_{v_0}	the constant used to describe the viscous friction	-1.544	-
β	the constant used to describe the viscous friction	21.15	-
a	the friction constant at the load end	-1.833	-
f_s	the friction constant at the load end	-311.83	-
$\dot{\theta}_v$	the friction constant at the load end	-4.9215	-

Table 3.5: Parameter identification results of the single joint system using the FOBW model in Equation (3.12) and Equation (3.14) using MCMC method.

Notation	Definition	Value	Unit
Ba	the output torque coefficient of PMSM motor	1.4e-4	$N \cdot m/\circ/sec$
ku	the post-yield stiffness	0.0498	$N/\circ$
kh	the initial stiffness of the hysteretic part	-22.660	$N/\circ$
ρ	the shape constant of the hysteresis curve	3.133e-05	$1/\circ$
n	the shape constant of the hysteresis curve	0.858	-
σ	the shape constant of the hysteresis curve	1411.64	-
λ_1	the fractional order	1.4787	-
λ_2	the fractional order	0.9832	-
a	the friction constant at the load end	0.3502	-

Table 3.6: The error between the simulated output torque value and the real output torque value of the three formulas.

The fitting degrees of MCMC and the least square	The FOBW model in Equation (3.12) and Equation (3.14) using the LS method	The FOBW model in Equation (3.12) and Equation (3.14) using the MCMC method	The CBW models in Equation (3.12) and Equation (3.13) using the LS method	The model in Equation (3.8) using the LS method
1. RMES	1.6198	1.2621	1.5883	4.4780
2.Fitness(R-Squared)	88.24%	91.3 %	83.42%	73.8%

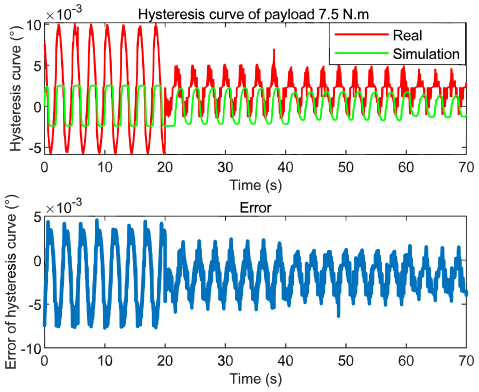

Figure 3.11: Identification results of the BW models in Equation (3.13). In the upper picture, the red one is the actual model hysteresis value, the blue one is the simulated hysteresis loop output, and the lower picture is the error value. The payload is 7.5 $N \cdot m$.

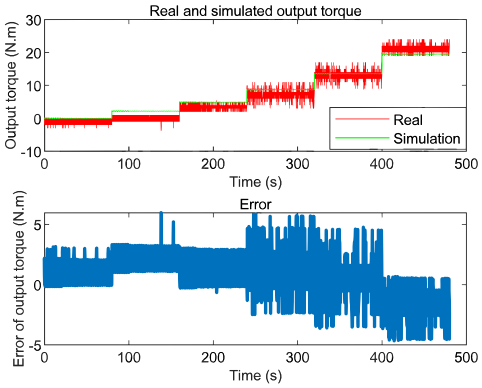

Figure 3.12: Identification results of the BW models in eqs. Equation (3.12). The red in the upper picture is the real value of the model torque output and the blue simulation value, and the lower picture is the error value of the model torque output. The load, respectively, is 0 $N \cdot m$, 2.5 $N \cdot m$, 3.75 $N \cdot m$, 5 $N \cdot m$, 6.25 $N \cdot m$, 7.5 $N \cdot m$.

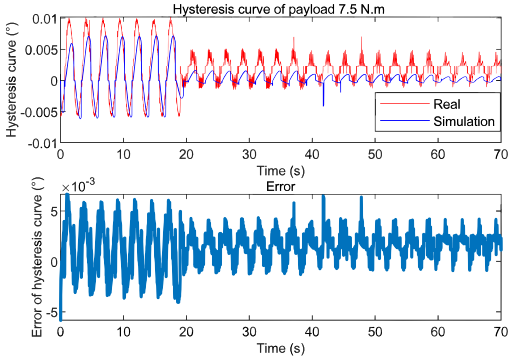

Figure 3.13: Identification results of the proposed FOBW models in Equation (3.14) using the LS method. In the upper picture, the red image is the actual model hysteresis value, the blue image is the simulated hysteresis loop output, and the lower picture is the error value. The payload is 7.5 $N \cdot m$.

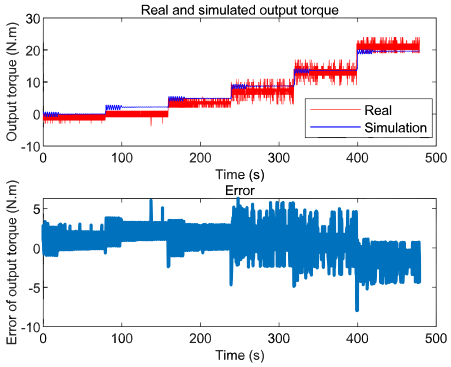

Figure 3.14: Identification results of the proposed FOBW models in Equation (3.12) using the LS method. The red picture is the actual model output torque value in the upper image and the blue simulation value, and the lower picture is the error value of the model output torque. The load, respectively, is 0 $N \cdot m$, 2.5 $N \cdot m$, 3.75 $N \cdot m$, 5 $N \cdot m$, 6.25 $N \cdot m$, 7.5 $N \cdot m$.

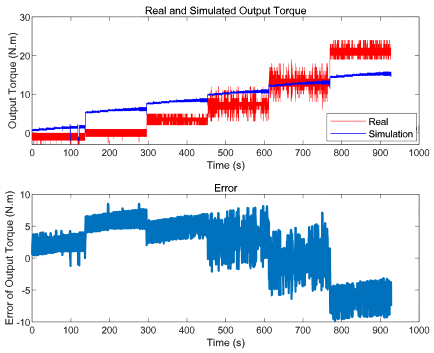

Figure 3.15: Identification results of the traditional mechanical modeling in Equation (3.8). The red in the upper picture is the real value of the model torque output and the blue simulation value, and the lower picture is the error value of the model torque output. The load, respectively, is 0 $N \cdot m$, 2.5 $N \cdot m$, 3.75 $N \cdot m$, 5 $N \cdot m$, 6.25 $N \cdot m$, 7.5 $N \cdot m$.

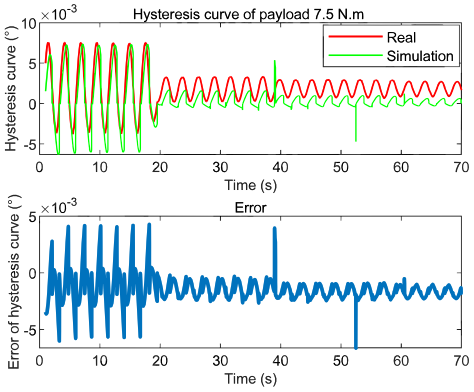

Figure 3.16: Identification results of the proposed FOBW models in Equation (3.14) using the MCMC method. In the upper picture, the red image is the identification results, the blue image is the output of the simulated hysteresis loop, and the lower image is the error value. The payload is 7.5 $N \cdot m$.

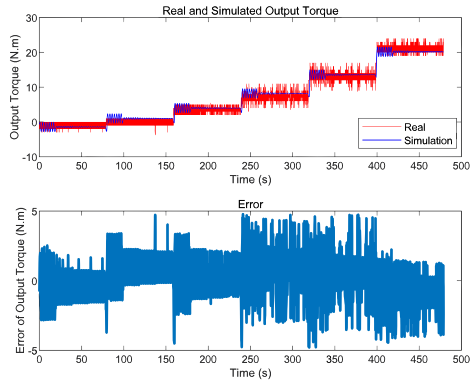

Figure 3.17: Identification results of the proposed FOBW models in eqs. Equation (3.12) using MCMC method. The red in the upper picture is the real value of the model torque output and the blue simulation value, and the lower picture is the error value of the model torque output. The load, respectively, is 0 $N \cdot m$, 2.5 $N \cdot m$, 3.75 $N \cdot m$, 5 $N \cdot m$, 6.25 $N \cdot m$, 7.5 $N \cdot m$.

In Figure 3.11 and Figure 3.13, the speed is gradually reduced from $30^\circ/s$ to $10^\circ/s$, so the hysteresis curve is also gradually reduced. By comparing Figure 3.11 and Figure 3.13, it is evident that Figure 3.13 has a superior simulation effect for hysteresis, which is attributable to the adoption of the new FOBW model suggested in this research. In Table 3.6 displays the RMES error of the data. We reduced the RMES from 4.48 to 1.26 while increasing the fitness from 73% to 91%. The accuracy has increased significantly. X_{RMSE} in Equation (3.19) is the root mean squard error. R^2 in

Equation (3.20) is the coefficient of determination (R-squared). R-squared is also called fitness, which eliminates the influence of dimensions. The closer the model is to 100%, the more accurate the model is.

$$X_{RMSE} = \sqrt{\frac{\sum_{i=1}^{N} (y_i - f_i)^2}{N}} \tag{3.19}$$

$$R^2 = (1 - \frac{SS_{\text{res}}}{SS_{\text{tot}}}) \times 100\% \tag{3.20}$$

Where y_i is is the observed value, f_i is the predicted value, $\bar{y}$ is the average value. $SS_{res} = \sum_{i=1}^{N} (y_i - f_i)^2$ is the residual sum of squares, $SS_{tot} = \sum_{i=1}^{N} (y_i - \bar{y})^2$ is the total square value.

We reidentify Equation (3.12) and Equation (3.14) using the MCMC technique to increase the FOBW model's accuracy even more. In Table 3.5 the results of the identification parameters are shown. Refer to Section 2.1 for details of the precise procedure and pseudocode of the MCMC method. RMES is 1.26 and the fitness is 0.91, which is more accurate than the LS technique.

In general, Figure 3.11 to Figure 3.17 tend to suggest that the use of the FOBW model can predict hysteresis curves at different speeds and loads, thus increasing the range of hysteresis problems that can be studied. In addition, the MCMC algorithm improves the accuracy of the model identification.

3.3.3 Experimental results of parameter identification using SGHMC

Figure 3.18 illustrates the identification results of the proposed FOBW models using the SGHMC (Stochastic Gradient Hamiltonian Monte Carlo) method. The upper picture shows the comparison between the identification results (red) and the simulated hysteresis loop output (blue). The lower picture represents the error values between the identification results and the simulated output. The payload for this experiment is 7.5 $N \cdot m$.

Figure 3.19 presents the identification results of the proposed FOBW models using the SGHMC method. The upper picture compares the real value (red) and the simulated value (blue) of the model torque output. The lower picture shows the error value of the torque output of the model. The experiments were carried out with different loads ranging from 0 $N \cdot m$ to 7.5 $N \cdot m$.

The Table 3.7 displays the parameter identification results of the single joint system using the FOBW (Fractional Order Bouc-Wen) model. The table lists the notation, definition, value, and unit of each identified parameter.

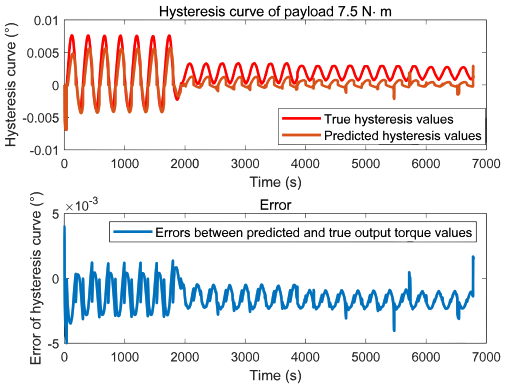

Figure 3.18: Identification results of the proposed FOBW models in Equation (3.14) using the SGHMC method. In the upper picture, the red image is the identification results, the blue image is the output of the simulated hysteresis loop, and the lower image is the error value. The payload is 7.5 $N \cdot m$.

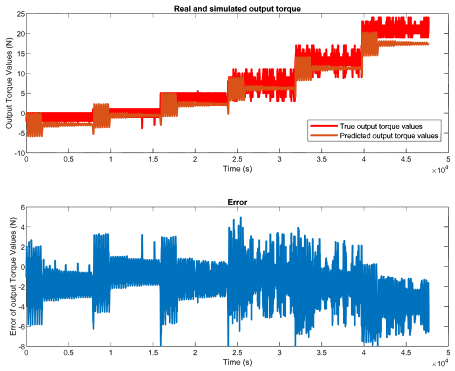

Figure 3.19: Identification results of the proposed FOBW models in Equation (3.12) using SGHMC method. The red in the upper picture is the real value of the model torque output and the blue simulation value, and the lower picture is the error value of the model torque output. The load, respectively, is 0 $N \cdot m$, 2.5 $N \cdot m$, 3.75 $N \cdot m$, 5 $N \cdot m$, 6.25 $N \cdot m$, 7.5 $N \cdot m$.

3.3.4 Comparison of average autocorrelation values: SGHMC versus MCMC experimental findings

The Figure 3.20 and Figure 3.21 illustrate the autocorrelation values of the samples obtained from the SGHMC and MCMC algorithms, respectively. These autocorrelation values provide insights into the correlation structure of the obtained samples.

The Table 3.8 compares the mean autocorrelation values for the MCMC and SGHMC

Table 3.7: Parameter identification results of the single joint system using the FOBW model in Equation (3.12) and Equation (3.14) using SGHMC method.

Notation	Definition	Value	Unit
Ba	the output torque coefficient of PMSM motor	1.4e-4	$N \cdot m/\circ/sec$
ku	the post-yield stiffness	-0.0334	$N/\circ$
kh	the initial stiffness of the hysteretic part	-48.6570	$N/\circ$
ρ	the shape constant of the hysteresis curve	2e-05	$1/\circ$
n	the shape constant of the hysteresis curve	0.8307	-
σ	the shape constant of the hysteresis curve	1566.61	-
λ_1	the fractional order	1.7348	-
λ_2	the fractional order	0.9075	-
a	the friction constant at the load end	0.3606	-

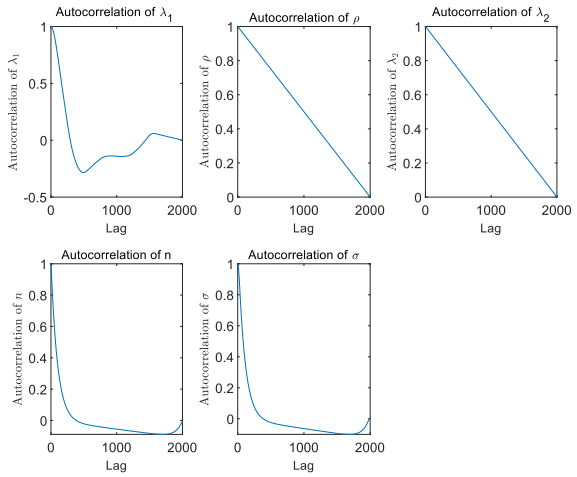

Figure 3.20: The autocorrelation values of the samples obtained from SGHMC algorithm in Equation (3.14).

methods. The table presents the autocorrelation values for each parameter obtained from both methods. Corresponding parameters of 1 to 5: λ_1, ρ, λ_2, n, σ.

By examining the density plot of the parameter during the sampling process, we can observe the shape of the distribution.

The Figure 3.22 displays the posterior distribution, and we can observe that the shape closely resembles that of the inverse gamma distribution, which aligns with the conjugate relationship between the prior and likelihood distributions. This similarity suggests that

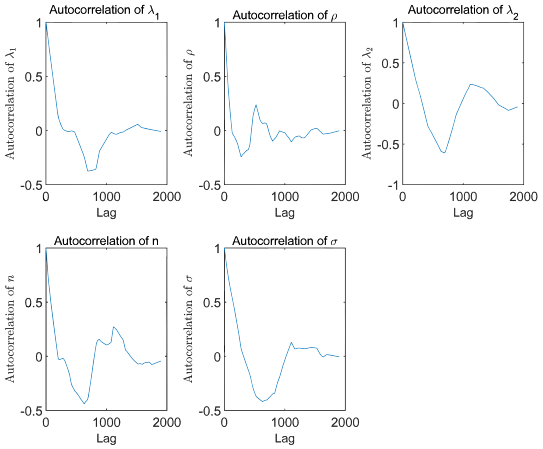

Figure 3.21: The autocorrelation values of the samples obtained from MCMC algorithm in Equation (3.14).

Table 3.8: Mean autocorrelation values for MCMC and SGHMC method.

No.	MCMC	SGHMC
1	3×10^{-4}	2.813×10^{-4}
2	3×10^{-4}	1×10^{-3}
3	1.5×10^{-3}	1×10^{-3}
4	9×10^{-4}	-2.1×10^{-3}
5	4×10^{-4}	-2.486×10^{-5}

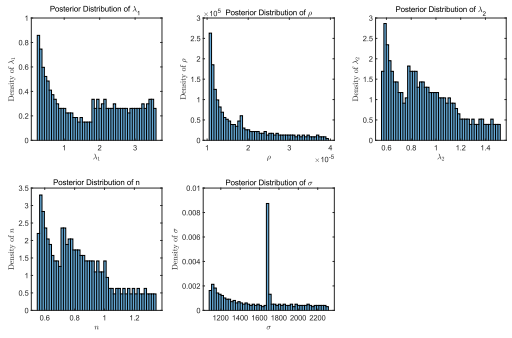

Figure 3.22: The density plot of the posterior distribution for the parameter of SGHMC algorithm of the samples obtained from the Equation (3.14).

the parameter has converged to a stable state, as indicated by the posterior distribution.

The convergence of the posterior distribution with an inverse gamma shape provides strong evidence that the SGHMC algorithm has achieved convergence.

This convergence indicates that the algorithm has effectively estimated the parameter's values and captured the underlying uncertainty. With the conjugate relationship between the prior and likelihood distributions, the SGHMC algorithm has successfully used the information from the data and the prior knowledge encoded in the inverse gamma prior to obtain reliable inference and analysis results.

Table 3.9: The error between the simulated output torque value and the real output torque value of the three formulas.

The fitting degrees of MCMC and the least square	The FOBW model in Equation (3.12) and Equation (3.14) using the SGHMC method	The FOBW model in Equation (3.12) and Equation (3.14) using the MCMC method
1. RMES	2.3681	1.2621
2.Fitness(R-Squared)	90.62%	91.3 %

The Table 3.9 provides the comparison of errors between the simulated output torque values and the real output torque values obtained from different methods. The table includes two columns, the first one for the FOBW model identification using the SGHMC method, and the other using the MCMC (Markov Chain Monte Carlo) method. Present the root mean square error (RMSE) and the fitness (R-squared) values.

From Table 3.8, which compares the mean autocorrelation values for the MCMC and SGHMC methods, we can observe the following.

The MCMC method shows autocorrelation values ranging from 3×10^{-4} to 1.5×10^{-3} for different parameters. In comparison, the SGHMC method exhibits autocorrelation values ranging from 2.813×10^{-4} to -2.1×10^{-3}. On the basis of these values, we can conclude that the autocorrelation in the SGHMC method is generally lower than that in the MCMC method. This suggests that the SGHMC algorithm has a faster convergence speed as it explores the parameter space more efficiently.

Moving on to Table Table 3.9, which presents the comparison of errors between simulated and real output torque values, we find the following:

The RMSE for the identification of the FOBW model using the SGHMC method is 2.3681. On the other hand, the RMSE for the FOBW model identification using the MCMC method is 1.2621. Additionally, the fitness values (R-squared) for the SGHMC and MCMC methods are 90.62% and 91.3%, respectively.

Based on these results, we can infer that the accuracy of the two methods is relatively

comparable, since the RMSE values are similar. However, the MCMC method exhibits slightly higher fitness, indicating slightly better accuracy in capturing the real output torque values.

In terms of convergence speed, the SGHMC method demonstrates faster convergence compared to the MCMC method. Lower autocorrelation values in the SGHMC method suggest more efficient exploration of the parameter space and quicker convergence to the desired posterior distribution.

Overall, the analysis of the provided data indicates that while the accuracy between the two methods is relatively similar, the SGHMC method shows a clear advantage in terms of convergence speed.

3.4 Discussion of results and findings

In this section, we discuss the results of the use of MCMC and Monte Carlo methods to identify friction and hysteresis in lightweight arms. The significance of this study lies in its potential to revolutionize the understanding of frictional dynamics and hysteresis phenomena, a cornerstone in ensuring optimal operation of lightweight arms.

Results for friction identification (Qi, Huapeng, Cheng, et al., 2022) : The application of the MCMC method to the identification of friction in harmonic drive joints produced encouraging results. When one digs deeper into MCMC, its statistical rigor provides a reliable framework that ensures confidence in the results. Using the Generalized Maxwell Slip (GMS) model and a Bayesian inference formulation, the MCMC algorithm efficiently sampled the posterior distribution of friction parameters. Furthermore, the choice of the GMS model, with its ability to represent complex frictional phenomena, is perfectly aligned with the research objectives. The parameter estimates obtained accurately characterized the non-linear and time-varying nature of friction, which yields important information on the friction behavior of lightweight arms.

Fitness R^2 and RMSE were used to evaluate the performance of the model. The predictions of the model matched closely with the experimental data, validating the efficacy of the MCMC method for the identification of friction.

Results of hysteresis identification: For hysteresis identification, the Monte Carlo-based method employing MCMC and SGHMC techniques demonstrated outstanding performance. The value proposition of Monte Carlo techniques is their adaptability and robustness, making them particularly suitable for the identification of hysteresis, a well-known phenomenon due to its complexity. The algorithms effectively sampled the parameter space and estimated optimal parameter values to minimize differences between model predictions and experimental data.

R^2 and RMSE were again used as evaluation criteria to determine the precision of hysteresis identification. High R^2 and low RMSE values indicated a strong correlation between the predictions of the model and the experimental data, demonstrating the dependability of the SGHMC method to identify hysteresis.

Comparative evaluation: Both MCMC-based and Monte Carlo-based methods are effective for parameter identification in lightweight arms with harmonic gear reducers, according to a comparison of the two approaches. To delve further, the MCMC method, with its strong theoretical foundation, is unparalleled in capturing frictional properties, making it the method of choice for friction studies. The SGHMC method, with its adaptability, demonstrated superior performance in addressing hysteresis effects.

In general, the findings demonstrate the importance of Bayesian inference and Monte Carlo-based methods for accurately identifying friction and hysteresis parameters. It provides a robust framework for parameter estimation by acting as a bridge between raw data and important findings, thereby underscoring the importance of Bayesian inference. Combining experimental data with intelligent inference techniques facilitates the comprehension and optimization of the dynamic behavior of lightweight arms with harmonic gear reducers.

4 Exploring inference methods for parameter identification in the CFETR CMOR robot arm

4.1 Parameter identification in the CMOR

Effective optimization of the performance of the CMOR robot arm is significantly dependent on the identification of parameters. The study referred to in (Qi, Huapeng, Yuntao, et al., 2023) dives deep into the intricacies of robotic arm dynamics. At the heart of any robot arm's efficiency is the understanding and precise identification of its parameters. Without this understanding, the movement might be erratic or inefficient. By focusing on heavy duty manipulators, the study covers machines that do a lot of heavy lifting in industry.

One of the main highlights of the research is the introduction of the SGHMC method. But why is this all important? Consider the application mentioned in the study, the CFETR superconducting Tokamak fusion device, to comprehend the significance. Fusion energy, often labeled the energy of the future, relies on extremely complex machinery to replicate the conditions inside the Sun. Any minor mistake may risk the entire procedure. The CMOR robot arm, which functions within this device, performs a crucial function.

The findings of (Qi, Huapeng, Yuntao, et al., 2023) are not just theoretical. They have a very real impact. By introducing a powerful algorithm to estimate the precise parameters of the robot arm, the study ensures that the CMOR robot arm operates at its best. This is crucial not only for the efficiency of the fusion device, but also for the safety of everyone involved.

In short, robotic arms, especially those used in critical applications such as fusion energy, are marvels of engineering. But to ensure that they operate as intended, a deep understanding of their parameters is essential. The (Qi, Huapeng, Yuntao, et al., 2023) study provides this understanding. By advancing knowledge and fine-tuning the operations of the CMOR robot arm, it will ensure that the dream of harnessing fusion energy becomes a reality.

4.1.1 Introduction to the CMOR robot arm of the CFETR

According to (Qi, Huapeng, Yuntao, et al., 2023), the mechanical arm of CMOR is not just an accessory, but a vital part of the CFETR superconducting Tokamak fusion device. Fusion devices like the Tokamak are complex pieces of engineering that aim to harness energy in the same way the sun does.

Among these essential components is the CMOR robot arm. Consider a machine that must operate in extreme heat and pressure, making human intervention impossible. Here, the CMOR robot arm enters play. Its construction is designed to withstand the

severe conditions of the fusion device. It is constructed from specialized materials that can withstand extreme heat and radiation.

In terms of movement, the CMOR robot arm has multiple degrees of freedom. This means that it can move in various directions, making it versatile and adaptable. Its flexibility ensures that it can reach different parts of the fusion device, perform repairs, or move materials as required.

Its applications within the fusion device are numerous. Beyond maintenance, the robot arm also helps with the installation of new components, monitors conditions inside the fusion chamber, and even assists with data collection. These data are invaluable as they help scientists better understand the fusion process and make improvements where necessary. This section aims to shine a light on this remarkable piece of engineering and to highlight its importance in the world of advanced energy research.

The CMOR mechanical system has been introduced in Section 1.2.2, as shown in Figure 4.1. In (Qi, Huapeng, Yuntao, et al., 2023), experimental methods were used to validate and evaluate the performance of parameter identification approaches for the CMOR robot arm.

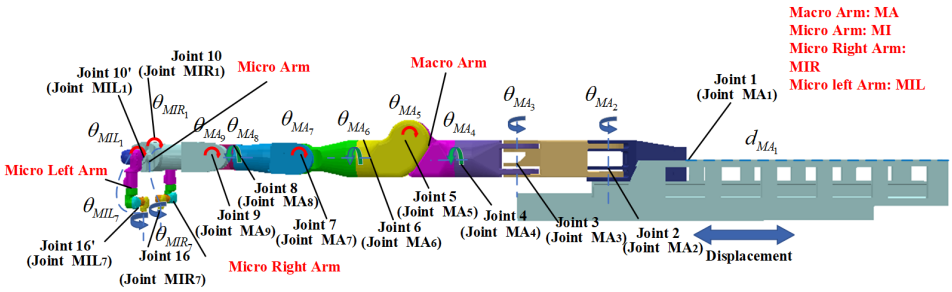

Figure 4.1: The configuration of the CMOR system include its overall structure.

The primary emphasis of (Qi, Huapeng, Yuntao, et al., 2023) was the use of the SGHMC method for the purpose of parameter identification in the CMOR robot arm. Observations of the behavior of the robot arm while it operates provided the data used for parameter estimation. The experimental procedures involved data collection, preprocessing, and validation. To acquire data, it was necessary to document the movements and behaviors of the robot arm under various conditions. The data were cleaned and organized prior to parameter identification in order to ensure suitability. To validate the identified parameters, the experimental results were compared with the simulated outputs of the identified models, and statistical measures such as the root mean square error (RMSE) were used to evaluate the precision of the parameter estimates. The experimental methods were essential to demonstrate the effectiveness and reliability of

parameter identification approaches.

4.1.2 Challenges in parameter identification for the CMOR robot arm

The main challenges comprise the identification of parameters in the CMOR robot arm, including friction and hysteresis effects, and the analysis of the complexities and uncertainties involved in parameter identification for the CMOR robot arm.

Identifying the parameters of the CMOR robot arm faces difficulties, as highlighted in (Qi, Huapeng, Yuntao, et al., 2023). This paper refines the estimation process by introducing the SGHMC method to deal with noisy data and wide-ranging parameter spaces.

1. Nonlinear dynamics: The CMOR robot arm operates in a complex and nonlinear environment, where nonlinearities are introduced by interactions with plasma, magnetic fields, and other Tokamak components. This complexity makes it difficult to develop mathematical models that accurately depict the behavior of the arm.

2. Hysteresis effects: (Qi, Huapeng, Yuntao, et al., 2023) discuss the effects of hysteresis, which refers to the phenomenon in which the output of the robot arm depends not only on its current inputs, but also on its historical inputs. It is difficult to identify and quantify hysteresis parameters due to their dynamic and time-dependent nature.

3. High-dimensional parameter space: The CMOR robot arm may have a large number of parameters that must be accurately estimated. This high-dimensional parameter space presents computational difficulties, as conventional parameter identification techniques may become computationally intensive and time-consuming.

4. The measurements acquired from the robot arm's sensors are frequently subject to noise and uncertainties. Unaddressed, dealing with noisy data during the parameter identification procedure can result in inaccurate estimations.

5. Differences between the mathematical models used for parameter identification and the actual behavior of the CMOR robot arm can result in estimation errors. To enhance the precision of parameter identification, it is essential to account for these model-experiment mismatches.

Alternatively, (Qi, Huapeng, Yuntao, et al., 2023) introduces the SGHMC method, which addresses noisy data and high-dimensional parameter spaces, providing a powerful instrument for parameter estimation in the CMOR robot arm.

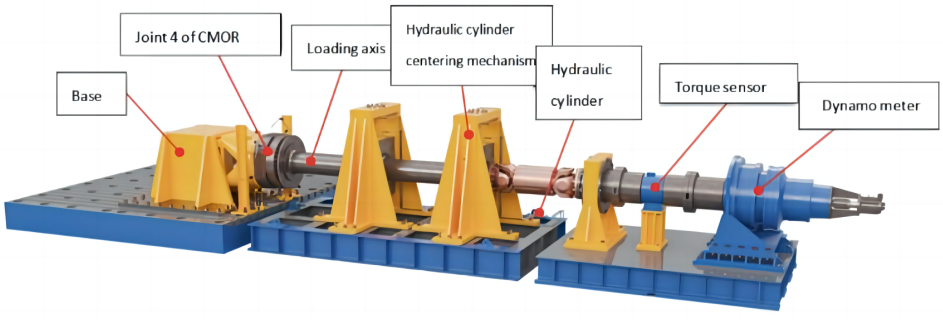

Figure 4.2: The fourth joint of the CMOR robot arm serves as the experimental platform for single-joint testing.

Successfully overcoming these obstacles will result in more accurate and reliable parameter identification for the CMOR robot arm, thereby improving its performance and contributing to the successful operation of the CFETR superconducting Tokamak fusion device.

4.2 Data collection and experimental setup

The CMOR robotic arm test platform consists of several key components that work together to achieve its functionalities as shown in Figure 4.2. These components include:

Base and mounting: The CMOR robot arm is securely mounted on a stable base within the Tokamak device. This ensures that the arm remains firmly anchored during its operations.

Linkages and joints: The robot arm is constructed using multiple interconnected links, allowing for smooth and flexible movements. These links are equipped with joints that provide rotational degrees of freedom, allowing the arm to move in various directions.

End effector: The end of the robot arm is equipped with a specialized end effector or tool that can be customized based on specific tasks. The end effector may include grippers, sensors, or other devices necessary to interact with Tokamak components.

Actuators: Actuators serve as the driving force for robot joint movements. These can be electric, hydraulic, or pneumatic actuators, depending on the requirements of the application.

Sensors and feedback systems: The CMOR robot arm is equipped with a variety of sensors that provide real-time feedback on its position, orientation, and interaction forces. This feedback is crucial for accurate and safe operations within the fusion device.

Control system: The control system of the CMOR robot arm is highly sophisticated and capable of executing complex motion trajectories with precision. Integrates advanced algorithms and software to optimize joint movements and ensure efficient completion of tasks.

The significance of the CMOR robot arm lies in its ability to perform critical tasks within the Tokamak fusion device. These tasks include the manipulation of plasma-facing materials, diagnostic systems, and other components.

The structure of the CMOR robot joint, combined with its precise control capabilities, enables it to adapt to different tasks and respond to dynamic changes within the Tokamak environment. This adaptability and reliability make it an indispensable tool for researchers and engineers working towards the successful operation of the CFETR superconducting Tokamak fusion device.

4.2.1 Dynamic modeling of robots using Lagrange's method

The dynamic model of a robot manipulator is crucial to understanding its behavior and accurately controlling its motion. It involves parameters such as joint angles, velocities, accelerations, as well as inertial, friction, and gravity effects. Dynamic modeling often relies on two commonly used approaches: the classical Lagrange method and the CBW model.

The classical Lagrange method is a widely used technique for dynamic modeling of robotic systems. It involves formulating the robot's equations of motion using Lagrangian mechanics. The dynamics equation governing a single joint mechanism can be expressed as follows:

$$M(q)\ddot{q} + C(q,\dot{q})\dot{q} + g(q) = \tau + J(q)^T F_{\text{ext}} \tag{4.1}$$

In Equation (4.1), the terms represent the following:

q: Joint angle vector. $\dot{q}$: Joint velocity vector. $\ddot{q}$: Joint acceleration vector. $M(q)$: Mass matrix. $C(q,\dot{q})$: Coriolis and centrifugal forces. $g(q)$: Gravitational forces. τ: Joint torque vector. $J(q)^T$: Jacobian transpose matrix. F_{ext}: Vector of external forces.

The equation captures the dynamic behavior of the manipulator, aiming to estimate the unknown parameters for each link in the robot, specifically the inertial and friction parameters. The robot dynamics model in (4.2) can be written in the linear form of its moment of inertia parameters without considering friction and presuming that all

connecting rods are rigid bodies (regardless of the flexibility of the connecting rods).

$$Y(q,\dot{q},\ddot{q})P = \tau \tag{4.2}$$

where P is the complete set of inertial parameters (standard parameters), which includes the unknown parameters of the robot model that need to be estimated or identified. These parameters can include the inertial parameters of the robot links (such as mass, center of mass, and inertia tensor components), friction parameters, and other parameters that affect the robot's dynamics. $Y(q,\dot{q},\ddot{q})$ represents the dynamic matrix that describes the relationship between joint positions q, joint velocities $\dot{q}$, and joint accelerations $\ddot{q}$. It captures the dynamic behavior of the system and is typically derived from the robot's equations of motion.

τ represents the joint torque vector, which represents the torques or forces applied to the robot joints. These torques can be generated by various factors, such as external loads, actuator dynamics, and control inputs. By solving this equation, we can estimate the unknown parameters of the robot model based on measured joint torques and kinematic information.

$$P_i = [I_{ixx}, I_{ixy}, I_{ixz}, I_{iyy}, I_{iyz}, I_{izz}, m_i r_x, m_i r_y, m_i r_z, m_i]^T \tag{4.3}$$

In Equation (4.3), the vector P_i represents the parameters associated with the i-th link of a robot manipulator. The meaning of each parameter is explained below:

I_{ixx} is the moment of inertia of the i-th link around the x-axis. I_{ixy} is the product of inertia of the i-th link between the x and y axes. I_{ixz} is the product of inertia of the i-th link between the x and z axes. I_{iyy} is the moment of inertia of the i-th link around the y-axis. I_{iyz} is the product of inertia of the i-th link between the y and z axes. I_{izz} is the moment of inertia of the i-th link around the z-axis. r_x is the distance from the center of mass of the i-th link to the x-axis. r_y is the distance from the center of mass of the i-th link to the y-axis. r_z is the distance from the center of mass of the i-th link to the z-axis. m_i is the total mass of the i-th link.

The Coulomb and viscous friction models are:

$$\tau_f = [f_v, f_c] \begin{bmatrix} \dot{q} \\ \text{sgn}(\dot{q}) \end{bmatrix} \tag{4.4}$$

In Equation (4.4), the vector τ_f represents the friction torque applied to the robot joints. Let us explain the meaning of each parameter:

f_v is the viscous friction coefficient. It represents the damping effect in the motion of the joint, where the magnitude of the friction torque is proportional to the velocity of the joint $\dot{q}$. f_c is the Coulomb friction coefficient. It represents static friction in joint motion, where the friction torque remains constant until a threshold velocity is reached. The sign function $\text{sgn}(\dot{q})$ is used to determine the direction of the Coulomb friction torque. This friction torque affects the dynamics of the manipulator and must be considered for accurate modeling and control of the robot's motion.

Consider the torque effect of friction at the joints. As a result, the following (4.5) exist:

$$\begin{aligned}\tau &= Y'p' \\ &= [\ddot{q},0,0,0,0,0,g\sin(q),g\cos(q),0,0,\dot{q},\text{sgn}(\dot{q})]\cdot \\ &[I_{xx},I_{xy},I_{xz},I_{yy},I_{yz},I_{zz},mr_x,mr_y,mr_z,m,f_v,f_c]^T\end{aligned} \tag{4.5}$$

In Equation (4.5), the vector τ represents the total torque exerted on the robot joints. The meaning of each parameter is explained below:

$\ddot{q}$ is the joint acceleration vector. g is the acceleration due to gravity. q is the joint angle vector. It represents the current positions of the robot joints. I_{xx}, I_{xy}, I_{xz}, I_{yy}, I_{yz}, I_{zz} are the elements of the inertia matrix. These parameters represent the moments of inertia of the robot links around different axes. m is the mass of the link. r_x, r_y, r_z are the center of mass position of the link. These parameters represent the distances between the joint axis and the center of mass of the links along different axes. f_v is the viscous friction coefficient. It represents the damping effect on joint motion. f_c is the Coulomb friction coefficient. It represents static friction or stiction in the joint motion. The equation computes the total torque τ experienced by the robot joints. This torque accounts for the effect of joint acceleration, gravity, inertia, mass distribution, and friction in the robot's dynamics.

4.2.2 Introduction to the classic Bouc-Wen model

For modeling flexible joints, the classic Bouc-Wen model (CBW) is commonly used. The CBW model is used to describe the effects of hysteresis on the joint and represents the relationship between the input position $u(t)$ and the output joint torsion as follows:

$$\Delta\theta(t) = q - \frac{\theta(t)}{N} = z(t) + x(t) \tag{4.6}$$

where $\Delta\theta(t)$ is the joint torsion (positional deviation), q is the position of the input joint, $\theta(t)$ is the position of the output joint, N is the joint reduction ratio, $z(t)$ is the joint torsion between the motor side and the load side, and $x(t)$ is the hysteresis variable representing positional deviation.

Using the CBW model, the joint torque can be represented as a function of joint position and speed:

$$T(t) = D \times \dot{\mathrm{u}}(t) + \Gamma(\mathrm{u}(t), t) \tag{4.7}$$

Where D is the internal damping coefficient, $T(t)$ is the joint torque. The following are the definitions of a Bouc-Wen-like hysteresis model:

$$\Gamma(u(t), t) = wk|u(t)| + (1-w)k|x(t)| \tag{4.8}$$

where $u(t)$ is the input position for the one-joint system, $\dot{u}(t)$ is the velocity. $\Gamma(u(t), t)$ represents the output torque of hysteresis, composed of an elastic term $wk|u(t)|$ and a purely hysteretic term $(1-w)k|x(t)|$ with parameters k and w. x is a hysteresis variable that is the solution of (4.9).

A plastic torque response (w=0) and a completely elastic torque response (w=1) are weighted differently. Stiffness is denoted by k.

The hysteresis output torque $\Gamma(u(t), t)$ is composed of two components: an elastic term $wk|u(t)|$ and a purely hysteretic term $(1-w)k|x(t)|$, where the parameters k and w represent stiffness and weight, respectively. The hysteresis variable $x(t)$ is governed by the following equation:

$$\dot{x}(t) = \alpha\dot{\mathrm{u}}(t) - \beta|\dot{\mathrm{u}}(t)|x(t)|^{n-1}x(t) - \gamma\dot{\mathrm{u}}(t)|x(t)|^{n} \tag{4.9}$$

The friction term f can be expressed as follows:

$$f = f_c \times \dot{u}(t) + f_v \times \mathrm{sgn}(\dot{u}(t)) + C \tag{4.10}$$

where f is the friction torque, f_c is the Coulomb friction coefficient, f_v is the viscous friction coefficient, and C is the constant term. The CBW model allows for accurate modeling of the hysteresis effects and friction in flexible robot joints, providing a more comprehensive representation of the joint's behavior.

The classical Bouc-Wen (CBW) model (Ikhouane and Rodellar, 2007) is developed to describe the hysteresis effect in (4.9) and the output torque in (4.11), we define the

constants $ku = wk$, $kh = (1-w)k$.

$$\begin{aligned} T(t) &= D \times \dot{\mathrm{u}}(t) + k_u \times u(t) + k_h \times x(t) \\ &+ f_c \times \dot{\mathrm{u}}(t) + f_v \times \mathrm{sgn}(\dot{\mathrm{u}}(t)) + C \end{aligned} \tag{4.11}$$

4.3 Results and discussion

The researchers conducted experiments to evaluate the performance of the SGHMC algorithm. This assessment focused on the identification of parameters for a heavy-duty manipulator. We used real-world data and compared the SGHMC method with the traditional LS method using the RMSE as an evaluation metric.

The findings demonstrated that the SGHMC algorithm exhibited superior accuracy and computational efficiency compared to the LS method. It provided more precise estimates of the model parameters, including inertial and friction parameters, thus improving the accuracy and reliability of the dynamic model.

Posterior parameter distributions of (4.5)

Table 4.1: The results of the Least Square method and SGHMC method in (4.5).

Parameter	Description	Unit	Least Square	SGHMC	95% Credible Interval
1	I_{xx}	$\mathrm{kg}\cdot\mathrm{m}^2$	6685.166	6681.266	[6599.640, 6753.321]
2	mr_x	$\mathrm{kg}\cdot\mathrm{m}$	20.779	20.780	[19.302, 22.305]
3	mr_y	$\mathrm{kg}\cdot\mathrm{m}$	-34.543	-34.523	[-38.549, -30.420]
4	f_v	$\mathrm{N}\cdot\mathrm{s}/\mathrm{m}$	8683.272	8682.911	[8663.980, 8702.206]
5	f_c	N	2352.660	2352.936	[2332.964, 2372.455]

In Table 4.1 parameters 1 to 5 represent the following variables: I_{xx} (Moment of inertia around the X-axis), mr_x (Product of mass and distance along the X-axis), mr_y (Product of mass and distance along the Y-axis), f_v (Viscous friction coefficient), and f_c (Coulomb friction coefficient).

The RMSE between the predicted output torque values using the estimated values of the

SGHMC method and the true output torque values is 2227.144.

The RMSE between the predicted output torque values using the estimated values of the LS method and the true output torque values is 2227.144.

Figure 4.11 displays the comparison between the true output torque values and the predicted output torque values obtained using the SGHMC method for (4.5). The graph illustrates that the SGHMC predictions closely align with the true values, indicating the method's effectiveness in accurately estimating the output torque. In Figure 4.12, the corner plot shows the posterior distributions of the parameters in Equation (4.5) obtained by the SGHMC method. The plot provides valuable insights into the uncertainties and correlations between the parameters, aiding in a comprehensive understanding of the system's dynamics.

Table 4.1 presents the results of the least squares (LS) method and the SGHMC method for Equation (4.5). The table highlights the estimated values for the parameters, along with their respective 95% credible intervals. It can be observed that the SGHMC method yields parameter estimates that are close to those obtained from the LS method.

Posterior parameter distributions of SGHMC in (4.11)

Table 4.2: The results of the Least square method and SGHMC method in (4.11).

Parameter	Description	Unit	Least square	SGHMC	95% Credible interval
1	k_u	-	-761.529	-689.076	[-1501.594, 16.680]
2	k_h	-	16909.986	16987.952	[16027.840, 17666.666]
3	f_v	$\mathrm{Nm}/(\mathrm{m}/\mathrm{s})$	9069.448	9305.415	[8137.896, 10057.360]
4	$D+f_c$	$\mathrm{Nm}/(\mathrm{m}/\mathrm{s})$	492.014	375.168	[-711.280, 1582.123]
5	C	Nm	-492.237	-412.486	[-1520.071, 631.033]

The parameters 1 to 5 in Table 4.2 are: k_u (proportional gain for input $u(t)$), k_h (proportional gain for input $x(t)$), f_v (viscous friction coefficient), $D+f_c$ (sum of Coulomb friction coefficient and inertia) and C (contant term) in (4.11).

The RMSE between the predicted output torque values using the estimated values of the SGHMC method and the true output torque values is 1705.926.

The RMSE between the predicted output torque values using the estimated values of the LS method and the true output torque values is 1845.883.

Figure 4.13 and Figure 4.14, along with Table 4.1, show the results of the LS and SGHMC methods applied to identify the parameters in (4.11). Figure 4.13 illustrates the comparison between the true output torque values and the predicted output torque values obtained using both the SGHMC method and the least squares (LS) method for (4.11). The graph shows that the SGHMC method achieves a closer fit to the true values compared to the LS method, indicating its superior performance in accurately estimating the output torque.

In Figure 4.14, the plot presents the posterior distributions of the parameters in Equation (4.11) obtained by the SGHMC method. This visualization provides valuable information about the uncertainties associated with the parameter estimates and facilitates a comprehensive understanding of their distributions.

Table 4.2 presents the results of the LS method and the SGHMC method for (4.11). The table shows the estimated values for the parameters, along with their respective 95% credible intervals. The effectiveness of the SGHMC method can be observed from the table. The provided RMSE values of 1705.926 and 1845.883 indicate the respective accuracies of the SGHMC and LS methods in predicting the output torque.

Efficiency comparison of MCMC and SGHMC method: mean autocorrelation and Rhat

The provided Figure 4.3 shows the comparison between the true output torque and the predicted output torque obtained using the MCMC method in (4.11). The Table 4.3

Table 4.3: The results of MCMC Method in (4.11).

Parameter	Description	Unit	MCMC	95% Credible Interval
1	k_u	-	-714.487	[-766.713, -666.645]
2	k_h	-	16921.728	[16876.993, 16953.551]
3	f_v	$\mathrm{Nm}/(\mathrm{m/s})$	9051.270	[9023.947, 9079.557]
4	$D+f_c$	$\mathrm{Nm}/(\mathrm{m/s})$	475.074	[436.007, 511.528]
5	C	Nm	-587.327	[-642.374, -503.742]

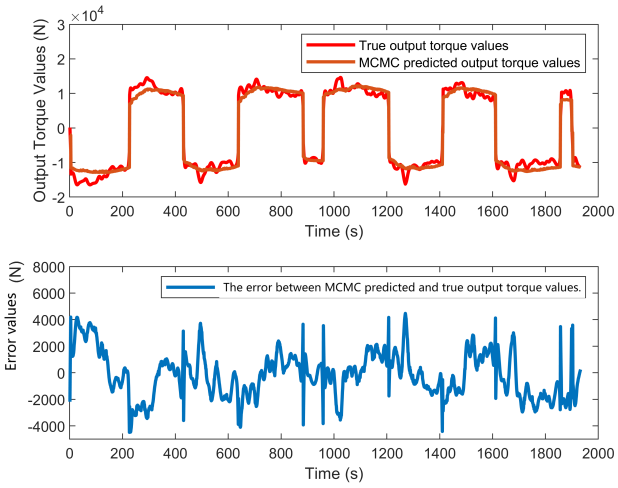

Figure 4.3: This image plots the true output torque and the MCMC method predicted output torque in (4.11).

presents the results of the MCMC method, including the estimated parameter values and their corresponding 95% credible intervals. The root mean squared error (RMSE) between the predicted output torque values (based on the estimated parameter values) and the true output torque values is 1741.990.

The figure visually demonstrates the agreement between the predicted and true output torques, indicating that the MCMC method captures the underlying patterns reasonably well. The relatively small RMSE value suggests that the MCMC method provides accurate predictions with a reasonable level of precision.

In general, based on visual comparison, parameter estimates, interval estimates, and RMSE, the MCMC method shows promising performance in predicting the output torque. We calculate the autocorrelation of the samples obtained from both algorithms

Table 4.4: Mean autocorrelation values for MCMC and SGHMC method.

No.	1	2	3	4	5
MCMC	0.7×10^{-3}	-0.8×10^{-3}	3.4×10^{-3}	-0.2×10^{-3}	1.9×10^{-3}
SGHMC	-0.599×10^{-3}	0.679×10^{-4}	-0.93×10^{-5}	0.293×10^{-3}	-0.747×10^{-4}

and compare them. Lower autocorrelation indicates higher efficiency, since it implies

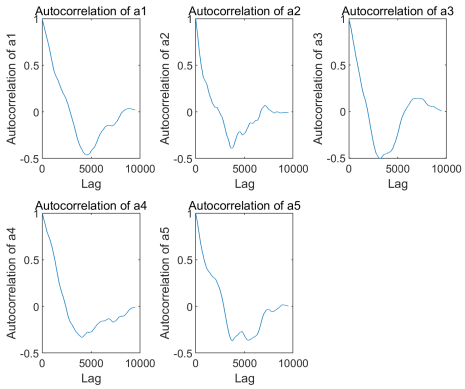

Figure 4.4: The autocorrelation values of the samples obtained from SGHMC algorithm in (4.11). For definitions and values of the parameters depicted in this figure, refer to Table 4.2.

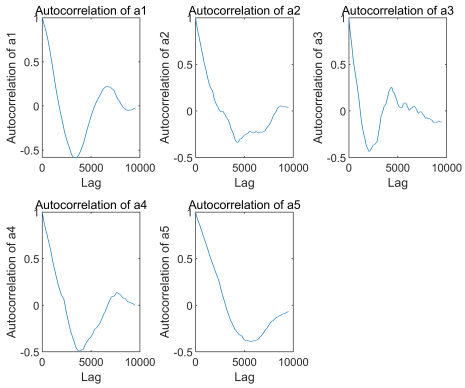

Figure 4.5: The autocorrelation values of the samples obtained from MCMC algorithm in (4.11). For definitions and values of the parameters depicted in this figure, refer to Table 4.2.

that subsequent samples are less dependent on each other. The autocorrelation function is presented in the third chapter of this article (Foreman-Mackey et al., 2013).

Based on the average autocorrelation values and in the provided Creffig32 and Figure 4.5, it can be observed that the SGHMC algorithm has values relatively smaller compared to the MCMC algorithm. Values range from -0.5994e-03 to 0.2927e-03 for SGHMC, while MCMC has values ranging from -0.0008 to 0.0034.

This suggests that the SGHMC algorithm exhibits faster convergence and better mixing properties compared to the MCMC algorithm. The lower autocorrelation values indicate

that the samples generated by SGHMC are less correlated and reach stationarity more quickly. This can lead to more efficient exploration of the parameter space and faster convergence to the target distribution. In summary, based on average autocorrelation values, the SGHMC algorithm demonstrates faster convergence compared to the MCMC algorithm. The smaller autocorrelation values indicate a faster exploration of the parameter space in SGHMC.

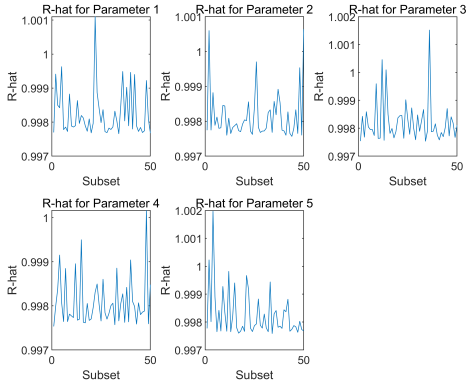

Figure 4.6: The RHat values of SGHMC algorithm of the samples obtained from the (4.11). For definitions and values of the parameters depicted in this figure, refer to Table 4.2.

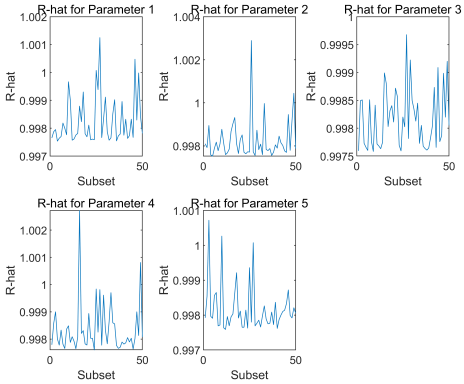

Figure 4.7: The RHat values of MCMC algorithm of the samples obtained from the (4.11). For definitions and values of the parameters depicted in this figure, refer to Table 4.2.

The Gelman-Rubin convergence statistic (RHat) (Vats and Knudson, 2021) is commonly used to assess the convergence of Monte Carlo chains. It provides a measure of how well multiple chains agree with each other and whether they have reached convergence to the desired distribution. In general, RHat values below 1.1 indicate that the chains have

Table 4.5: RHat average values for MCMC and SGHMC

Parameter	1	2	3	4	5
MCMC	0.9982	0.9982	0.9984	0.9983	0.9984
SGHMC	0.9983	0.9981	0.9982	0.9981	0.9983

converged. Therefore, RHat values less than 1.1 are typically considered indicative of satisfactory convergence to the desired distribution.

Compare the number of iterations required for both algorithms to converge to a reasonable estimate of the target distribution. In Figure 4.6, Figure 4.7, and Table 4.5, the number of iterations for both algorithms is set to 10000. We calculate the Rhat value every 200 points. By observing the convergence behavior, we can assess which algorithm converges faster. According to the results of the calculation, the RHat values of the MCMC and SGHMC algorithms are close to 1, indicating that they have a good convergence in parameter estimation.

However, from the results, the RHat value of the SGHMC algorithm is relatively slightly lower, indicating that it may be slightly better than the MCMC algorithm in terms of convergence speed. This may be because the SGHMC algorithm introduces randomness when updating the parameters and utilizes stochastic gradient estimation to speed up the convergence process. On the contrary, the MCMC algorithm uses Metropolis-Hastings sampling and its update process is relatively conservative.

Overall, the SGHMC algorithm may achieve better convergence in a shorter number of iterations, while the MCMC algorithm may require more iterations to achieve similar results.

Posterior parameter distributions of SGHMC in (4.9)

Table 4.6: The results of the least square method and SGHMC method in (4.9).

Parameter	Description	Least square	SGHMC	95% Credible interval
1	α	0.003	0.040	[-0.028, 0.121]
2	β	0.002	0.012	[-0.047, 0.072]
3	γ	-0.042	-0.011	[-0.160, 0.149]

Parameters 1 to 3 in Table 4.6 represent the following variables: α (the shape constant

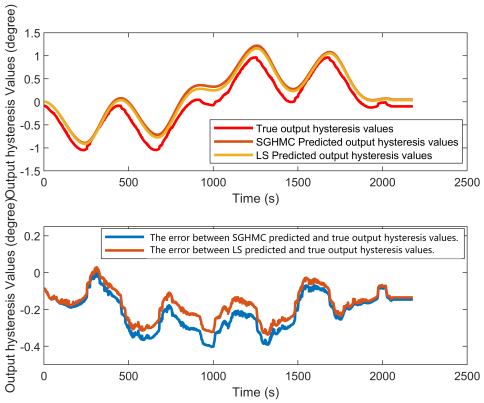

Figure 4.8: True hysteresis values, the SGHMC method, and Least square method predicted hysteresis values in (4.9).

of the hysteresis curve), β (the shape constant of the hysteresis curve), and γ (the shape constant of the hysteresis curve) in equation (4.9). They are coefficient factors that affect the behavior of the equation, so they do not have specific units of measurement.

Determine n = 1 first and then proceed with the calculation, as a slight change in the value of n will result in a significant change in the results of hysteresis. Sensitivity analysis will be conducted in the next section.

The RMSE between the predicted hysteresis values using the estimated values of the SGHMC method and the true hysteresis values is 0.234. The RMSE between the predicted hysteresis values using the estimated values of the LS method and the true hysteresis values is 0.545.

Lastly, Figure 4.8, Figure 4.9, and Figure 4.10, along with Table 4.6, exhibit the results of LS and SGHMC methods for the identification of parameters in Equation (4.9).

Figure 4.8 showcases the comparison between the true hysteresis values and the predicted hysteresis values obtained using the SGHMC method and the least squares (LS) method for Equation (4.9). It can be observed that the SGHMC method provides a closer match to the true values compared to the LS method, indicating its superior performance in accurately estimating the hysteresis behavior of the system.

In Figure 4.9, the corner plot of the posterior distributions for Equation (4.9) is displayed. This plot provides a comprehensive visualization of the uncertainties associated with the estimated parameters. When examining the intersections of the histograms, valuable insights can be gained regarding the correlations and probability distributions of the parameters. Figure 4.10 presents the posterior distributions for

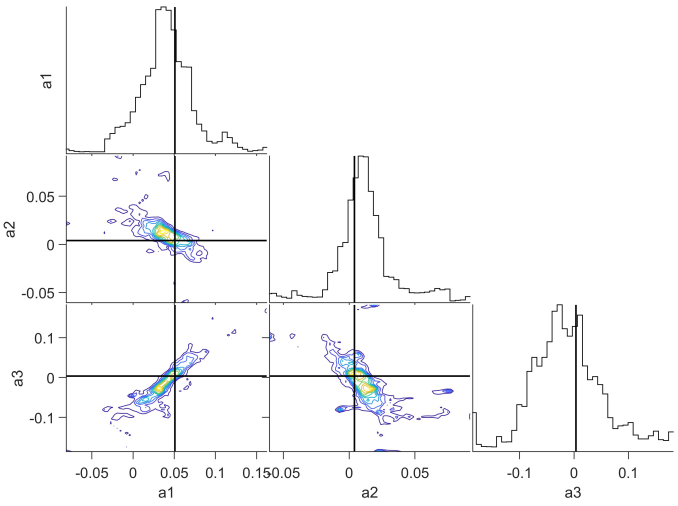

Figure 4.9: This image plots the corner plot of the posterior distributions in (4.9). For definitions and values of the parameters depicted in this figure, refer to Table 4.6.

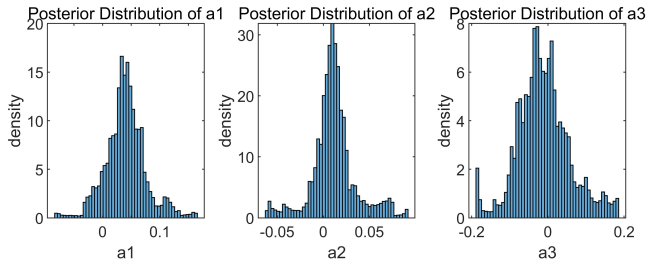

Figure 4.10: This image plots the posterior distributions in (4.9). For definitions and values of the parameters depicted in this figure, refer to Table 4.6.

Equation (4.9). This plot provides a detailed representation of the probability density functions for each parameter.

Table 4.6 summarizes the results obtained from the LS method and the SGHMC method for Equation (4.9). The table shows the estimated values for the parameters, along with their respective 95% credible intervals. It can be observed that the SGHMC method yields parameter estimates that differ from those obtained by the LS method. The RMSE values represent the prediction accuracy of the SGHMC and LS methods when estimating hysteresis values, respectively. The SGHMC method exceeds the LS method in capturing the hysteresis behavior of the system, which is shown by a lower RMSE value.

Furthermore, the researchers performed sensitivity analysis to identify key parameters

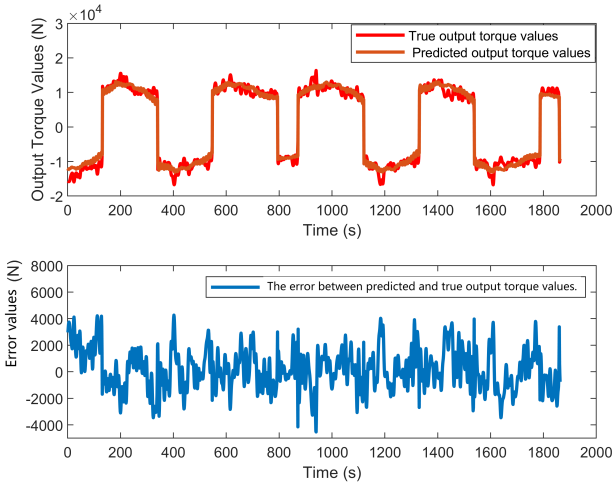

Figure 4.11: The observed actual output torque values and the output torque values predicted by the SGHMC method in (4.5).

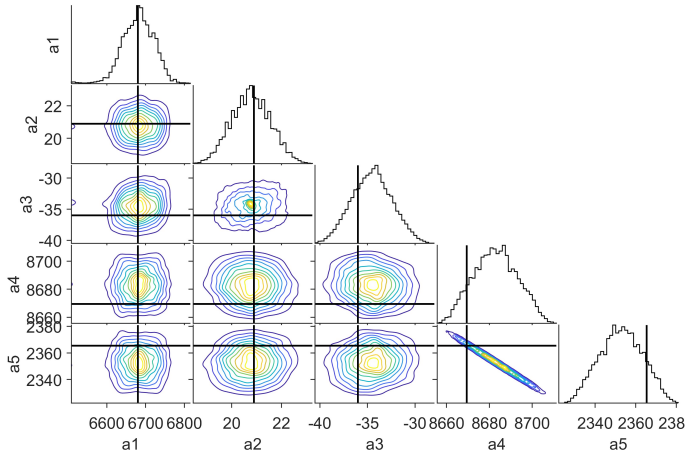

Figure 4.12: The corner plot of the posterior distributions (4.5) is illustrated in the provided image. For definitions and values of the parameters depicted in this figure, refer to Table 4.1.

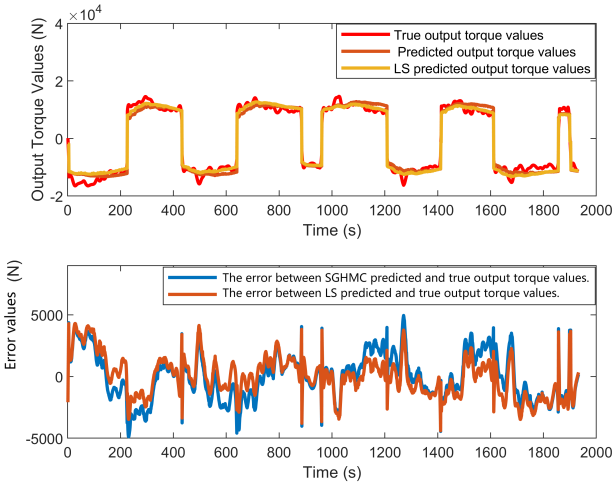

Figure 4.13: The given plot presents a comparison of the true output torque values with the predicted output torque values obtained using the SGHMC method and the least square method in (4.11).

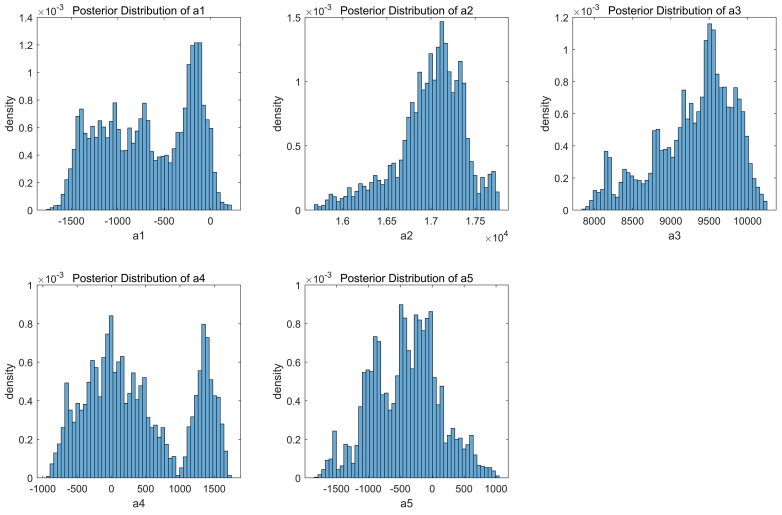

Figure 4.14: The provided image visualizes the posterior distributions in (4.11). For definitions and values of the parameters depicted in this figure, refer to Table 4.2.

.

that significantly influenced the manipulator's output torque. Using first-order and total-effect sensitivity indices, this study investigated the impact of various parameters on the output torque. Please refer to (Qi, Huapeng, Yuntao, et al., 2023) for specific parameters.

Discussion of results and findings
After comparing the RMSE values of the predicted output torque obtained using both methods for two different equations (Equation (4.5) and Equation (4.7)), the superiority of the SGHMC method over the LS method in Equation (4.7) was evident. The SGHMC method achieved an approximate 8.16% reduction in RMSE in Equation (4.7), indicating its superior predictive performance in modeling the hysteresis effect.

Figure 4.11, Figure 4.12, Figure 4.13, Figure 4.14, and Figure 4.9 displayed the results of parameter identification using both methods for different equations. In Figure 4.11 and Figure 4.13, the SGHMC algorithm has been shown to be a powerful tool to achieve accurate parameter estimation, showing closer alignment with true values compared to the LS method. The corner plots in Figure 4.12, Figure 4.14, and Figure 4.9 provided information on parameter uncertainties and correlations. Using the SGHMC algorithm, a comprehensive understanding of the system's dynamics and hysteresis behavior was obtained.

This discovery has a great impact on the development of heavy-duty robotic arms. SGHMC outperforms LS for parameter estimation. Through sensitivity analysis, key parameters that affect system behavior are identified, aiding the design of reliable robotic joints. This research improves the methods of estimating robotic arm parameters, demonstrating the potential of the SGHMC algorithm.

Despite the encouraging results, the study acknowledges certain limitations. To acquire a more complete understanding of the manipulator's performance under real-world conditions, future research should also consider external factors such as temperature and disturbances.

In the field of robotics, parameter identification is a cornerstone of enhancing performance, accuracy, and reliability. This is demonstrated by the work described in (Qi, Huapeng, Yuntao, et al., 2023). The authors have paved the way for a deeper understanding of the complexities involved in robotic arms, with a special emphasis on the CMOR robot arm and its implications for heavy-duty manipulators.

The adoption of the SGHMC method in parameter identification is illustrated in (Qi, Huapeng, Yuntao, et al., 2023). The deviation from conventional MCMC methods is justified by the obvious benefits that SGHMC provides. In a world where computational speed and precision are of the highest priority, SGHMC's faster convergence and decreased computational time make it an indispensable instrument, especially for robotic systems.

Furthermore, the emphasis on the Bouc-Wen model and the subsequent validation of the effectiveness of the SGHMC algorithm provide an academic foundation for future research endeavors. Our findings impact the design and optimization of robotic systems, leading to improved performance and reliability in real-world usage.

5 Conclusions and future directions

This chapter evaluates techniques for robot parameter identification, highlighting MCMC and SGHMC for their exceptional performance and practical benefits. We intend to provide a concise comparative analysis suited to various robotic scenarios. In Sections 5.2 and 5.3, the limitations, applications, and prospective research directions of these methods are elaborated.

5.1 Key findings from the comparative study of inference methods

In this section, we provide a brief summary of our comparative study of inference methods for heavy-duty and lightweight robotic arms. We emphasize the advantages and disadvantages of each method and discuss its applicability to various robotic systems.

Key findings in (Qi, Huapeng, Cheng, et al., 2022):

Friction is an essential but frequently neglected factor in robotic mechanics. The complexity of this physical phenomenon can determine the efficacy, control, and even longevity of robotic operations. Recognizing this, our investigation journey, as detailed in (Qi, Huapeng, Cheng, et al., 2022), strived to shed light on the nuances of friction estimation, particularly for harmonic drive joints.

Our exploration delved deep into the MCMC methodology, juxtaposing it with traditional methods to discern its efficacy. This rigorous comparison bore several critical insights:

1. In addition to its accuracy, the MCMC method demonstrated remarkable resistance to background disturbances. In scenarios where external factors such as different velocities, changes in ambient temperature, or load conditions are prevalent, the MCMC approach maintained its precision. This robustness, especially in the face of friction noise interference, is a method designed for the rigors of real-world applications.

2. Furthermore, while precision in prediction is crucial, the ability to gauge the inherent uncertainty of those predictions is equally important. This dual capacity of the MCMC method – to not only predict but also quantify the associated uncertainty – provides researchers and practitioners with a holistic tool that aids both theoretical studies and practical implementations.

3. We also outline a comprehensive framework that uses the MCMC method to identify friction in harmonic drive joints.

To summarize, the findings of (Qi, Huapeng, Cheng, et al., 2022) accentuate the pivotal role of sophisticated friction modeling in robotic joints. The MCMC method emerges not

only as an alternative, but also as a superior model in this field, creating the groundwork for robotics that are more reliable.

Key findings in Section 3.3:

The complex phenomenon of hysteresis within robotic arms requires a deep understanding, particularly when aiming to optimize their functioning in real-world environments. As described in Section 3.3, our academic investigation deeply explored the domain of these dynamics, finding a wealth of information on the behavior of robotic arms under a variety of operational conditions. Here are some further reflections and elaborations on our central findings:

1. Although the least-squares method laid the foundational groundwork for our research, its true prowess was manifested in its compatibility with the MCMC and SGHMC algorithms. By supplying initial values, the method not only facilitated a seamless transition to more sophisticated algorithms but also bolstered the overall reliability of our analytical framework.

2. The decision to employ the fractional-order Bouc-Wen model stemmed from the realization that conventional models often fell short of capturing the torque and responses exhibited by robotic arms. This model, with its intricate incorporation of a fractional-order derivative, acts as a beacon in comprehending and, more importantly, replicating the nonlinear dynamics inherent in these systems. It should be noted that the SGHMC method, given its rapid convergence rate compared to MCMC, establishes itself as an indispensable tool in the repertoire of any researcher in this domain.

3. The interaction between the FOBW model and the SGHMC method demonstrated their combined efficacy. The resulting insights not only fortified the theoretical underpinnings of robotic arm dynamics, but also paved the way for practical advancements. Specifically, the enhanced accuracy in torque prediction and control is a testament to the applicability of our findings in real-world scenarios.

In conclusion, Section 3.3 shows the advances in understanding hysteresis dynamics in lightweight robotic arms. Beyond technical insights, this work emphasizes the need for ongoing innovation and methodological refinement in the rapidly advancing field of robotics.

Key findings in (Qi, Huapeng, Yuntao, et al., 2023):

In our study, as detailed in (Qi, Huapeng, Yuntao, et al., 2023), we explored inference methods for parameter identification in heavy-duty and lightweight robotic arms. Here is a condensed summary of our findings:

The SGHMC method stands out for parameter identification in heavy-duty manipulators. It surpasses conventional least squares (LS) methods in terms of accuracy and computational efficiency. It succeeds in anticipating output torque and modeling hysteresis behavior, making it an indispensable instrument for modeling dynamic systems.

Although we reviewed other inference methods suitable for heavy-duty and lightweight robotic arms, none rivalled the performance of SGHMC for heavy-duty applications. Although these methods show potential in specific contexts, they warrant further exploration and validation.

The study highlights the importance of tailoring the chosen inference method to the specific robotic system. While SGHMC is designed for heavy-duty manipulators and handles large datasets efficiently, lightweight robotic arms might benefit from alternative methods.

In essence, (Qi, Huapeng, Yuntao, et al., 2023) makes a significant contribution by showcasing SGHMC's efficiency in parameter identification for heavy-duty robots. Still, the choice of inference method should always consider the specific characteristics of the system.

5.2 Limitations and implications of inference methods

This section discusses the limitations of the various inference methods analyzed in this study. We discuss the potential obstacles and uncertainties that may arise during parameter identification and provide recommendations to address these problems.

Limitations in (Qi, Huapeng, Cheng, et al., 2022):

Although the MCMC method is effective in identifying friction for harmonic drive joints, it faces the following obstacles:

1. Monte Carlo sampling requires a large number of samples, which increases the computational complexity of the method. For an efficient approximation, particularly in complex robotic systems, it is essential to improve sampling techniques.

2. The method is sensitive to data disturbances. Noise may affect parameter estimates and diminish the reliability of the model.

3. The accuracy of the MCMC method is dependent upon the selection of appropriate prior distributions. When people make bad choices, the results can be unfair.

Despite these obstacles, the MCMC remains a valuable instrument for identifying friction in harmonic drive joints.

Limitations in Section 3.3:

The SGHMC methods evaluated for identifying hysteresis in lightweight robotic arms, though effective, have certain limitations:

1. Obtaining quality data from real-world robotics can be challenging. Better data acquisition is crucial to improving the accuracy of hysteresis models.

2. Robotic arm hysteresis is inherently complex. Traditional linear methods may fail to capture this complexity, necessitating advanced nonlinear regression techniques. However, even these might not fully represent the hysteresis behavior.

3. The choice of models is vital for an accurate representation of hysteresis. The selected model can significantly influence the accuracy and applicability of the results, so it is imperative to consider the characteristics and data of the system.

In summary, while the methods studied show potential for hysteresis identification in lightweight robotic arms, they come with inherent challenges.

Limitations in (Qi, Huapeng, Yuntao, et al., 2023):

The study of inference methods for the identification of the heavy-duty manipulator parameter showed both positive results and highlighted challenges. We address these limitations and offer potential solutions:

1. Choosing the right model for the dynamics of the system is crucial. The inference methods analyzed require varied model structures, making selection complicated. A deep understanding of the system and relevant data can guide this decision.

2. Data quality and quantity play a crucial role in parameter identification. Precise experimental data is challenging to obtain, often leading to uncertainty in estimation.

3. Certain methods, such as SGHMC, require hyperparameter tuning for peak performance.

In summary, while methods such as SGHMC offer potential in parameter identification, challenges such as model selection, data accuracy, and hyperparameter tuning remain.

After examining the limitations of various inference methods, we found that it is essential

to implement solutions.

1. For computational complexity problems, an algorithm structure that can be optimized, such as a modular design or hierarchical structure, may help improve computational efficiency and make the algorithm more adaptable to complex industrial environments.

2. Secondly, for the issue of data sensitivity, future research should not only focus on the quality of the data, but also require in-depth preprocessing of the data. By employing advanced data processing, filtering techniques, and outlier detection, we can reduce the impact of noise and other anomalous data, thus improving the reliability of the model.

3. Furthermore, choosing an appropriate prior distribution is a critical step for many inference methods. Future research could consider the use of data-based methods to estimate the most appropriate distribution. This method can not only increase the robustness of the model, but also improve its generalization ability, so that the model can perform well in various scenarios.

In summary, to maximize the performance of inference methods, we need to understand their potential limitations and adopt effective strategies for addressing them.

5.3 Proposed Strategies for Advancing Robotic Manipulators in Industrial Applications

In this section, we outline future research strategies aimed at improving robotic performance in industrial settings, especially addressing the limitations mentioned in Section 5.2. By integrating recent technological advancements, we suggest focusing on improved inference techniques, experimental methods, and control algorithms to optimize robotic operations.

Proposed strategies and outlook in (Qi, Huapeng, Cheng, et al., 2022):

In the ever-changing field of robotics, it is necessary to strategically align our research directions with the evolving technological trends and obstacles. A number of practical options for future development emerge from (Qi, Huapeng, Cheng, et al., 2022):

1. Expanding test scenarios: While primary research has been conducted in a laboratory setting, a thorough validation of the MCMC method requires it to undergo a variety of stress tests. These could range from high-speed operations to environments with variable temperature and pressure conditions, thereby assessing the method's resilience.

2. Incorporation of AI and machine learning: Integrating AI-driven predictive models with the MCMC method can be useful as we enter an era dominated by artificial intelligence. These integrations could facilitate friction adjustments in real time, thus preventing operational failures.

3. Customization based on robotic application: While general applicability is desired, specific customization for autonomy systems, based on their operational domain and functional requirements, could increase efficiency. Such specialized modifications can address the specific frictional challenges encountered by various robots.

Ultimately, advances in sensor technology and data collection can further enhance the precision of the method for industrial robotic manipulators.

Proposed strategies and outlook in Section 3.3:

For the identification of hysteresis in harmonic drive joints, future research should prioritize the following:

1. Combining with other optimization algorithms or deep learning to improve the accuracy of identification.

2. Expanding the experimental data to involve a variety of conditions, thereby enhancing the general applicability of the model.

3. In-depth analysis and validation of the SGHMC method for broader applications.

These advances will strengthen the role of SGHMC in improving robotic control and precision.

Proposed strategies and outlook in (Qi, Huapeng, Yuntao, et al., 2023):

Given the substantial significance and possible effects of our research findings, it is crucial to adopt a rigorous and systematic approach when implementing and advancing these ideas. Expanding upon the methods discussed above, we offer the following viewpoints.

1. Broadening applications: The efficacy of SGHMC in the context of heavy-duty manipulators requires a comprehensive evaluation of its adaptability across a diverse range of robotic designs. This involves performing comprehensive evaluations on a variety of systems, including mobile robots and industrial assembly line robots. Conducting comprehensive trials of this nature would provide a comprehensive perspective on the strengths and potential areas for improvement of SGHMC.

2. **I**nfrastructure and computation: As SGHMC scales to handle more complex robotic systems, the underlying computational infrastructure needs to be enhanced. This might require investment in high-performance computing clusters and the development of specialized software to ensure efficient and accurate parameter estimation.

The investigation of techniques for the identification of robot parameters was emphasized throughout this study, with a particular focus on the potential and applicability of the MCMC and SGHMC methods. Both approaches demonstrated outstanding abilities in resolving the complex challenges posed by heavy-duty and light-weight robotic systems. The importance of accurately modeling and comprehending properties such as friction and hysteresis in robotic joints was emphasized, and the effectiveness of the MCMC method in high-noise situations was demonstrated. Similarly, the SGHMC method, with its proficiency in parameter identification for heavy-duty manipulators, emerged as the winner in terms of precision and computational efficiency.

The focus of the research is on refining the application of these inference methods, integrating them with advanced control strategies, improving sensor technologies, and developing additional optimization algorithms. With the rapid evolution of industrial robotics and its increasing participation in complex operations, this body of work lays the foundations for enhancing robotic performance in industrial settings, highlighting the need for continuous innovation and improvement in parameter identification techniques.

References

Astrom, K. J. and Canudas-De-Wit, C. (2008). Revisiting the LuGre Friction Model STICK-SLIP MOTION AND RATE DEPENDENCE. In: *Ieee Control Systems Magazine* 28.(6), pp. 101–114. DOI: 10.1109/mcs.2008.929425.

B'Elanger, P. R. and Taghirad, H. D. (2002). An Experimental Study on Modelling and Identification of Harmonic Drive Systems. In: *Proceedings of 35th IEEE Conference on Decision and Control*.

Al-Bender, Farid, Lampaert, V., and Swevers (2005). The generalized Maxwell-Slip model: A novel model for friction simulation and compensation. In: *IEEE Transactions on Automatic Control* 50.(11), pp. 1883–1887.

Boschert, Stefan and Rosen, Roland (2016). Digital twin—the simulation aspect. In: *Mechatronic futures: Challenges and solutions for mechatronic systems and their designers*, pp. 59–74. ISSN: 3319321544.

Brooks, Steve P., Gelman, Andrew, Jones, Galin L., and Meng, Xiao-Li (2011). Handbook of Markov Chain Monte Carlo. In.

Cai, Jingnan, Dong, Wei, and Nagamune, Ryozo (2023). A survey of Bouc-Wen hysteretic models applied to piezo-actuated mechanical systems: Modeling, identification, and control. In: *Journal of Intelligent Material Systems and Structures*, p. 1045389X231157361. ISSN: 1045-389X.

Chen, Tianqi, Fox, Emily, and Guestrin, Carlos (2014). Stochastic gradient hamiltonian monte carlo. In: *International conference on machine learning*. PMLR, pp. 1683–1691.

Chia-Pei, Wang, Kaan, Erkorkmaz, John, McPhee, and Serafettin, Engin (2020). In-process digital twin estimation for high-performance machine tools with coupled multibody dynamics. In: *CIRP Annals* 69.(1), pp. 321–324. ISSN: 0007-8506.

Chitta, Sachin, Marder-Eppstein, Eitan, Meeussen, Wim, Pradeep, Vijay, Tsouroukdissian, Adolfo Rodríguez, Bohren, Jonathan, Coleman, David, Magyar, Bence, Raiola, Gennaro, and Lüdtke, Mathias (2017). ros control: A generic and simple control framework for ROS. In: *The journal of open source software* 2.(20), pp. 456–456.

Chunxia, Li, Linlin, Li, Guoying, Gu, and Limin, Zhu (Aug. 2016). Modeling of rate-dependent hysteresis in piezoelectric actuators using a Hammerstein-like structure with a modified Bouc-Wen model. In: *Intelligent Robotics and Applications: 9th International Conference, ICIRA 2016, Tokyo, Japan, Proceedings, Part I 9*. Springer, pp. 672–684. ISBN: 3319435051.

De León, Carlos Leopoldo Carreón-Díaz, Vergara-Limón, Sergio, Vargas-Treviño, María Aurora D, López-Gómez, Jesús, Gonzalez-Calleros, Juan Manuel, González-Arriaga, Daniel Marcelo, and Vargas-Treviño, Marciano (2022). Parameter identification of a robot arm manipulator based on a convolutional neural network. In: *IEEE Access* 10, pp. 55002–55019. ISSN: 2169-3536.

Dewit, C. C., Noel, P., Aubin, A., and Brogliato, B. (1991). ADAPTIVE FRICTION COMPENSATION IN ROBOT MANIPULATORS LOW VELOCITIES. In:

International Journal of Robotics Research 10.(3), pp. 189–199. DOI: 10.1177/027836499101000301.

Dhaouadi, R. (2003). A New Dynamic Model of Hysteresis. In: *Ieee T Ind Electron* 50, p. 1165. DOI: 10.1109/tie.2003.819661.

Do, T. N., Tjahjowidodo, T., Lau, M. W. S., and Phee, S. J. (2014). An investigation of friction-based tendon sheath model appropriate for control purposes. In: *Mechanical Systems and Signal Processing* 42.(1-2), pp. 97–114. DOI: 10.1016/j.ymssp.2013.08.014.

Ema, B, Osr, A, Db, A, and Xz, B (2020). Comprehensive modeling and identification of nonlinear joint dynamics for collaborative industrial robot manipulators. In: *Control Engineering Practice* 101.

Ema, B, Osr, A, Db, A, and Xz, B (2021). Adaptive feedforward control of a collaborative industrial robot manipulator using a novel extension of the Generalized Maxwell-Slip friction model. In: *Mechanism Machine Theory* 155.

Foreman-Mackey, D., Hogg, D. W., Lang, D., and Goodman, J. (2013). emcee: The MCMC Hammer. In: *Publications of the Astronomical Society of the Pacific* 125.(925), pp. 306–312. DOI: 10.1086/670067.

Friel, N. and Wyse, J. (2012). Estimating the evidence – a review. In: *Statistica Neerlandica* 66.(3), pp. 288–308.

Gandhi, P. S., Ghorbel, F. H., and Dabney, J. (2002). Modeling, identification, and compensation of friction in harmonic drives. In: *IEEE*.

Gargiulo, Laurent, Bayetti, Pascal, Bruno, Vincent, Hatchressian, Jean-Claude, Hernandez, Caroline, Houry, Michael, Keller, Delphine, Martins, Jean-Pierre, Measson, Yvan, and Perrot, Yann (2009). Operation of an ITER relevant inspection robot on Tore Supra tokamak. In: *Fusion Engineering and Design* 84.(2-6), pp. 220–223. ISSN: 0920-3796.

Gautier, Maxime and Poignet, Ph (2001). Extended Kalman filtering and weighted least squares dynamic identification of robot. In: *Control Engineering Practice* 9.(12), pp. 1361–1372. ISSN: 0967-0661.

Grieves, Michael and Vickers, John (2017). Digital twin: Mitigating unpredictable, undesirable emergent behavior in complex systems. In: *Transdisciplinary perspectives on complex systems: New findings and approaches*, pp. 85–113. ISSN: 3319387545.

Han, Bangcheng, Ma, Jijun, and Li, Haitao (2016). Research on nonlinear friction compensation of harmonic drive in gimbal servo-system of DGCMG. In: *International Journal of Control, Automation and Systems* 14.(3), pp. 779–786.

Hao, Lei, Pagani, Roberto, Beschi, Manuel, and Legnani, Giovanni (2021). Dynamic and Friction Parameters of an Industrial Robot: Identification, Comparison and Repetitiveness Analysis. In: *Robotics* 10.(1), p. 49. ISSN: 2218-6581. URL: https://www.mdpi.com/2218-6581/10/1/49.

Ikhouane, Fayçal and Rodellar, José (2007). *Systems with hysteresis: analysis, identification and control using the Bouc-Wen model*. John Wiley Sons. ISBN: 0470513195.

Jan, Swevers, Al-Bender, F., Ganseman, C. G., and Prajogo, T. (2000). An integrated friction model structure with improved presliding behavior for accurate friction compensation. In: *Ieee Transactions on Automatic Control* 45.(4), pp. 675–686. DOI: 10.1109/9.847103.

Jatta, F., Legnani, G., and Visioli, A. (2006). Friction compensation in hybrid force/velocity control of industrial manipulators. In: *Ieee Transactions on Industrial Electronics* 53.(2), pp. 604–613. DOI: 10.1109/tie.2006.870682.

Jiasheng, Liu, Kun, Lu, Pan, Hongtao, Cheng, Yong, and Yao, Zhixin (2020). Vision-based tile recognition algorithms for robot grasping task in EAST. In: *Fusion Engineering and Design* 152, p. 111422.

Kalan, Satyam, Chauhan, Sanket, Coelho, Rafael F, Orvieto, Marcelo A, Camacho, Ignacio R, Palmer, Kenneth J, and Patel, Vipul R (2010). History of robotic surgery. In: *Journal of Robotic Surgery* 4, pp. 141–147. ISSN: 1863-2483.

Kennedy, C. W. and Desai, J. P. (2003). Estimation and modeling of the harmonic drive transmission in the Mitsubishi PA-10 robot arm. In: *IEEE/RSJ International Conference on Intelligent Robots and Systems*.

Kennedy, C. W. and Desai, J. P. (2005). Modeling and control of the Mitsubishi PA-10 robot arm harmonic drive system. In: *Ieee-Asme Transactions on Mechatronics* 10.(3), pp. 263–274. DOI: 10.1109/tmech.2005.848290.

Kesner, S. B. and Howe, R. D. (2011). Position Control of Motion Compensation Cardiac Catheters. In: *Ieee Transactions on Robotics* 27.(6), pp. 1045–1055. DOI: 10.1109/tro.2011.2160467.

Kim, Dong-Hyun and Oh, Jun-Ho (2019). Hysteresis Modeling for Torque Control of an Elastomer Series Elastic Actuator. In: *IEEE/ASME Transactions on Mechatronics* 24, pp. 1316–1324.

Kingma, Diederik P and Ba, Jimmy (2014). Adam: A method for stochastic optimization. In: *arXiv preprint arXiv:1412.6980*.

Kircanski, N. M. and Goldenberg, A. A. (1997). An experimental study of nonlinear stiffness, hysteresis, and friction effects in robot joints with harmonic drives and torque sensors. In: *International Journal of Robotics Research* 16.(2), pp. 214–239. DOI: 10.1177/027836499701600207.

Krizhevsky, Alex, Sutskever, Ilya, and Hinton, Geoffrey E (2012). Imagenet classification with deep convolutional neural networks. In: *Advances in neural information processing systems* 25.

Kun, Wang, Qi, Wang, Huapeng, Wu, and Kun, Jiang (2018). A Geometric Algorithm for Redundant Inverse Kinematics with Obstacle Avoidance in a Known Environment. In: *Int. Rev. Mech. Eng.* 12.(8).

Kun, Wang, Qi, Wang, Yong, Cheng, Huapeng, Wu, Yuntao, Song, and Bruno, Vincent (2019). Optimization of the geometric parameters of the EAST articulated maintenance arm (EAMA) with a collision-free workspace determination in EAST. In: *Fusion Engineering and Design* 139, pp. 155–162. ISSN: 0920-3796.

Lampaert, V., Swevers, J., and Al-Bender, F. (2002). Modification of the Leuven integrated friction model structure. In: *IEEE Transactions on Automatic Control* 47.(4), pp. 683–687.

Liang, F., Liu, C., and Carroll, R. J. (2010). Advanced Markov Chain Monte Carlo Methods (Learning from Past Samples) || Index. In: pp. 353–357.

Llorens-Bonilla, Baldin and Asada, H. Harry (2014). A robot on the shoulder: Coordinated human-wearable robot control using Coloured Petri Nets and Partial Least Squares predictions. In: *2014 IEEE International Conference on Robotics and Automation (ICRA)*, pp. 119–125.

Llorente, F., Martino, L., Delgado, D., and Lopez-Santiago, J. (2020). Marginal likelihood computation for model selection and hypothesis testing: an extensive review. In: *arXiv e-prints*.

Luca, A. D. and Mattone, R. (2005). Sensorless Robot Collision Detection and Hybrid Force/Motion Control. In: *Robotics and Automation, 2005. ICRA 2005. Proceedings of the 2005 IEEE International Conference on*.

Marchand, Robert C, Sodhi, Nipun, Anis, Hiba K, Ehiorobo, Joseph, Newman, Jared M, Taylor, Kelly, Condrey, Caitlin, Hepinstall, Matthew S, and Mont, Michael A (2019). One-year patient outcomes for robotic-arm-assisted versus manual total knee arthroplasty. In: *The journal of knee surgery* 32.(11), pp. 1063–1068. ISSN: 1538-8506.

Martino, Luca (2018). A review of multiple try MCMC algorithms for signal processing. In: *Digit. Signal Process.* 75, pp. 134–152.

Marton, Lrinc and Lantos, Bla (2007). Modeling, Identification, and Compensation of Stick-Slip Friction. In: *IEEE Transactions on Industrial Electronics* 54, pp. 511–521.

Metzner, Maximilian, Leurer, Sebastian, Handwerker, Andreas, Karlidag, Engin, Blank, Andreas, Hefner, Florian, and Franke, Jörg (2021). High-precision assembly of electronic devices with lightweight robots through sensor-guided insertion. In: *Procedia CIRP* 97, pp. 337–341. ISSN: 2212-8271.

Morel, G. and Dubowsky, S. (1996). The precise control of manipulators with joint friction: a base force torque sensor method. In: *IEEE International Conference on Robotics and Automation*.

Mukhopadhyay, Rajarshi, Chaki, Ritartha, Sutradhar, Ashoke, and Chattopadhyay, Paramita (2019). Model learning for robotic manipulators using recurrent neural networks. In: *TENCON 2019-2019 IEEE Region 10 Conference (TENCON)*. IEEE, pp. 2251–2256. ISBN: 1728118956.

Neal, Radford M (2012). *Bayesian learning for neural networks*. Vol. 118. Springer Science Business Media. ISBN: 1461207452.

Nguyen, Hoai-Nhan, Zhou, Jian, and Kang, Hee-Jun (2015). A calibration method for enhancing robot accuracy through integration of an extended Kalman filter algorithm and an artificial neural network. In: *Neurocomputing* 151, pp. 996–1005. ISSN: 0925-2312.

Ni, Fenglei, Li, Tian, Liu, Yiwei, Liu, Hong, Li, Yang, Zhao, Liangliang, and Chen, Zhaopeng (2018). Dynamic modeling and controller design for SEA joints. In: *Assembly Automation*.

Pan, Hongtao, He, Kaihui, Cheng, Yong, Song, Yuntao, Yang, Yang, Villedieu, Eric, Shi, Shanshuang, and Yang, Songzhu (2017). Conceptual design of EAST multi-purpose maintenance deployer system. In: *Fusion Engineering and Design* 118, pp. 25–33. ISSN: 0920-3796.

Qahmash, Ayman, Al-Darraji, Izzat, Khadidos, Adil O, Tsaramirsis, Georgios, Khadidos, Alaa O, and Alghamdi, Mohammed (2023). On-Board Digital Twin Based on Impedance and Model Predictive Control for Aerial Robot Grasping. In: *Journal of Sensors* 2023. ISSN: 1687-725X.

Qi, Wang, Huapeng, Wu, Cheng, Yong, Pan, Hongtao, Yang, Yang, and Qin, Guodong (2022). Friction-identification of harmonic drive joints based on the MCMC method. In: *IEEE Access* 10, pp. 125893–125907. DOI: 10.1109/ACCESS.2022.3226036.

Qi, Wang, Huapeng, Wu, Yuntao, Song, Heikki, Handroos, Yong, Cheng, and Guodong, Qin (2023). Parameter identification of heavy-duty manipulator using stochastic gradient Hamilton Monte Carlo method. In: *IEEE Access* 11, pp. 78561–78583. ISSN: 2169-3536. DOI: 10.1109/ACCESS.2023.3298570.

Qian, Xuesen., Dai, Ruwei., and He, Shan. (2007). *Engineering control theory (New Century Edition)*. Shanghai Jiaotong University Press.

Qiang, Zhang, Ling, Zhou, and Zengfu, Wang (2017). Design and implementation of wormlike creeping mobile robot for EAST remote maintenance system. In: *Fusion Engineering and Design* 118, pp. 81–97. ISSN: 0920-3796.

Qin, Guodong (2022). Research on key technologies of snake arm maintainers in extreme environments. In: ISSN: 9523359096.

Qin, Guodong, Cheng, Yong, Pan, Hongtao, Zhao, Wenlong, Shi, Shanshuang, Ji, Aihong, and Wu, Huapeng (2022). Systematic design of snake arm maintainer in nuclear industry. In: *Fusion Engineering and Design* 176, p. 113049. ISSN: 0920-3796.

Qin, Guodong, Ji, Aihong, Cheng, Yong, Zhao, Wenlong, Pan, Hongtao, Shi, Shanshuang, and Song, Yuntao (2021). Position error compensation of the multi-purpose overload robot in nuclear power plants. In: *Nuclear Engineering and Technology* 53.(8), pp. 2708–2715. ISSN: 1738-5733.

Radivojevi, Tijana and Akhmatskaya, Elena (2019). Modified Hamiltonian Monte Carlo for Bayesian inference. In: *Statistics and Computing* (10).

Ramadhan, Ardityo Dimas, Usman, Koredianto, and Pratiwi, Nor Kumalasari Caecar (2021). Comparative analysis of various optimizers on residual network architecture for facial expression identification. In: *Proceedings of the 2nd International Conference on Electronics, Biomedical Engineering, and Health Informatics: ICEBEHI 2021, 3–4 November, Surabaya, Indonesia*. Springer, pp. 279–288.

Ravenzwaaij, D. van, Cassey, P., and Brown, S. D. (2018). A simple introduction to Markov Chain Monte-Carlo sampling. In: *Psychonomic Bulletin and Review* 25.(1), pp. 143–154. DOI: 10.3758/s13423-016-1015-8.

Rens van de Schoot Sonja D Winter, Oisin Ryan (2017). A systematic review of Bayesian articles in psychology: The last 25 years. In: *Psychological Methods* 22.(2), pp. 217–239.

Ruderman, M., Hoffmann, F., and Bertram, T. (2009). Modeling and Identification of Elastic Robot Joints With Hysteresis and Backlash. In: *Ieee Transactions on Industrial Electronics* 56.(10), pp. 3840–3847. DOI: 10.1109/tie.2009.2015752.

Sarkis, J. and Dhavale, D. G. (2015). Supplier selection for sustainable operations: A triple-bottom-line approach using a Bayesian framework. In: *International Journal of Production Economics* 166, pp. 177–191.

Sato, R. (2012). Mathematical Model of a CNC Rotary Table Driven by a Worm Gear. In: *International Journal of Intelligent Mechatronics and Robotics* 2.(4), pp. 27–40.

Shengzheng, Kang, Wu, Hongtao, Li, Yao, Xiaolong, Yang, and Jiafeng, Yao (2021). A fractional-order normalized Bouc–Wen model for piezoelectric hysteresis nonlinearity. In: *IEEE/ASME Transactions on Mechatronics* 27.(1), pp. 126–136. ISSN: 1083-4435.

Shi, Shanshuang, Song, Yuntao, Cheng, Yong, Villedieu, Eric, Bruno, Vincent, Feng, Hansheng, Wu, Huapeng, Wang, Peng, Hao, Zhiwei, and Li, Yang (2016). Conceptual design main progress of EAST Articulated Maintenance Arm (EAMA) system. In: *Fusion Engineering and Design* 104.(Mar.), pp. 40–45.

Shoujun, Wang, Xingmao, Shao, Yang, Liusong, and Nan, Liu (2020). Deep learning aided dynamic parameter identification of 6-DOF robot manipulators. In: *IEEE Access* 8, pp. 138102–138116. ISSN: 2169-3536.

Sim, Okkee, Oh, Jaesung, Lee, Kang Kyu, and Oh, Jun-Ho (2018). Collision Detection and Safe Reaction Algorithm for Non-backdrivable Manipulator with Single Force/Torque Sensor. In: *Journal of Intelligent and Robotic Systems* 91, pp. 403–412.

Simoni, L., Beschi, M., Legnani, G., and Visioli, A. (2015). FRICTION MODELING WITH TEMPERATURE EFFECTS FOR INDUSTRIAL ROBOT MANIPULATORS. In: *2015 Ieee/Rsj International Conference on Intelligent Robots and Systems*, pp. 3524–3529.

Simoni, Luca, Beschi, Manuel, Legnani, Giovanni, and Visioli, Antonio (2017). Modelling the temperature in joint friction of industrial manipulators. In: *Robotica*, pp. 1–22.

Song, Yanshu, Huang, Hailin, Liu, Fei, Xi, Fengfeng, Zhou, Dawei, and Li, Bing (2020). Torque Estimation for Robotic Joint With Harmonic Reducer Based on Deformation Calibration. In: *IEEE Sensors Journal* 20, pp. 991–1002.

Song, Yuntao, Wu, S., Li, Jiangang, Wan, Bao Nian, Wan, Yuan Xi, Fu, Peng, Ye, Min You, Zheng, Jin Xing, Lu, Kun, and Gao, Xianggao (2014). Concept design of CFETR tokamak machine. In: *IEEE Transactions on Plasma Science* 42.(3), pp. 503–509. ISSN: 0093-3813.

Suh, Jung-Il, Joonwook, Lee, and Dong-Eun, Lee (2020). Development and Application of Motor-Equipped Reaction Torque Sensor with Adjustable Measurement Range and Sensitivity. In: *Applied Sciences*.

Sun, Yongjun, Yiwei, Liu, Tian, Zou, Jin, Ming-He, and Liu, Hong (2015). Design and optimization of a novel six-axis force/torque sensor for space robot. In: *Measurement* 65, pp. 135–148.

Taghirad, H. D. and Belanger, P. R. (1998). Modeling and parameter identification of harmonic drive systems. In: *Journal of Dynamic Systems Measurement and Control-Transactions of the Asme* 120.(4), pp. 439–444. DOI: 10.1115/1.2801484.

Tao, Z., Yongping, S., Cheng, Yong, Zeng, Yishan, Zhang, Xin, and Liang, Sheng (2023). The design and implementation of distributed architecture in the CMOR motion control system. In: *Fusion Engineering and Design* 186, p. 113357. ISSN: 0920-3796.

Team, Tore Supra (2002). Tore Supra experience on actively cooled high heat flux components. In: *Fusion engineering and design* 61.(3), pp. 71–80.

Thrane, E. and Talbot, C. (2019). An introduction to Bayesian inference in gravitational-wave astronomy: Parameter estimation, model selection, and hierarchical models. In: *Publications of the Astronomical Society of Australia* 36.

Ticker, Ronald L, Cepollina, Frank, and Reed, Benjamin B (2015). NASA's in-space robotic servicing. In: *AIAA Space 2015 Conference and Exposition*, p. 4644.

Traversaro, Silvio, Prete, Andrea Del, Ivaldi, Serena, and Nori, Francesco (2015). Inertial parameters identification and joint torques estimation with proximal force/torque sensing. In: *2015 IEEE International Conference on Robotics and Automation (ICRA)*, pp. 2105–2110.

Tri, V. M., Tjahjowidodo, T., Ramon, H., and Van Brussel, H. (2011). A New Approach to Modeling Hysteresis in a Pneumatic Artificial Muscle Using The Maxwell-Slip Model. In: *Ieee-Asme Transactions on Mechatronics* 16.(1), pp. 177–186. DOI: 10.1109/tmech.2009.2038373.

Trumper, David L. and Yoon, Jun Young (2014). Friction modeling, identification, and compensation based on friction hysteresis and Dahl resonance. In: *Mechatronics: The Science of Intelligent Machines*.

Tuttle, T. D. and Seering, W. (1993). Modeling a harmonic drive gear transmission. In: *IEEE International Conference on Robotics and Automation*.

Vasilev, Momchil, MacLeod, Charles N, Loukas, Charalampos, Javadi, Yashar, Vithanage, Randika KW, Lines, David, Mohseni, Ehsan, Pierce, Stephen Gareth, and Gachagan, Anthony (2021). Sensor-enabled multi-robot system for automated welding and in-process ultrasonic NDE. In: *Sensors* 21.(15), p. 5077. ISSN: 1424-8220.

Vats, Dootika and Knudson, Christina (2021). Revisiting the gelman–rubin diagnostic. In: *Statistical Science* 36.(4), pp. 518–529. ISSN: 0883-4237.

Vojić, Samir (2020). Applications of collaborative industrial robots. In: *Machines. Technologies. Materials.* 14.(3), pp. 96–99. ISSN: 1313-0226.

Wahrburg, Arne, Bös, Johannes, Listmann, Kim D., Dai, Fan, Matthias, Björn, and Ding, Hao (2018). Motor-Current-Based Estimation of Cartesian Contact Forces and Torques for Robotic Manipulators and Its Application to Force Control. In: *IEEE Transactions on Automation Science and Engineering* 15, pp. 879–886.

Wang, K., Wang, Q., Cheng, Y., Wu, H., Song, Y., and Engineering, V Bruno (2019). Optimization of the geometric parameters of the EAST articulated maintenance arm (EAMA) with a collision-free workspace determination in EAST. In: *Fusion and Design* 139.(FEB.), pp. 155–162.

Wei, Huo. (2005). *Robot Dynamics and Control (in chinese)*. Higher Education Press.

Welling, M. and Teh, Y. (2011). Bayesian learning via stochastic gradient langevin dynamics. In.

Yeon, Kang, Donghan, Kim, and Kwangjin, Kim (2019). URDF generator for manipulator robot. In: *2019 Third IEEE International Conference on Robotic Computing (IRC)*. IEEE, pp. 483–487. ISBN: 1538692457.

Yuhsiu, Lee, Hsu, S.C., Du, Y.Y., Hu, J.S., and Tsao, T. C. (2019). A Nested-Loop Iterative Learning Control for Robot Manipulators. In: *Ifac Papersonline* 52.(15), pp. 358–363. DOI: 10.1016/j.ifacol.2019.11.701.

Zhang, Hongwei (2013). Development and multiple mode control of modular and reconfigurable robot. Thesis. DOI: 10.1109/ROBOT.2008.4543746.

Zhen, S. C., Peng, X., Liu, X. L., Li, H. M., and Chen, Y. H. (2021). A new PD based robust control method for the robot joint module. In: *Mechanical Systems and Signal Processing* 161, p. 107958.

Zhiguo, Shi, Yuankai, Li, Guangjun, and Systems, Liu (2017). Adaptive torque estimation of robot joint with harmonic drive transmission. In: *Mechanical and Processing, Signal*.

ACTA UNIVERSITATIS LAPPEENRANTAENSIS

1066. JANTUNEN, NIKLAS. Development of liquid–liquid extraction processes for concentrated hydrometallurgical solutions. 2023. Diss.

1067. GULAGI, ASHISH. South Asia's Energy [R]evolution – Transition towards defossilised power systems by 2050 with special focus on India. 2023. Diss.

1068. OBREZKOV LEONID. Development of continuum beam elements for the Achilles tendon modeling. 2023. Diss.

1069. KASEVA, JANNE. Assessing the climate resilience of plant-soil systems through response diversity. 2023. Diss.

1070. HYNNINEN, TIMO. Development directions in software testing and quality assurance. 2023. Diss.

1071. AGHAHOSSEINI, ARMAN. Analyses and comparison of energy systems and scenarios for carbon neutrality - Focus on the Americas, the MENA region, and the role of geo-technologies. 2023. Diss.

1072. LAKANEN, LAURA. Developing handprints to enhance the environmental performance of other actors. 2023. Diss.

1073. ABRAMENKO, VALERII. Synchronous reluctance motor with an axially laminated anisotropic rotor in high-speed applications. 2023. Diss.

1074. GUTIERREZ ROJAS, DANIEL. Anomaly detection in cyber-physical applications. 2023. Diss.

1075. ESANOV, BAKHTIYOR. Adaptive user-controlled personalization for virtual journey applications. 2023. Diss.

1076. SILTANEN, JUKKA. Laser and hybrid welding of high-strength structural steels. 2023. Diss.

1077. NOUSIAINEN, JALO. Model-based reinforcement learning and inverse problems in extreme adaptive optics control. 2023. Diss.

1078. USTINOV, STANISLAV. Fast and accurate simulation of fluid power circuits in the presence of small volumes using advanced methods and models for numerical stiffness elimination. 2023. Diss.

1079. HUSSAIN, HAFIZ MAJID. Heuristic-based packetized energy management for residential electricity demand. 2023. Diss.

1080. HÄMÄLÄINEN, MINNA. Principals managing entrepreneurship education in schools. 2023. Diss.

1081. WANG, ZHAO. Photocatalytic degradation of pharmaceutical and person care products (PPCPs) by commercial and synthesized catalysts under UV irradiation. 2023. Diss.

1082. LOHRMANN, ALENA. The water footprint of the global power sector: Status quo, challenges, and opportunities for tackling the global water crisis. 2023. Diss.

1083. PONOMAREV, NIKOLAI. A salt and alkali synergy for synthesising active carbons from lignin: porosity development and techno-economic assessment. 2023. Diss.

1084. AFANASYEVA, SVETLANA. Wind farm layout optimization: project economics and risk. 2023. Diss.

1085. VOSTROV, KONSTANTIN. Reduction of non-circulating bearing currents by electrical machine design. 2023. Diss.

1086. CARILLO MELGAREJO, DICK. Improving the design of cellular networks beyond 5G for smart grids. 2023. Diss.

1087. MALACINA, IRYNA. Zooming in and out: The strategic management of innovation across multiple levels of complex supply networks. 2023. Diss.

1088. SORE, SARISEELIA. Impact of information system capabilities on business value creation: Aspects of IT-producing and IT-consuming companies. 2023. Diss.

1089. IMMONEN, EERO. Advances in optimal design of shapes and processes by computational fluid dynamics. 2023. Diss.

1090. LAVOYE, VIRGINIE. Augmented reality in consumer retail: a presence theory approach. 2023. Diss.

1091. HÄRKÖNEN, KALEVI. Smart buildings in the green energy transition. 2023. Diss.

1092. TSYTSYNA, EVGENIYA. Motives, uncertainties, and imbalances in the evolution of a sustainable business ecosystem. 2023. Diss.

1093. JÄÄSKELÄINEN, ATTE. Business model innovation opportunities when news has become a public good. 2023. Diss.

1094. ADEDIPE, TAIWO. Atmospheric boundary-layer characteristics and their significance in wind energy and urban air quality assessment. 2023. Diss.

1095. SOSUNOVA, INNA. Model and guidelines for designing Internet-of-Things-enabled smart waste management system in smart cities. 2023. Diss.

1096. VUORELA, JYRI. Operative business development through system model and changing business structures. 2023. Diss.

1097. TRIAPITCIN, ILIA. Knowledge injection method for real-time decision support. 2023. Diss.

1098. RÄISÄNEN, OTTO. Open data in distribution network asset management. 2023. Diss.

1099. MATELA, MIKA. Procurement improvement in the public agency. 2023. Diss.

1100. SHAH, DIPAL. Quantification of synchronization. 2023. Diss.

1101. GHAFOURI, MEHRAN. Thermomechanical finite element simulation of welding, and elevated-temperature mechanical behaviour of high and ultra-high strength steels. 2023. Diss.

1102. NEUVONEN, RIKU. Numerical ductile fracture assessment of weldments in direct-quenched, ultra-high-strength steel. 2023. Diss.

1103. HUPPONEN, MARI. Long-term evolution of greenhouse gas emissions from municipal solid waste management. 2023. Diss.

LUT University

ISBN 978-952-412-002-9
ISBN 978-952-412-003-6 (PDF)
ISSN 1456-4491 (Print)
ISSN 2814-5518 (Online)
Lappeenranta 2023